The Long-Term Ecological Research (LTER) site Istituto scientifico Angelo Mosso

SECOND JOINT MEETING
ON SOIL AND PLANT
SYSTEM SCIENCES

FROM ALPINE GLACIERS TO RICE PADDIES

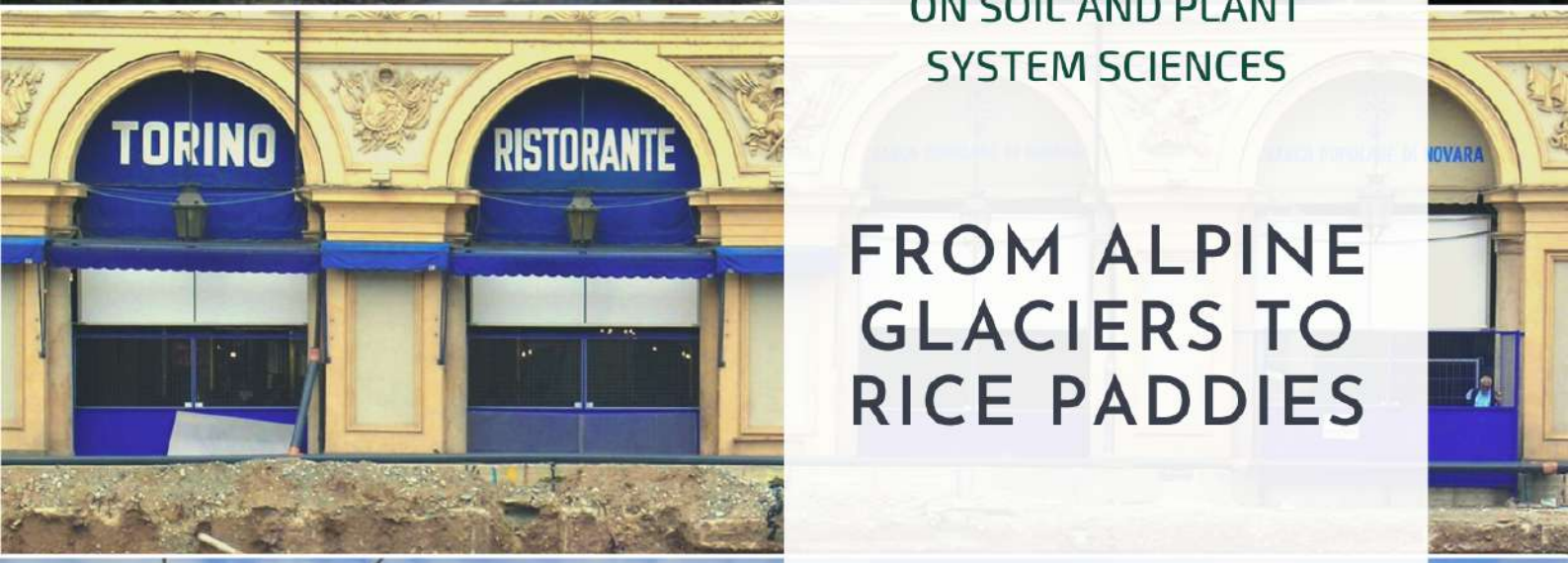

Excursion guide

SPSS 2021

SECOND JOINT MEETING
ON SOIL AND PLANT SYSTEM SCIENCES

FROM ALPINE GLACIERS TO RICE PADDIES

Excursion guide

20th-23rd September 2021
Online - Torino, Italy

Edited by
Eleonora Bonifacio
Luisella Celi
Michele Freppaz

Graphic layout
Marta Iannicelli
Veronica Santoro
Michela Schiavon

Cover images (from the top)
Michele Freppaz
Andrea Samorè
Franco Ajmone Marsan
Sara Martinengo

Printed by
Biblion Graphic – Grugliasco (TO)

INTRODUCTION

Following water: from alpine glaciers to rice paddies

With the virtual SPSS2021 field trip, we aim at showing you a range of sites that could not be reached in normal field trips. We will travel more than 250 km and move from 3000 m to less than 100 m a.s.l. All sites have been the subject of various multidisciplinary studies over the last years carried out either by us or by expert colleagues from other fields of research. To better link the field trip to the topics of the scientific sessions, we divided it into four parts. By doing so we hope to keep you interested and stimulate the discussion. The virtual field trip will follow the course of water and lead all participants through the exploration of some of the most interesting environments of North-Western Italy. We will start from Alpine glacial lakes and ponds, high mountain vegetation and striking, hidden soils at the LTER site Istituto Mosso (Monte Rosa Massif). At an elevation ranging between about 2600 and 3300 m, the long seasonal snow cover and the cold air temperature shape the landscape, with the presence of periglacial landforms and snowbed ecosystems.

Then, following alpine rivers down to the Stura di Lanzo floodplain we will stop at one of few remaining forests that once covered the Po plain. We will show you soils that are more likely to be found in tropical areas than 100 km far from the Alps. However, after having escaped to changes in land use, these sites are now at risk because of the presence of non-indigenous tree species that through physiological adaptations sharply impact nutrient biogeochemical cycles.

Torino is just 10 km away, where the Stura di Lanzo merges with the Po River. Soil contamination is a problem here, as in many big cities that have been heavily industrialized. Industrial districts are now converted in urban parks where plant selection, decontamination techniques and architectural design meet to improve city life quality.

Still following the Po River, we will then leave Torino eastwards and look at how agriculture can shape the landscape. Lowland rice fields harbour a large biodiversity, and have been proposed to be listed among the UNESCO world heritage sites. Water management in rice paddies is the main driver of rice yield and quality, but also a key factor determining soil characteristics and processes. However, sustainable agriculture in these areas is now facing emerging challenges that require new

approaches to combine crop production, resource management and environmental issues.
We will thus end the field trip in Lombardia.

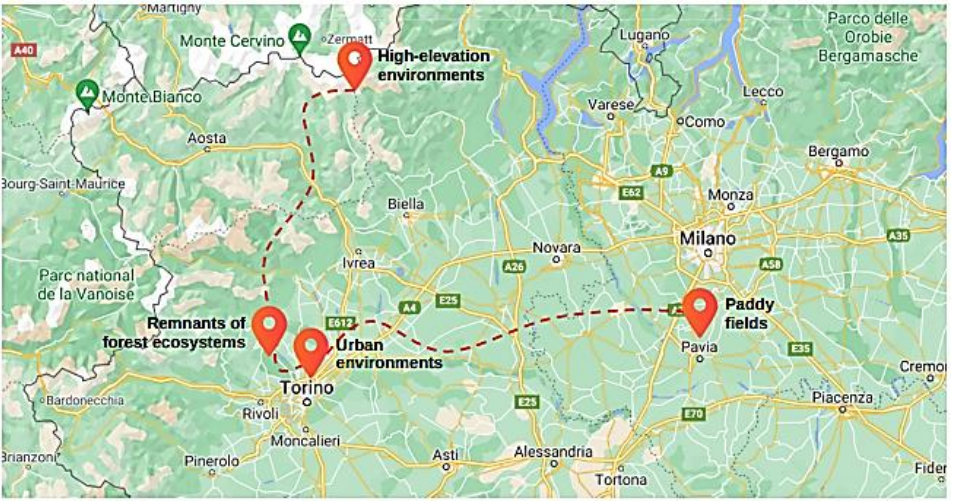

Chapter 1.1

Running waters as living elements of territorial, ecological and cultural identities

Bona, F., Fenoglio, S.

Rivers represent 0.0002% of the water present on the Earth and ecological functioning, biodiversity and human life strongly depend on this infinitesimal fraction. The rivers that flow down from the Alps are of particular importance, as they constitute one of the most important water reserves in terms of both quality and quantity. Unfortunately, global climate change and local anthropogenic pressures are increasingly altering hydrology, morphology, chemistry and temperature regimes of these streams. Running waters are key elements connecting different territories and shaping the external (natural) and the inner (cultural) landscape of entire regions. Here we present a small snapshot of four aquatic environments typical of the Piedmont region, ideally but also literally connected by the same waters (Fig. 1.1).

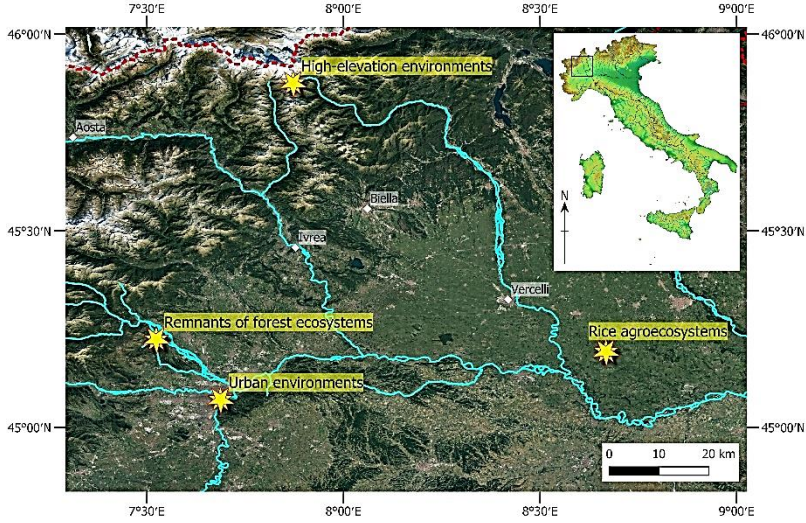

Figure 1.1. Localization of the study sites and the main rivers from the Alps to the plain.

Different aquatic environments have peculiar natural, biological and ecological characteristics, but also different history of water-man relationship, cultural and socio-economical heritages.

High-elevation environment

Alpine rivers have unique characteristics, and their presence has profoundly characterized not only natural history but also the human colonization of these mountain areas. Located in the largest and most important mountainous area in Europe, still currently in a phase of active orogenesis, Alpine rivers are generally characterized in their upper sections by steep slopes, great erosion capacity and coarse substrate. Other characteristics are high riverbed instability, conspicuous daily variations in the flow rate, with a maximum in the late afternoon, low summer temperatures (generally below the 10 °C), high turbidity and solid transport, noticeable oligosalinity (Fig. 1.2).

Figure 1.2. A high altitude alpine river, fed by the melting of snow and ice, with the peculiar turbid aspect due to the solid transport.

In the Monte Rosa area, rivers belong to the 'Kryal' type, i.e., they show a single seasonal hydrological peak in late spring-summer due to the melting of glaciers. In the same area, at lower altitudes there are 'Rhithral' streams, whose hydrology is dominated by seasonal melting of snow and precipitation. Biodiversity in these high-

altitude environments is generally low, because of the harsh environmental conditions, but the presence of endemism and highly adapted taxa is remarkable.
Considering the importance of Alpine running waters, we decided two years ago to found the Alpine Stream Research Center – ALPSTREAM, a center located in Ostana, near the sources of the Po River (Fig. 1.3). Researchers from three Universities (UNITO, UPO, POLITO) and technicians from the Parco del Monviso collaborate here to study the human impact on lotic environments and to promote the sustainable use of water resources through three main missions: research, teaching and public engagement. More information at: info.alpstream@gmail.com.

Figure 1.3. View from the window of the Alpine Stream Research Center Alpstream.

Remnants of forest ecosystems

In highly populated regions such as Piemonte the presence of forest ecosystems are often limited to protected areas. In the region, the "Parco Naturale della Mandria" represents in this sense a valuable example of historical balance between human activities and biodiversity conservation. The Mandria Park covers 6500 ha at the boundary of the metropolitan area of the city of Turin. It hosts a rich network of aquatic ecosystems, some of them included in the Habitat EU Directive, which represents a clear example of the functional and mutual connections between rivers and perifluvial environments. Indeed, the Park includes several wetlands composed

of artificial lakes created for hunting purpose in the XIX century, ponds and temporary pools often surrounded by woodland. All these wetlands host remarkable biodiversity elements, especially aquatic plants, such as *Phragmites australis*, *Typha latifolia, Alisma plantago-aquatica* and amphibians (9 species). Running waters include a typical rithral stream (Ceronda) and by a network of irrigation channels created by the Savoy Monarchy in the XIX century.

Figure 1.4. Rio Valsoglia, Parco Naturale della Mandria. A typical example of stream flowing in the protected area, with natural features despite its artificial origin.

The channels are now almost re-naturalized and are very similar to natural streams with rhitral features (Fig. 1.4), such as high aquatic diversity reflecting a rather good hydromorphological diversification, as confirmed by the presence of seven fish species listed in the Annex II of the Habitat Directive.

The University of Turin has been collaborating with the Park for many years and, in this regard, a Field Station has recently been created in the Park for educational activities regarding the study of aquatic ecosystems.

Urban environments

Many cities around the world can be defined as “river cities” as they developed along watercourses and experienced the incorporation of nature into the fabric of urban life. Urban cities concentrate people, economic wealth, cultural heritage and activities that historically largely depend on the proximity of water. Turin is not an exception: the city arose on two important rivers, the Po and the Dora Riparia already in Roman times and subsequently incorporated two others, the Sangone and the Stura di Lanzo, coming from two other Alpine valleys. The Po River, in particular, marks the Turin area separating the city from the hill for about 15 km of its urban course. Upon entering Turin, the Po River radically changes its appearance: most of the natural elements are replaced by anthropogenic ones. Human interventions follow one another along the river: artificial banks, works for recreational use of the banks, the production of energy, and water purification (Fig. 1.5).

Figure 1.5. The Po River flowing through the town of Torino

Yet, there are also evident traces of interventions for environmental restoration, which are the result of careful planning that began in recent decades with the creation of a system of protected areas along the Po River. The city of Turin is characterized by large urban parks, most of them lying along the Po and connected to each other: the Valentino, Colletta and Meisino Parks. Their presence provides important natural elements, allowing the nesting of numerous species of birds, so much so that Turin hosts the only urban heronry in Europe. The riparian vegetation,

dense in some places even if not always native, helps to maintain a fair ecological functionality of the river: it provides shade, mitigates the temperature of the waters, and provides organic matter to feed the food chain of the waters. These natural elements contribute making the water quality of the Po acceptable even if far from the objectives of the Water Framework Directive, which aims to achieve "good" quality for all European rivers by 2027. Indeed, several key- issues should be addressed by scientific research in the coming years towards the efficient management of urban streams. Among the main environmental issues of Turin rivers, common to many other urban rivers, are emerging pollutants, including pharmaceuticals and microplastics, for which wastewater treatments are still lacking; the shortage of summer flows connected to climate change and the growing water requirement; the invasion of alien plants and animals that pose a serious threat to aquatic biodiversity.

Rice agroecosystems

The proximity to the Alps and their rich lotic systems has allowed the development of the largest European rice growing area, the so-called Vercelli, Novara, Pavia district (Fig. 1.6). Here, humans have created unique artificial environments that have changed the natural characteristics and economy of the Piedmont plains.

Figure 1.6. The large rice fields of Piedmont Region are fed by the waters of Alpine rivers.

The water in rice fields is present intermittently and has created a unique habitat, which has some negative impacts (e.g., favouring the spread of some harmful species, such as mosquitoes or invasive taxa), but on the other represents one refugee for numerous taxa that would otherwise disappear in a heavily anthropized environment, as numerous odonates, molluscs and crustaceans. Moreover, here water chemical-physical characteristics change drastically, due to the use of fertilizers and biocides and because confined waters undergo greater thermal excursus, reaching such high temperatures during summer days that the availability of oxygen can be strongly reduced.

Chapter 1.2

From Monte Rosa to the plains of the Po River: a climate introduction

Mercalli, L., Cat Berro, D.

The sites chosen for this virtual tour among pedological and paleo-environmental evidences are located at the southern flank of the Alps, between Monte Rosa (one of the most relevant massifs of the Alps, which culminates at 4634 m) and at the western Po Valley (Northwestern Italy).

The climate of the area is strongly affected by the presence of mountainous reliefs and the prevailing Atlantic winds, which however, flowing from the West, discharge the greatest precipitations on the French and Swiss side of the Alpine range (windward), leaving the Italian side (leeward) sometimes in foehn conditions (warm and dry wind) especially in winter. The most important rains and snowfalls occur instead when the winds orient themselves between South-West, South and Southeast, drawing moisture from the nearby Mediterranean Sea (Fig. 1.7).

Figure 1.7. In summer days, cumulus and stratocumulus clouds often cover the south-eastern side of Monte Rosa (Val Sesia) due to local winds that carry moist air from the Po plain (photo taken from the plane, August 30th, 2015; f. D. Cat Berro/SMI).

In this case, the moist maritime air is barred by the southern slope of the Alps, encouraging the formation of clouds and precipitation to the point that much of the mean annual precipitation amounts rises rapidly from 600-1000 mm in the plain between Turin, Vercelli, Alessandria and Pavia - where rice paddies are an iconic landscape - up to over 2000 mm in the mountainous area of Biellese and Valsesia, one of the rainiest regions in Italy.

A common climatic feature of all these places is the bimodal precipitation regime, with maximum in spring and autumn (April-May, October-November), when low atmospheric pressures around the gulf of Genoa direct the humid winds towards the Alps. Winter is drier due to prolonged high pressures or recurring foehn periods, while summer, although less rainy than spring and autumn, still see frequent diurnal clouds (cumulus) and thunderstorms in the mountains North of Turin, toward Monte Rosa and Lago Maggiore.

The meteorological observatory of Oropa (altitude 1181 m, near Biella) is representative of the climate of this mountain area known for its huge rainfall: it receives on average 2130 mm of precipitation per year (rain and melted snow), distributed over 105 days (reference period 1991-2020), with monthly values ranging from a minimum of 65 mm in January (6 rainy or snowy days) to a maximum of 292 mm in May (13 days) and 273 mm in November (9 days). July, the driest month of the summer, still receives 135 mm of rain (9 days) due to frequent afternoon thunderstorms.

From this very wet and green pre-alpine belt, precipitation amounts decrease proceeding both towards the interior of the Alps, more protected from the flow of maritime moist air, and towards the plain, where the orographic barrier effect on the Mediterranean winds is less felt: 1085 mm in Gressoney-D'Ejola (1850 m, Aosta Valley), 896 mm in Turin, 827 mm in Vercelli and just 611 mm in Alessandria, less than a third compared to the Biellese mountains (Fig. 1.8). In addition to the average precipitation, the territory is shaped by extreme rainfalls.

Large floods and geo-hydrological events occur mostly in autumn, when the warm and humid sirocco wind causes heavy and prolonged rains for 2-5 consecutive days even at high altitudes as at the beginning of November 1968 (up to 500 mm in 2 days and serious destruction in the eastern Biella area, vast flooding of the Vercelli plain and 66 victims throughout the Italian North-West), again at the beginning of November in 1994, at early and mid-October 2000 and early October 2020, while

more local flash-floods can develop during summer cloudbursts (June 5th, 2002 in Biella and surroundings, 191 mm of rain in 5 hours in Oropa).

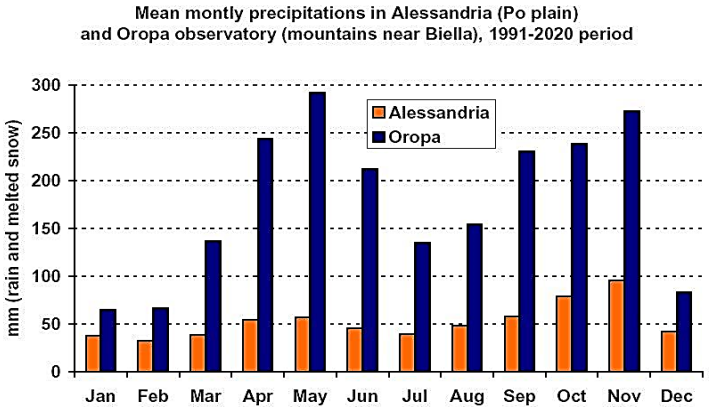

Figure 1.8. Monthly precipitations peak at Oropa observatory in May, and in Alessandria in November.

Temperatures behaviour follows the relief with an average annual thermal gradient of about 0,5 °C/100 m of altitude. In high mountain regions, the average annual freezing level (0 °C isotherm) fluctuates at 2700-2800 m, also delineating the limit of permafrost extension. At lower altitudes, average annual temperatures are 4.7 °C in Gressoney-D'Ejola (1850 m), 8.7 °C in Oropa (1181 m), 14.4 °C in downtown-Turin and at 13.1 °C in Alessandria (rural location). While long-term total precipitation is approximately stable, and the recent increase in rainfall intensity is still under debate, the effects of ongoing climate change are evident especially in rising temperatures.
In the last 50 years (1971-2020), mean annual temperatures have increased by 2.1 °C in Gressoney-D'Ejola, 2.2 °C at Gran San Bernardo, 2.3 °C in Turin and 2.7 ° C at Oropa observatory (Fig. 1.9). This has caused an upward shift of the climatic and ecosystemic zones of about 300-400 m in half a century, a very quick variation that might undermine the adaptability of many living species.

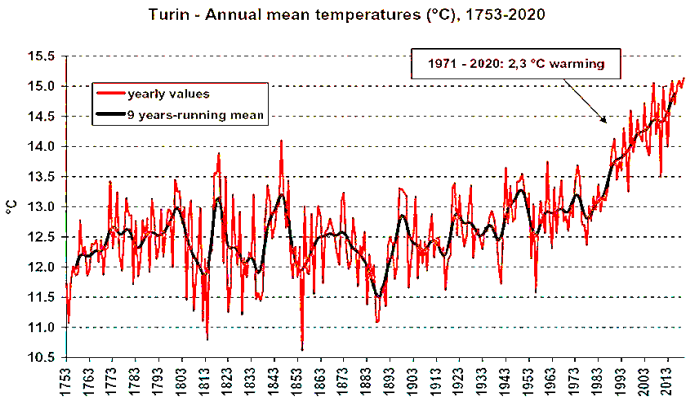

Figure 1.9. The rise in mean temperatures has become strongly evident since 1980's. In 1971-2020 period the atmosphere in Turin (city with one of the longest meteorological series in Italy, since 1753) has warmed by 2,3 °C (data elaboration: SMI – www.nimbus.it).

Extreme cold spells are becoming increasingly rare, one of the most intense in recent decades was that of February 2012 which brought minimum temperatures of -20.5 °C at Bocchetta delle Pisse, -19.0 °C in Gressoney-D'Ejola and even -24 °C in the southern surroundings of Turin due to the intense thermal inversion on the snow-covered plain.

At the same time, heat extremes events are more and more frequent. In this region, maximum temperatures on record, above 40 °C in the plains for the first time in centuries, were reached under the subtropical anticyclones of August 2003 (41.9 °C in Alessandria) and especially at the end of June 2019 (30.5 °C in Gressoney, 40.9 °C in Turin-Mirafiori) with the contribution of foehn-effect.

Warming temperatures lead to decreasing snow cover, due to the lower amount of snowfall especially below 2000 meters (the fraction of precipitation that falls in the form of rain increases at the expense of the snow) and due to the faster melting in spring. At Bocchetta delle Pisse (2410 m), in the southeastern side of Monte Rosa (Val Sesia), very close to the “Angelo Mosso” Institute, 687 cm of mean yearly snowfall is measured (2001-2020 period) and snow covers the ground for 8 months. Further downstream, the Gressoney-D'Ejola observatory detects 383 cm of snowfall (-14% compared to the previous thirty years period, 1971-2000) and 162 days of snow-

covered ground (-9%), and Oropa observatory respectively 161 cm (-19%) and 74 days (-34%) (Fig. 1.10).

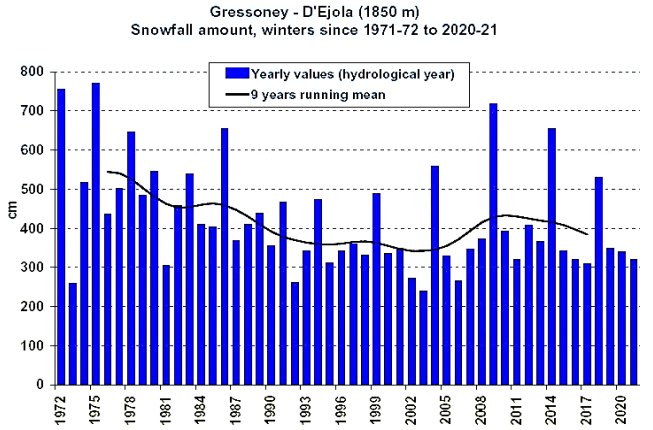

Figure 1.10. The decrease in annual snowfall amount at Gressoney-D'Ejola (1850 m, Monte Rosa): -14% in 2001-2020 compared to the previous period 1971-2000.

In the western Po plain the snow has become ephemeral: it often lasts on the ground only few hours after events that usually do not deposit more than 5 cm, and average annual snowfall amounts are reduced to 18 cm in Turin (-28%).

Although in a context of atmospheric warming and decreasing snow, large snowfalls and avalanches sometimes can still occur in high mountains during seasons with very high precipitation, as in 2013-14 and 2017- 18 winters, while rain prevails at lower altitudes.

Less snow and warmer summers badly affects mountain glaciers, whose surface area in the Alps as a whole decreased by 60% between the maximum of Little Ice Age (1820-1850) and nowadays. In addition, with further dramatic warming, up to +4 °C and more at the end of the 21st century without significant reductions in greenhouse gas emissions (business-as-usual scenario), the Alpine range may become almost entirely ice-free except for small residual ice caps above 4000 m. Then the glaciers of Monte Rosa will remain among the few relicts of the former Alpine glacialism.

Will there still be enough water for rice fields?

Chapter 1.3

Regional geological and local morphodynamic approaches to the northern Piemonte field trip

Giardino, M.

For approaching the fieldtrip to Northern Piemonte, an introduction to the relationships between geodiversity, soils and water within urban, piedmont, plain and alpine landscapes is necessary. A twofold analysis is here proposed, including a Regional Geological Approach (RGA) and a Local Morphodynamic Approach (LMA).

Application of the RGA analysis to large-scale, long-term geomorphological, lithological and structural features of Northern Piemonte implies the location of the fieldtrip stops within the regional framework (Piana *et al.*, 2017). The simplified geological map of Piemonte region (Fig. 1.11), illustrates the main lithological "groups" constraining the regional diversity of geomorphological landscapes:

a) the main units of unconsolidated Quaternary superficial deposits (Pleistocene to present-day fine to coarse alluvial and debris flow deposits, Pleistocene glacial deposits, "Villafranchian" clay, silts and sands; 1-3 in Fig. 1.11), buillding up floodplains channels and terraces, morainic amphitheatres and large alluvial fans at the Alpine piedmont;

b) a composite succession of sedimentary units of marine origin (Pliocene sands; Miocene clays and evaporites; Oligo-Miocene marls; calcareous sandstones and sandy-muddy turbidite layers; 4-7 in Fig. 1.11) infilling the Padan gulf and the Tertiary Piemonte Basin, and sedimentary units of the Alpine foreland basin (silico-clastic sandstones, conglomerates, marles, and undifferentiated clayely chaotic units of Cretaceous- Eocene age; 8-9 in Fig. 1.11). These successions identify the hilly areas of Central Piemonte (Torino Hill, Monferrato and Langhe) and the piedmont of Ligurian Alps and Apennines (southern Piemonte);

c) a complex section of the Alps-Apennines orogenic system: lower crust, lithospheric mantle, metaophiolites and associated metasediments of the Mesozoic

Piemonte-Liguria and Valais oceans (10-12 in Fig. 1.11), intermediate crust and metasedimentary cover of both European and Adriatic palaeocontinents, either as massive and schistous metamorphites ("internal" and "external crystalline massifs", 13-14 in Fig. 1.11), Ercynian and late Alpine magmatites (plutonic, volcanic and volcanoclastic sequences; 15 in Fig. 1.11) constituting the whole arched structure of the mountain range, including the Ligurian, Maritime, Cottian, Graian, and Lepontine Alps.

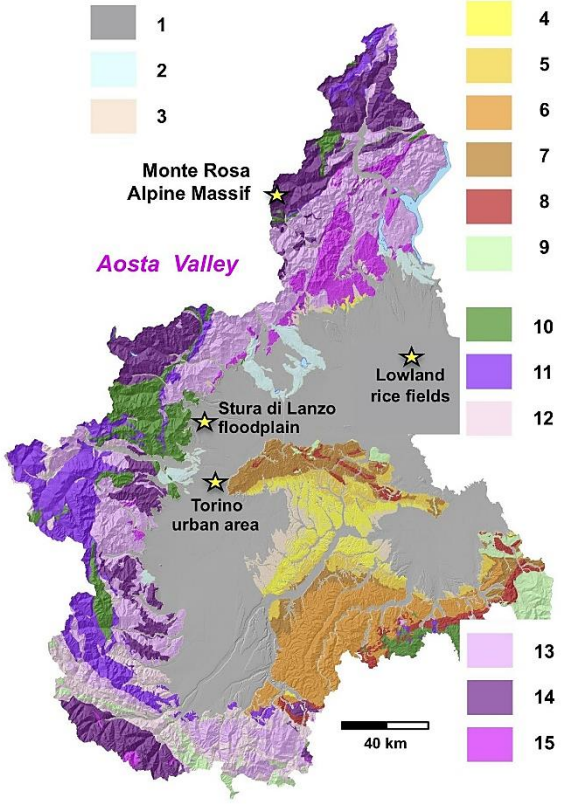

Figure 1.11. Location of the fieldtrip stops within the simplified geological map of the Piemonte Region (modified by ARPA-Piemonte). See text for description of the lithological groups of the legend and their relationships with the regional diversity of geomorphological landscapes (floodplain and piedmont groups: 1-3; hilly areas groups: 4-9; c) mountain range groups: 10-15).

Main lithological characters and the regional structures of the Alps (a deep-rooted double-vergent collisional belt with a series of metamorphic folds and wedges separated by steep fault zones) and Apennine (a shallower thrust and fold belt) are here interpreted as general conditioning factors for modelling the stability of the relief. In the long-term "geological" perspective, they represent independent variables, offering "static" conditionings to the geomorphological landscape (e.g. constrains on hydrographic network, predisposition to slope instability as "internal" causes, lowering shear strength of slopes material).

Application of RGA approach to the "Torino" and the "Stura di Lanzo" fieldtrip stops, clearly indicates the whole urban area of Torino is "pinched" in between the above-described main orogenetic features: the internal side of the metamorphic Western Alps (to the West) and the sedimentary Torino Hill. Tectonic constraints and diversity of both history of crustal mobility and lithological resistance to erosion allowed contrasting geomorphological landscapes in the two orogens and the development of a threshold in between the southern and northern Po plain, controlling channel trends and location of confluences within the fluvial network of the area (Fig. 1.12) (Forno *et al*. 2018).

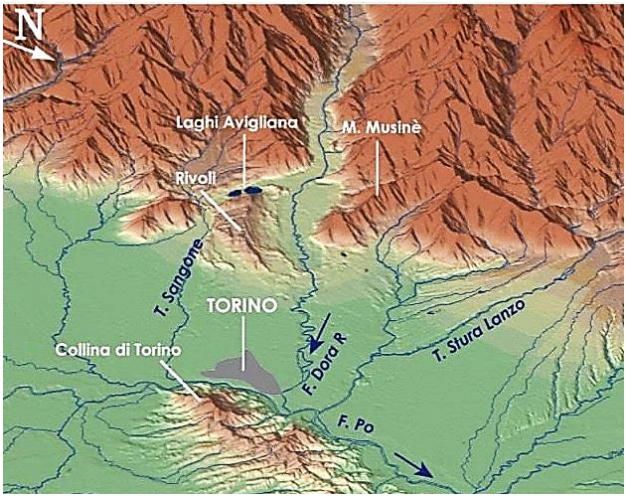

Figure 1.12. Geomorphological landscape of the Torino-Lanzo area, between the internal side of the metamorphic Western Alps (West) and the sedimentary Torino Hill (East).

The diversity of lithological and tectonic characters allowed different geomorphic responses also within the internal side of the Alps Perrone *et al*., 2013). Continuous deep erosion concentrated along linear deformation zones allowed long-term development of major alpine valleys (e.g. Susa Valley), recording the Middle-Upper Pleistocene glacial expansions till the piedmont area (i.e. Rivoli Avigliana Morainic Amphitheatre). Pulsed long-term uplift within resistant rocks units facing the alpine front range allowed long term development of large alluvial fan and the preservation of pre-glacial environments, such as the Stura di Lanzo "Villafranchian" finer grained fluvial deposits of lower Pleistocene age.

Within the RGA perspective, properties of lithological units are also extremely relevant for assessing the constraints imposed to water resources. By migrating to the northernmost stops of the fieldtrip, we can appraise the results of a recent study on lithological geodiversity constraining hydrological features (Perotti *et al*., 2019) within the Sesia Val Grande Unesco Global Geopark, from the Monte Rosa massif, to the Ossola and Vigezzo Valleys, an area bordering the Lake Maggiore and degrading towards the Po plain. Here, the higher mountain range is characterized by crystalline lithological units (10, 11, and 13 in Fig. 1.11) whose permeability mainly depends on fractures density. Lower mountains include also volcanic rocks (15 in Fig. 1.11) and limestones (soluble rocks; 12 in Fig. 1.11), while fluvial and fluvioglacial deposits (1 in Fig. 1.11), characterize the valley floors and the piedmont. These last units represent the reloading areas of the high productivity aquifers present in the territory. Factor map of permeability (Fig. 1.13) of the Sesia Val Grande Geopark shows the low predisposition of crystalline rocks within the Monte Rosa - Istituto Mosso site in contributing to water resources, with respect to the very high contributions of permeable deposits of the lowland in developing multi-layered aquifers.

Moreover, the lowland has the ideal regional geomorphological conditions (low elevation and energy relief and gentle southeast dip of the whole Piedmont) to collect channelized superficial water and distribute to the rice agroecosystems of the Vercellese area.

Switching to the Local Morphodynamic approach, we can now analyse the mountain fieldtrip stops for recognizing local lithological and geomorphological features (small scale heterogeneity of geomechanical properties, landforms indicating active geomorphological processes) and assessing their relevant contribution for: 1) understanding recent and present day mechanisms of relief evolution, 2) interpreting

dynamic factors of natural instabilities (e.g. “external” causes of slope instability, increasing shear stress), and 3) contributing to process modelling and hazards assessment in this fragile high mountain environment, deeply affected by climate change.

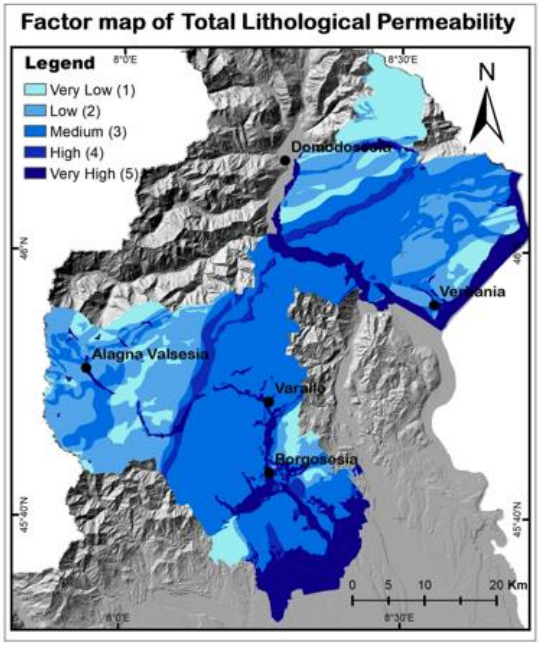

Figure 1.13. Factor map of lithological permeability for assessing hydrogeodiversity of the fieldtrip stops in the Sesia Val Grande UNESCO Global Geoapark (mod. by Perotti et al. 2019).

Within this perspective, the Monte Rosa Massif, the Indren basin and the Stolemberg and Cimalegna highplains offers both “natural” and “antropogenic” applications of the Local Morphodynamic Approach (Fig. 1.14). Here, recent and present-day “dynamic” controls to the alpine landscape are evidenced by six main geomorphological elements: 1) Glacial landforms are the most widespread, suggesting the main role of glaciers in shaping large part of the area (a, b in Fig. 1.14); 2) Periglacial and nival landforms indicate the presence of permafrost-related features (c); 3) Ice and snow related features are widespread around Indren and Garstelet glaciers and their forefields (a in Fig. 1.14); 4) fluvial and fluvioglacial landforms trace past and present proglacial environment evolution (a,b); 5)

Gravitational landforms evidence of most recent and active control on slope dynamics. 6) Man-made landforms are present and linked to ski and mountaineering activities (d).

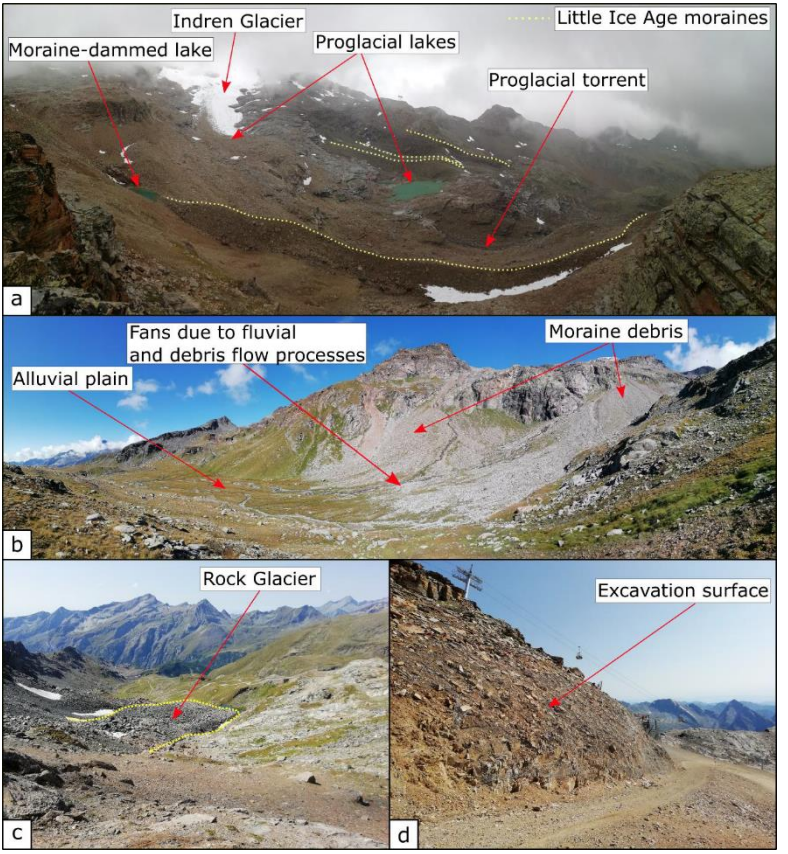

Figure 1.14. Natural and antropogenic landforms within the Indren-Cimalegna area show main present-day "dynamic" controls to the alpine landscape of the Monte Rosa Massif.

According to Gray (2013), geodiversity gives a character to the landscape, based on contents from geology and geomorphology, but also provides the foundation of biodiversity and other essential processes (biogeochemical, geomorphological, pedological), relevant for ecosystem functions. Geodiversity components within the fieldtrips stops demonstrate the abiotic and biotic components of nature are linked,

thus proving “geodiversity is an integral part of ecosystems and natural capital, and of the services and benefits they provide” (Gordon *et al*., 2013).

Mountains, piedmont fans, floodplains and urban areas visited by the fieldtrip additionally show that not only landforms and natural materials are affected by regional geodiversity, but also human activities and culture.

Finally, the knowledge of local morphodynamics, relief forms and landscape evolution allow proper modelling of geomorphological systems and scenarios. By increasing our understanding of natural instabilities, we can properly manage hazards and risks, and thus perform better land planning.

Chapter 2

HIGH-ELEVATION ENVIRONMENTS

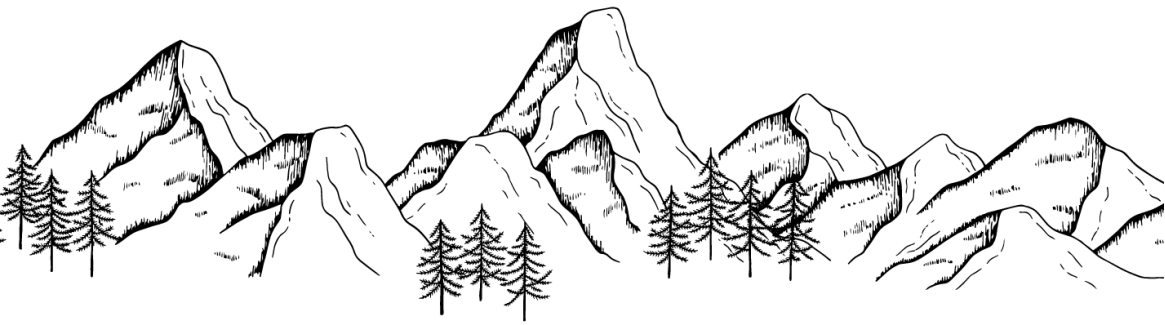

Chapter 2.1

The Long-Term Ecological Research (LTER) site Istituto scientifico Angelo Mosso

Freppaz, M., Pintaldi, E., Colombo, N., D'Amico, M.E.

The vast majority of studies in the ecological literature last less than three years, and only a small portion of studies capture unusual events. To detect changes in high-mountain ecosystems, long-term research is mandatory, as these areas are important bellwethers of climate change.

The first Long-Term Ecological Research (LTER) Network was established by the National Science Foundation, USA, in 1980. The Italian LTER Network (LTER-Italy) entered the European and International LTER Network in 2006, following a long lasting scientific and organizing process at national level, which involved many scientific institutions (e.g., National Research Council, Universities, Public Agencies).

In agreement with International LTER and LTER-Europe, the driving aims of LTER-Italy are, first of all, to foster collaboration and coordination among LTER ecosystems, researchers and institution; then, to improve comparability and exchange of LTER data and findings; finally, to deliver information to policymakers and the public. LTER-Italy has a strong interdisciplinary nature, being made-up of 25 terrestrial, marine, and freshwater ecosystems, with 79 research sites (Fig. 2.1).

Figure 2.1. Italian Long-Term Ecological Research (LTER-Italy) sites. The colours of the dots correspond to the main ecosystem typologies: Dark blue = marine, light blue = freshwater, green = transitional water, brown = terrestrial. The main features of the sites can be found on DEIMS-SDR, the LTER-Europe repository for research sites and datasets. (https://deims.org). http://doi.org/10.5281/zenodo.5116392

Among them, the LTER macrosite “Northwestern Italian Alps” includes the research site “Istituto Scientifico Angelo Mosso”, located in the alpine tundra close to the Monte Rosa Massif (Fig. 2.2; Table 2.1).

The core of the LTER site is the Istituto Scientifico Angelo Mosso (Col d’Olen, 2901 m a.s.l.), founded in 1907 by Angelo Mosso, professor of human physiology at the University of Turin. Over the years, the Institute has given support to scientists and scholars from all over the world, who could stay there even for long periods, while conducting their research activities in different research fields.

At present times, it includes permanent plots (Fig. 2.2), where different variables are constantly monitored, such as soil temperature (Fig. 2.3), snow cover duration, soil water content, and C and N forms. Moreover, the chemical characteristics of rainwater and snowfall are measured, as well as the water chemistry in ponds, focusing for example on how the soil properties control many hydrochemical properties such as the C and N content in water, following the critical zone paradigm.

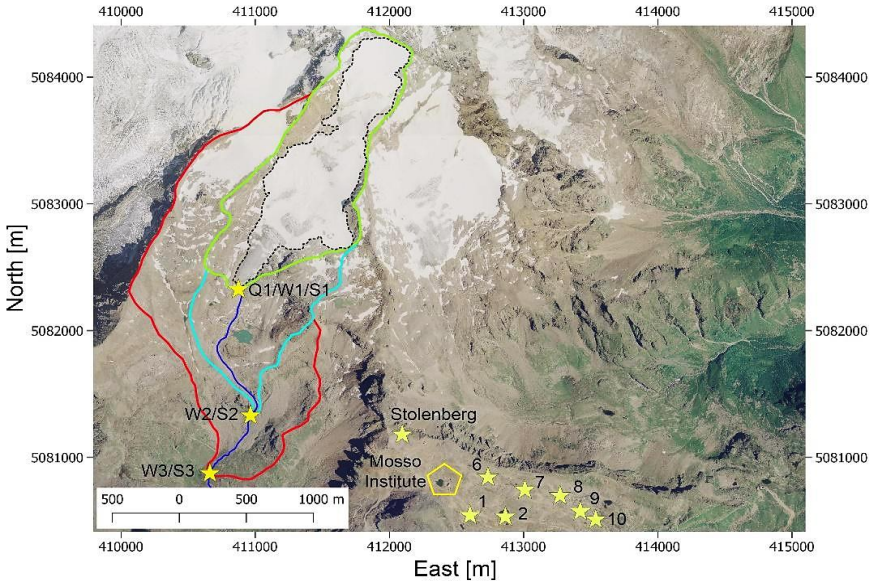

Figure 2.2. Aerial overview of the LTER study area (orthoimage year 2006, www.pcn.minambiente.it; coordinate system WGS84/UTM 32 N). Sites 1, 2, 6, 7, 8, 9, and 10: snowbed areas; Site Stolenberg: paleosol area; Sites Q1/W1/S1; W2/S2; W3/S3: proglacial and periglacial areas; Mosso Institute: Istituto Scientifico Angelo Mosso.

Table 2.1. LTER research site characteristics.

Coordinates	45° 52’ 30’’ N; 7° 52’ 19’’ E
Elevation	2605 - 3083 m a.s.l.
Aspect	S-SE
Slope	~ 0-20%
Climate	Mean annual air temperature = -2.4 °C, mean annual cumulative snowfall = 800 cm, mean annual rainfall = 370 mm
Vegetation	Alpine grassland, snowbed or pioneer scree vegetation dominated by: *Silene exscapa, Carex curvula, Salix herbacea, Festuca halleri, Poa alpina, Ranunculus glacialis, Leucanhtemopsis alpina, Cerastium uniflorum, Alchemilla pentaphyllea, Luzula alpinopilosa, Gnaphalium supinum, Agrostis rupestris, Euphrasia minima, Oxyria Digyna*
Geology	Gneiss and mica-schists (Monte Rosa nappe, pennidic basement), metabasites (Zermatt-Saas ophiolitic unit)
Morphology	Plateau and gentle slopes
Landforms	Frost shattered rocks, blockfield, blockstream, solifluction lobes, stone pavement, roche moutonnée, moraines
Classification (WRB)	Skeletic Umbrisols (Arenic, Turbic); Dystric Leptic Regosols; Dystric Skeletic Cambisols; Skeletic Umbrisols (Arenic); Eutric Skeletic Regosols; Dystric Skeletic Regosols

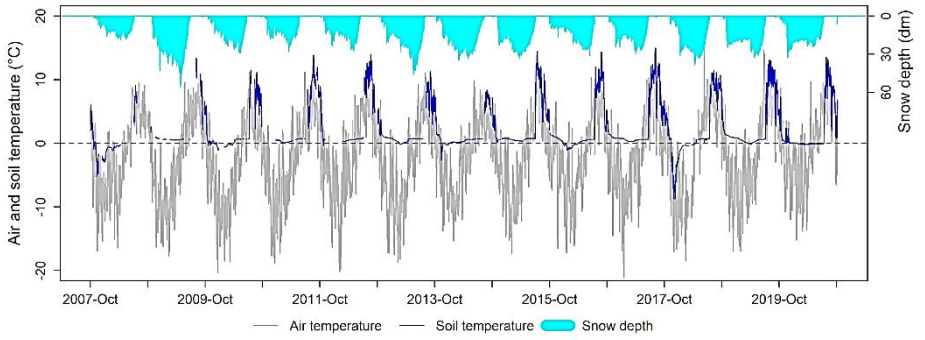

Figure 2.3. Snow depth, soil and air temperature measured at the automatic weather station (2901 m a.s.l., Comando Truppe Alpine - Servizio Meteomont, measured from 2005 to 2020). During winter, the presence of a consistent snow cover decouples air and soil temperatures.

Other permanent plots have been established in order to carry out investigations on paleoclimate through the information that could be derived from soils, integrating the information obtained in the same study area by ice core drilling. There is evidence that the paleoclimate influenced the cycling of soil carbon through shifting biomes and by altering soil physicochemical properties. The current distribution of soil carbon stocks thus contains footprints of the paleoclimate at timescales ranging from centuries to millennia (Ding *et al*., 2019; Delgado-Baquerizo *et al*., 2017).

Chapter 2.2

Paleosols study on the Stolenberg Plateau

Pintaldi, E., D'Amico, M.E., Colombo, N., Said-Pullicino, D., Giardino, M., Freppaz M.

Within the LTER site, this work was carried out in the periglacial environment of the Stolenberg Plateau, located at 3030 m a.s.l., at the boundary between Valle d'Aosta and Piemonte regions (Fig. 2.2), at the foot of the southern slope of Monte Rosa (4634 m a.s.l.) (NW Italian Alps). The study area is also a Site of Community Importance and a Special Protection Area (SCI/SPA IT1204220 "Ambienti glaciali del Gruppo del Monte Rosa") (Directive, 1992) belonging to the Natura 2000 network. On the plateau, the slope steepness is below 10%, with large flat portions. The area is characterized by active periglacial landforms. In particular, the plateau is covered by a thick layer of stones with variable size (from decimeter to meter), well organized in blockfields, blockstreams/sorted stripes, gelifluction lobes, tilted stones, and weakly developed sorted circles (Fig. 2.4).

Figure 2.4. Overviews of the Plateau.

In particular, blockstreams, partly rearranged into sorted stripes, are visible on sloping surfaces, while blockfields, partly rearranged into patterned ground and rich in standing stones, dominate the flatter surfaces.
The stony/blocky layer was 10-60 cm thick, and it was usually well graded with depth, with the coarsest stones on the surface and fine ones at the bottom, associated with the uppermost A horizons, as typically observed in blockfields and blockstreams (Wilson, 2013). Below the stone layer, the profiles showed thick (between 30 and 65 cm) and continuous, dark A and A@ horizons with subangular-blocky, platy or granular structure (Table 2.2, Fig. 2.5). These horizons contained few living or dead roots and very few, extremely weak, isolated, biogenic fine granular aggregates.

Table 2.2. Soil profile description. Soil horizons are reported following the scheme of sampling shown in Fig. 2.6.

Profile P1			
Sample number	**Horizon**	**Boundaries (cm)**	**Description**
6	**A**	15/20-20/25	5 cm thickness below the stone layer; black (10YR 2/1, moist), "salt and pepper appearance"; subangular blocky structure, very weakly developed, loose consistence; stone fragments 30%; few very fine roots; clear wavy lower boundary.
7	**A@**	32/40-40	Discontinuous "cryoturbations" (disrupted portions of very dark surface A materials), up to 8 cm thick; very dark greyish brown (10YR 3/2, moist); primary structure platy/laminar strongly developed, secondary coarse blocky subangular, strongly developed; crunchy consistence; stone fragments 10%, few very fine roots; abrupt limits.
8	**A2**	20-32/42	20 cm thick; dark brown (10YR 3/3, moist); coarse blocky subangular structure, well developed; crunchy consistence; stone fragments 30%; few very fine roots; abrupt wavy lower boundary.
9	**A1**	8/10-10	10 cm thick; very dark greyish brown (10YR 3/2, moist), "salt and pepper appearance"; very fine granular structure, weakly developed; stone fragments 70%; common very fine roots; clear lower boundary.
10	**BC**	40/60-60/80	20 cm thick; dark yellowish brown (10YR 4/4, moist); platy/laminar primary structure, strongly developed,

			partly derived from the weathered parent rock; secondary coarse blocky subangular, strongly developed; stone fragments 70%; roots absent; abrupt irregular upper and clear irregular lower boundaries.
11	**CB**	60/80-90	Discontinuous, up to 20 cm thick; greyish brown (10YR 5/2, moist); subangular blocky structure, weakly developed; stone fragments 70%, strongly weathered clasts; roots absent; abrupt irregular lower boundary, above the broken weathered rocky substrate.
12	**Bw**	25/40-40/50	20 cm thick; dark yellowish brown (10YR 3/4, moist); coarse subangular blocky structure, well developed; stone fragments 60%, strongly weathered; roots absent. Abrupt wavy lower boundary, discontinuous.
13	**A**	5/10-20/30	Up to 15 cm thick, below the surface stone layer; very dark greyish brown (10YR 3/2, moist), coarse blocky structure, weakly developed; soft consistence; fine stone fragments 30%, strongly weathered; few very fine roots; abrupt wavy lower boundary.
14	**BA**	20/25-40	20 cm thick; dark brown (10YR 3/3, moist); coarse columnar/prismatic structure, well developed, columns/prisms separated by open fissures, 0.1-1 cm wide; stone fragments 50%; few very fine roots; abrupt linear boundary.
15	**A**	5/10-20/25	15 cm thick; very dark greyish brown (10YR 3/2, moist); very fine granular structure, weakly developed; stone fragments 10%; few very fine roots; abrupt wavy lower boundary.
16	**Silt caps**		3 cm thick; abrupt upper limit; light yellowish brown (10YR 6/4, moist); fine platy structure, weakly developed; stone fragments 10%; roots absent.

The horizons were classified as Umbric according to WRB (IUSS Working Group WRB, 2015). Below the Umbric horizons, Cambic Bw ones were often developed although discontinuous, characterized by brown colour and well-developed subangular-blocky structure (Table 2.2, Fig. 2.5).

Stones were quite scarce, particularly in A horizons, evidencing frost sorting and cryoexpulsion. The stones were moderately weathered and could be easily broken with a spade, particularly in Bw horizons, while they were weakly weathered in the surface layer. Cryoturbation features, such as inclusions of surface A materials at

depth (A@ horizons in Fig. 2.5) and convolutions, were often observed within the profiles. Thick, dense silt caps were also observed on the upper faces of stone fragments.

Below the Bw, BC and CB horizons, the highly fractured bedrock was always observed. The soils were classified as Skeletic Umbrisol (Arenic, Turbic), according to IUSS Working Group WRB (2015). Considering the overall C-Stock of each sector within the profile (Fig. 2.5), the values spanned from 1.5 to approx. 3 kg m^{-2} (Pintaldi *et al*., 2021).

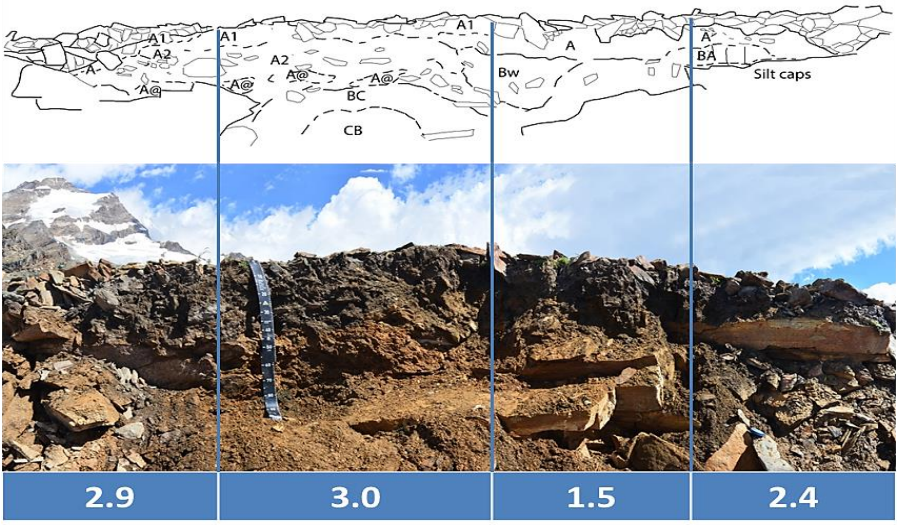

Figure 2.5. Estimated C-stock (kg m^{-2}) (adapted from Pintaldi et al., 2021).

The main physical and chemical features of soil samples are shown in Table 2.3. ^{14}C datings ranged between 6.5-6.3 (P1-7), 8.6-8.3 (P1-8) and 17.9-17.3 ka cal. BP (Fig. 2.6). The results indicated that these soils are paleosols, probably developed during the main warming phases (e.g., Holocene climatic optimum and Early Late Glacial) that have occurred since the end of the Last Glacial Maximum. The $\delta^{13}C$ signatures of soils hidden inside periglacial features (Table 2.4, Fig. 2.7), despite the sparse vegetation cover, corresponded very well with those of present-day vegetated soil, thus indicating that the soil organic carbon probably originated from alpine plants with the same isotopic signature of present-day vegetation in the snowbed areas.

Table 2.3. Main soil physical and chemical properties (adapted from Pintaldi et al., 2021).

Sample number	Horizon	Clay (%)	Silt (%)	Sand (%)	pH	TOC (%)	TN (%)
6	**A**	2.6	20.8	76.5	4.3	0.80	0.08
7	**A@**	2.3	23.2	74.5	5.6	2.05	0.11
8	**A2**	1.9	18.3	79.8	4.7	1.10	0.08
9	**A1**	2.5	12.1	85.4	4.4	1.13	0.11
10	**BC**	1.4	27.6	71.0	5.3	0.14	0.00
11	**CB**	1.0	26.3	72.7	5.9	0.00	0.00
12	**Bw**	0.9	25.7	73.4	5.2	0.26	0.03
13	**A**	4.3	24.1	71.6	4.8	1.09	0.08
14	**BA**	2.8	29.3	67.9	4.9	1.10	0.07
15	**A**	3.9	14.0	82.1	4.5	0.71	0.09

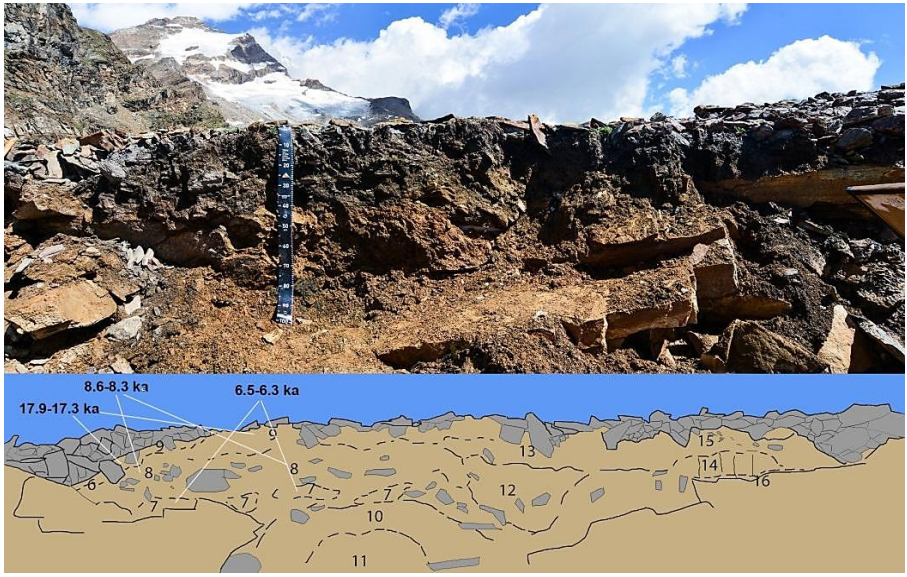

Figure 2.6. Soil profile P1 with the corresponding scheme (below) reporting sampling points (number) and the age of soil samples 7, 8, and 9 (ka cal. BP).

Table 2.4 and Figure 2.7. $\delta^{13}C$ comparison between (A) soil under present-day snowbed communities (Vegetation, snowbed sites 1, 2, and 6) and (B) soils under periglacial features (Blockstream/Blockfield, profile P1, samples 7, 8, and 9) at the Plateau (adapted from Pintaldi et al., submitted).

Site	Elevation (m a.s.l.)	Cover type	$\delta^{13}C$ (‰)
1	2840	Vegetation	-23.3
2	2800	Vegetation	-25.1
6	2854	Vegetation	-23.4
P1-7	3030	Blockstream/Blockfield	-24.2
P1-8	3030	Blockstream/Blockfield	-23.9
P1-9	3030	Blockstream/Blockfield	-24.5

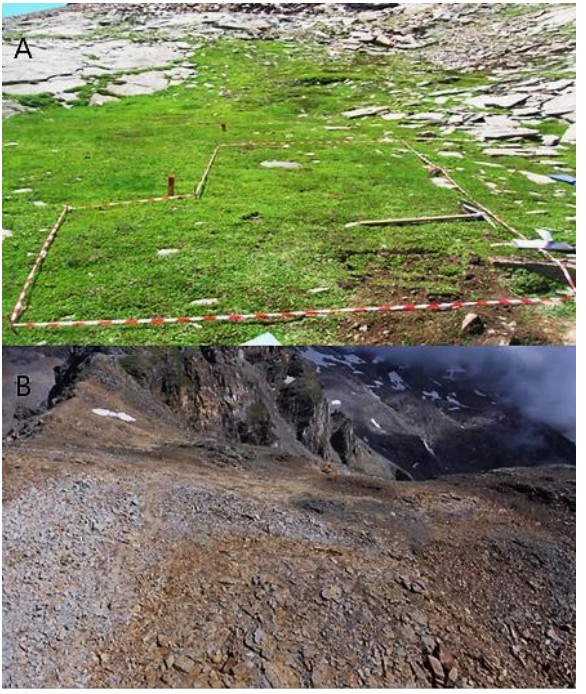

Chapter 2.3

Soils and plants in snowbed areas

Pintaldi, E., D'Amico, M.E., Colombo, N., Lonati, M., Lombardi, G., Ravetto Enri, S., Freppaz, M.

The work was performed on 7 permanent snowbed plots located between 2686 (site 10) and 2850 m a.s.l. (site 6) (Fig. 2.2), characterized by Dystric Leptic Regosols, Skeletic Umbrisols (Arenic) and Dystric Skeletic Cambisols (Table 2.5, Fig. 2.8), according to WRB classification (2015). The vegetation of the sites was included in the 'Siliceous alpine and boreal grasslands' (habitat 6150, according to the EU Habitat Directive). Small differences in plant species composition were observed among the sites, but all of them can be reconducted to the association *Salicetum herbaceae* (Fig. 2.9). The species found in the plots can be described, based on their vegetative optimum, as either snowbed specialists, debris or grassland species, according to Aeschimann *et al*. (2004). *Salix herbacea* L., which was largely the most abundant plant in all sites, is classified as a snowbed specialist.

The uptake of elements depends on both plant phenology and the availability of soil nutrients; however, it is not easy to distinguish between the factors (e.g., pedoclimatic conditions) affecting the availability of soil nutrients and those influencing their acquisition by plants. Nitrogen (N) supply often shows a pronounced seasonality, because of the rate of mineralization and seasonal variations of soil temperature and/or moisture levels, while its uptake is associated with different phenological phases of plants (Tian *et al.*, 2017). As the early phenological stages (i.e., foliation and flowering) are the most demanding for the majority of alpine plants, the highest nutrient uptake occurs during these phases. The uptake of the mobile elements is proportional to the plant transpiration (Nord and Lynch, 2009), which affects the availability of N and the carbon (C) pools in soil. However, in turn, both plant phenology and floristic composition are highly sensitive to micro variations in soil characteristics (Sterling *et al.*, 1984; Sakai and Ohsawa, 1993).

Table 2.5. Main soil physical and chemical properties (adapted from Pintaldi et al.*, 2021).*

Site	Soil (WRB)	Elev. (m a.s.l.)	Horizon	Depth (cm)	pH
1	Dystric Leptic Regosol	2840	A	0-7	4.6
			AC	7-20	5.4
			C	20-40	7.2
7	Dystric Skeletic Cambisol	2813	A	0-5	4.2
			AB	5-10	4.8
			BW	10-33+	5.4
10	Skeletic Umbrisol (Arenic)	2686	A1/OH	3-5	4.6
			A2	5-28/35	4.8
			BC	28/35-60+	5.1

Site	TOC (%)	TN (%)	C/N	Clay (%)	Silt (%)	Sand (%)
1	1.84	0.14	13	1	13	86
	0.65	0.05	14	1	17	82
	1.49	0.08	18	1	17	82
7	5.4	0.36	15	2	18	80
	0.8	0.07	12	1	14	85
	0.7	0.06	11	0	32	68
10	18.4	1.23	15	2	16	82
	1.4	0.12	12	6	14	80
	1.0	0.07	15	1	18	81

Figure 2.8. Soil profiles from site 1 (A), 7 (B), and 10 (C).

Figure 2.9. Typical example of a snowbed environment: (A) site 7 (2813 m a.s.l.); (B) site 10 (2686 m a.s.l.); the location of the sites is reported in Fig. 2.2.

During the four-years monitoring, the phenology of *S. herbacea* was significantly different only in 2017 and 2018, when plant growth was anticipated and delayed respectively (Fig. 2.10). These differences may be related to the different climatic and pedoclimatic conditions during 2017 and 2018, i.e., greater gravimetric water content

and the earlier melt-out day in 2017, lower gravimetric water content and delayed melt-out day in 2018. Thus, based on our observations, the soil water content and melt-out day can be considered the key factors influencing phenology in alpine ecosystems, as also reported by Ernakovich *et al*. (2014). Furthermore, these abiotic variables are significantly related to topsoil C and N forms, resulting in the main drivers of C and N transformations in these high-elevation microhabitats (e.g., Magnani *et al*., 2017).

Considering the vegetation variables, *S. herbacea* phenology played a fundamental role, affecting ammonium and DOC concentrations in soil. Ammonium plant uptake increased with advancing phenophases until senescence, while DOC content was influenced by the release of root exudates into the soils, as reported aLso by Hütsch *et al*. (2002). Since snowbed habitats are considered extremely vulnerable to climate warming, the identified abiotic and biotic factors could be proposed as indicators of the response of these high-elevation ecosystems against changes in climatic conditions, which, in current years, are strongly affecting the components of the cryosphere, such as the extension of glaciers.

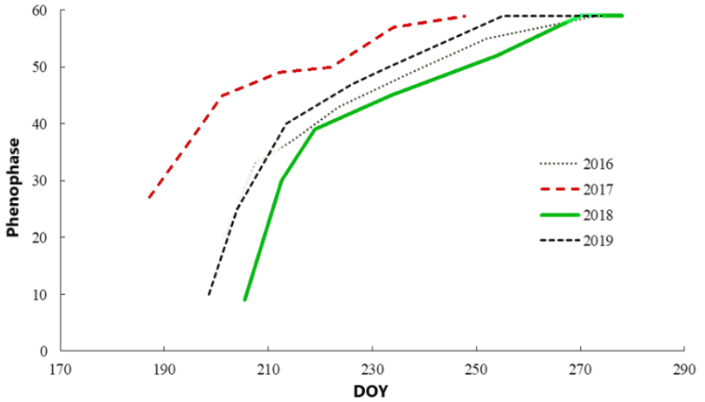

Figure 2.10. Phenology of the species Salix herbacea throughout the four-year monitoring period. Phenophases are indicated in the y axis as a progressive number following the adaptation of the BBCH scale (Hack et al*., 1992), while on the x axis Day Of Year is reported as a variable. This scale is characterized by a series of progressive integer numbers ranging from 0 to 59, where the tens represent the major phenophases in chronological order (Shoots emergence, Leaves development, Flower buds, Flowering, Fruiting, Seed dispersal) and the units represent the advancement of such phenophases. For every year, the lines represent the median phenophase of the 7 sites in each survey date (adapted from Pintaldi* et al*., submitted).*

Chapter 2.4

Glacier meltwater characteristics along an elevational gradient with differing soil covers

Colombo, N., Bocchiola, D., Martin, M., Confortola, G., Salerno, F., Godone, D., D'Amico, M.E., Freppaz, M.

Nitrate concentrations in surface waters are generally inversely related to the areal extensions of soils, indicating the fundamental role that the soil biological community plays in the retention and loss of nitrogen (N) and therefore the strict connection between soil and waters in mountain remote ecosystems (Balestrini *et al.*, 2013) (Fig. 2.11).

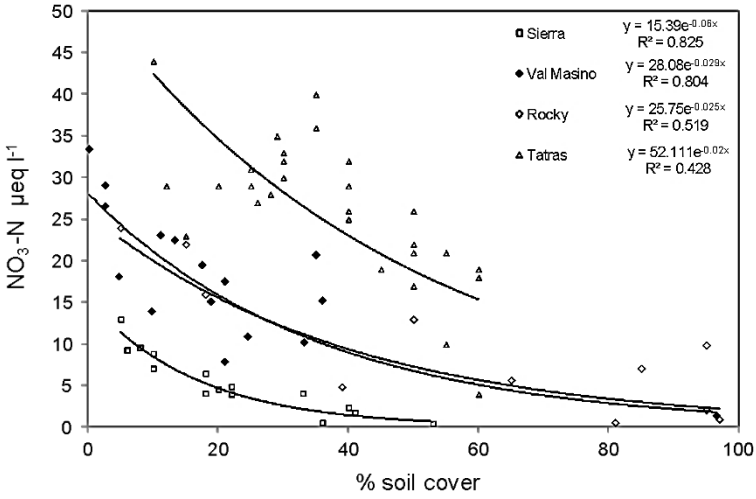

Figure 2.11. Relationship between the mean nitrate concentration in catchment outflow and soil cover (%) for high elevation watersheds of the Val Masino, the Sierra Nevada, the Rocky Mountains, and the Tatra Mountains. Adapted from Balestrini et al. *(2013).*

Streams and lakes fed by mountain glaciers are known to be enriched in nitrate compared to snow/groundwater-fed surface waters. Non-mutually exclusive factors could explain the N enrichment of glacier meltwaters, such as enhanced nitrification in subglacial environments and reduced contact with watershed soils (Slemmons *et al*., 2017, and reference therein). Moreover, several authors reported that dissolved organic carbon (DOC) increases in water with increasing distance from the glacier fronts (e.g., Li *et al*., 2018) and decreasing glaciated areas (e.g., Hood and Scott, 2008), due to the loss of terrestrial DOC from unglaciated terrains, implying a strong relationship between soil C pool and DOC export to surface water. Regarding dissolved organic nitrogen (DON), previous studies reported similar yields among catchments with different glacier covers, suggesting that glacial runoff is an important contributor to DON (Hood and Scott, 2008).

This study was carried out at the Indren Glacier foreland, located in the NW Italian Alps (Valle d'Aosta Region, Fig. 2.2) within the LTER site Istituto Scientifico Angelo Mosso. A proglacial pond is located close to the glacier front, and a glacial stream originates from the outflow thereby, crossing surfaces with soils at different degrees of development. Meltwater samples were collected in the period 2012–2015 and modelled glacier discharge was used to elucidate the role of glacial hydrology on N and C export. Water samples were also collected in the period 2012–2014 at two lower-elevation sites (Fig. 2.2, Table 2.6) along the glacial stream in order to investigate the downstream variability of N forms and DOC in glacial meltwater (further details in Colombo *et al*., 2019), evidencing a potential contribution from the surrounding soils.

Since the lowermost average modelled discharge at Q1 measuring site (Fig. 2.2, Table 2.6) during the melting period (April–October) was 0.05 $m^3\ s^{-1}$ (year 2014), this threshold was chosen to discriminate between samples collected during low-flow (< 0.05 $m^3\ s^{-1}$) and high-flow (≥ 0.05 $m^3\ s^{-1}$) periods. At W1 sampling site (Fig. 2.2), electrical conductivity (EC) was significantly higher during low-flow periods than during high-flow periods (Fig. 2.12a, Table 2.7). A similar behaviour was found for the dominant major anion (SO_4^{2-}-S, Fig. 2.12b, Table 2.7) and cation (Ca^{2+}, Fig. 2.12c, Table 2.7). Similar to EC and major ions, nitrate was significantly higher during low-flow periods than during high-flow periods (Fig. 2.12d, Table 2.7). In contrast, mean DON and DOC concentrations did not show statistically significant differences between low-flow and high-flow periods (Fig. 2.12e,f; Table 2.7). Estimated area-weighted

yields (analyte flux divided by the contributing area) for NO_3^--N, DON, and DOC were 220, 210, and 1,279 kg km^{-2} $year^{-1}$, respectively.

Table 2.6. Morphometric characteristics of the Indren Glacier, and morphometric and land cover characteristics of the sampling sites. Locations and details of sampling sites are reported in Fig. 2.2.

Parameter	Indren Glacier	Parameter	Q1/W1/S1 sampling site	W2/S2 sampling site	W3/S3 sampling site
Elevation range (m a.s.l.)	3083–4081	Elevation (m a.s.l.)	3083	2695	2605
Area, year 2006 (km^2)	0.92	Basin area (km^2)	1.43	2.12	3.59
Length/width (m)	2310/740	Distance from the glacier (km)	-	1	1.4
		Basin land cover	Glacier: 64.1% Bedrock: 32% Coarse sediment: 3.7% Soil: 0% Water surface: 0.2%	Glacier: 43.1% Bedrock: 38.9% Coarse sediment: 16.9% Soil: 0.4% Water surface: 0.7%	Glacier: 31% Bedrock: 29.2% Coarse sediment: 33.7% Soil: 5.6% Water surface: 0.4%

Soils displayed different properties according to the different elevations. Organo-mineral horizons enriched in organic carbon (OC) were observed in soils located at S2 and S3 sites, deglaciated since the Little Ice Age (LIA), while the few-decade-old till (S1) was OC-depleted (Table 2.8). Total nitrogen (TN) was significantly correlated with OC (r = 0.99) and had an increasing trend with decreasing elevation, showing the highest content in surface A horizons at S2 and S3. S2 and S3 also showed the presence of vegetation, dominated by *Carex curvula* All. and other species belonging to the *Caricetum curvulae* association. Along the elevation gradient, no significant variations were found in water nitrate, DON, and DOC concentrations (Fig. 2.13).

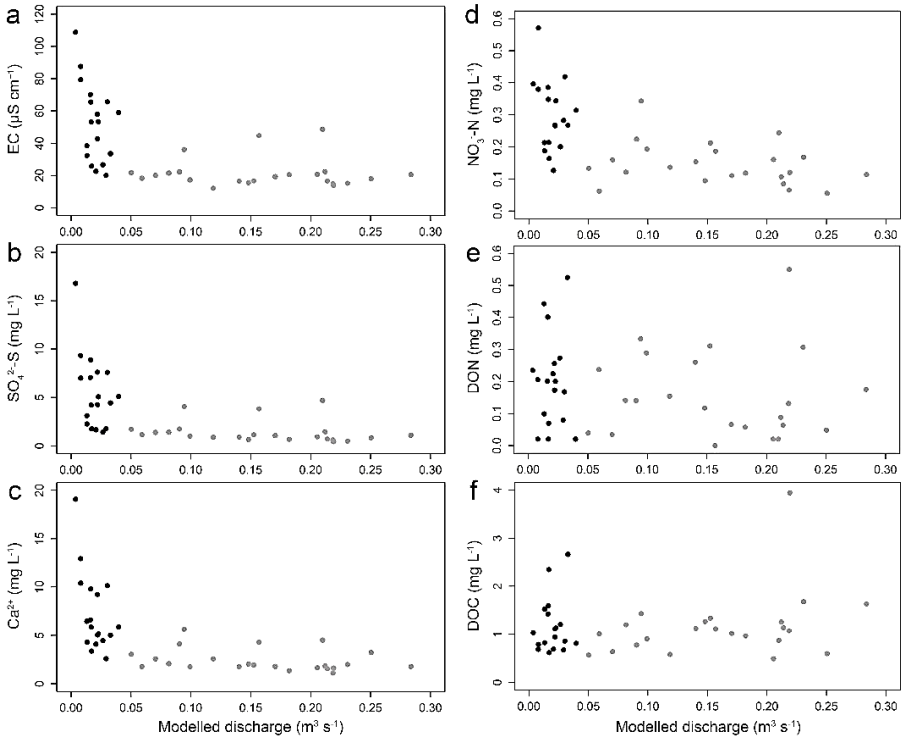

*Figure 2.12. Modelled glacier discharge vs. (a) EC, and (b) SO_4^{2-}-S, (c) Ca^{2+}, (d) NO_3^--N, (e) DON, and (f) DOC concentrations (*n *= 41). Black and grey dots indicate the sampling dates during low- and high-flow periods, respectively. Adapted from Colombo* et al*. (2019).*

Table 2.7. EC, and SO_4^{2-}-S, Ca^{2+}, NO_3^--N, DON, and DOC concentrations during low- and high-flow periods. Mean ± standard deviations are reported.

Parameter	Low-flow period	High-flow period
EC (µS cm^{-1}, 20 °C)	52.3 ± 24.6	21.3 ± 9.3
SO_4^{2-}-S (mg L^{-1})	5.50 ± 3.82	1.41 ± 1.16
Ca^{2+} (mg L^{-1})	7.23 ± 4.08	2.42 ± 1.17
NO_3^--N (mg L^{-1})	0.30 ± 0.11	0.15 ± 0.07
DON (mg L^{-1})	0.20 ± 0.15	0.15 ± 0.14
DOC (mg L^{-1})	1.16 ± 0.57	1.15 ± 0.69

Table 2.8. Soil characteristics across the elevation gradient. Locations and details of sampling sites are reported in Fig. 2.2 and Table 2.6.

Sampling site	Soil (WRB)	Horizon	Depth (cm)	OC (%)	TN (%)
S1	Eutric Skeletic Regosol	C	0–10	0.14	0.01
S2	Dystric Skeletic Regosol	A1	0–2	3.86	0.27
		A2	2–10	0.96	0.07
		AC	10–20+	0.35	0.02
S3	Dystric Skeletic Regosol	A	0–2	5.52	0.37
		CA	2–7	0.87	0.05
		2CB	7–20+	0.22	0.02

Nitrate-N mean concentration (0.21 ± 0.12 mg L^{-1}) was consistent with concentrations measured in other glaciated sites and high-elevation surface waters (with varying glacial cover) in Europe, although it was higher than those measured in other glaciated environments across the globe, such as in Nepal Himalaya, Svalbard, Northern Patagonia, and Greenland Ice Sheet (Colombo *et a*l., 2019, and reference therein). Only NO_3^-, among the N forms and DOC, was positively correlated to the major ions and negatively correlated to glacier discharge, showing higher concentration in meltwater during low-flow periods. This occurrence suggests that NO_3^- derived mainly from subglacial environment. Microbial activity could contribute to NO_3^- export from the Indren Glacier catchment, thanks to enhanced nitrification from microbial populations in subglacial environment (Wadham *et al.*, 2016).

Dissolved organic carbon average value (1.16 ± 0.63 mg L^{-1}) in glacial meltwater was approximately three and two times higher than the average global values for mountain glaciers reported by Hood (2015) (0.37 mg L^{-1}) and Li *et al*. (2018) (0.54 mg L^{-1}), respectively. This resulted in a high yield (1279 kg km^{-2} $year^{-1}$) confirming the high DOC export estimates in the European Alps recently proposed by Li *et al*. (2018), and far higher than previous average regional estimate for the European Alps (170 kg km^{-2} $year^{-1}$) (Singer *et al*., 2012). This high DOC export could derive from atmospheric deposition, considering the location of the Indren Glacier, close to the Po Valley, a European atmospheric pollution hotspot from where air masses can be transported to the NW Alps. DOC deposition in the Indren Glacier area was 15.5 kg C ha^{-1} $year^{-1}$,

with rain contributing 43% (6.6 kg C ha^{-1} $year^{-1}$) of the total DOC deposition, which highlighted its relevance in C dynamics in the investigated area.

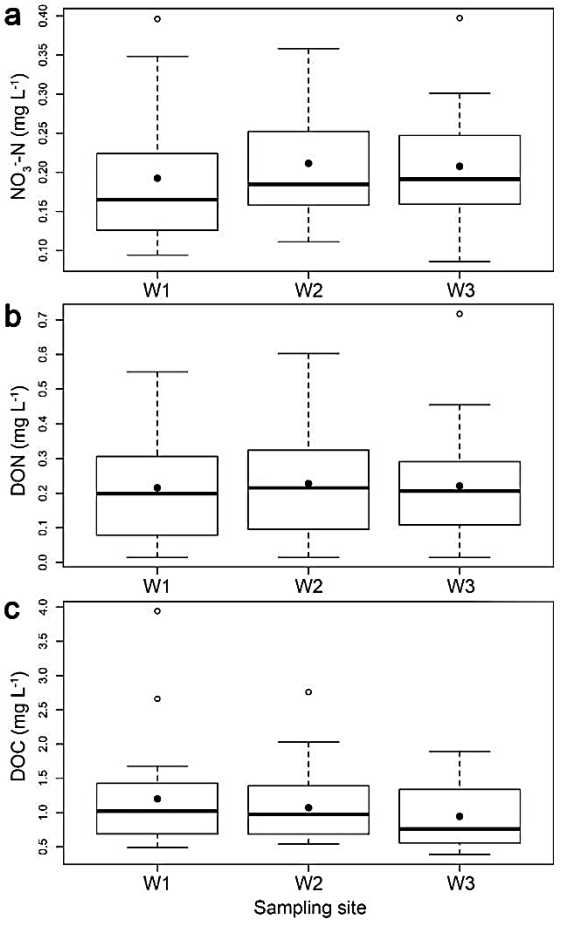

*Figure 2.13. (a) NO_3^--N, (b) DON, and (c) DOC concentrations in the glacial stream along the elevation gradient (*n *= 26). Black dots indicate the mean. Locations and details of sampling sites are reported in Fig. 2.2 and Table 2.6. Adapted from Colombo* et al. *(2019).*

In contrast to major ions, DOC and DON concentrations were similar during low- and high-flow periods, showing no dependence upon glacier discharge. This occurrence points towards a different origin of DOC and DON, which could derive from different pools of DOC and DON within glaciers. DOC could be leached during the ablation period from wet snow and/or the glacier surface in the supraglacial ecosystems (e.g., cryoconites). DOC could originate also at the glacier base; indeed, several authors reported the presence of OC in subglacial environments (e.g., Stibal *et al*., 2012). Sources of terrestrially derived DOC might exist beneath the glacier, such as glacially overridden soil and vegetation (Vione *et al*., 2021). The acquisition of DON could also occur both in surface and basal ecosystems, with the presence of a significant N-rich component to dissolved organic matter exported from glacier ecosystems in runoff (e.g., Bhatia *et al*., 2013).

Along the elevation gradient, the percentage of soil cover increased downstream, reaching a value close to 6% at S3 site, but without any relevant effect on NO_3^- concentration. This could be attributed to the slope steepness and to the fact that the area was recently deglaciated (LIA) with soils showing little development (soil age ca. 170 years), covering a small % of the basin area. OC and TN concentrations in soil increased at lower elevation, without any corresponding increase in DOC and DON in stream water. In our site, the higher (although not significant) DOC concentrations at the glacier front and the similar DON concentrations along the elevation gradient point towards the limited effect of soil on water characteristics due to its reduced surface area. At the same time, this underlines the importance of the glacier melting in determining N and C dynamics in surface water in this high-elevated, remote environment.

L'Adieu des glaciers

IL MON-TE CERVINO

Ricerca fotografica e scientifica

Forte di Bard
Valle d'Aosta
9 luglio
17 ottobre
2021

fortedibard.it
T. +39 0125.833811

Chapter 3

REMNANTS OF FOREST ECOSYSTEMS

Chapter 3.1

The soils of the Pleistocene terraces of the Stura di Lanzo glacio-fluvial fan

D'Amico, M.E., Raimondo, E., Negri, S., Stanchi, S., Bonifacio, E.

The study area (45°13'31.03'' N, 7°31'29.83'' E) is the South-Western side of the Stura di Lanzo (SL) alluvial fan, located in Turin Metropolitan area, Piedmont. This terraced glaciofluvial and alluvial fan stretches over 300 km^2, at an elevation between 210 and 550 m a.s.l. The glaciofluvial and alluvial materials are derived from the Stura di Lanzo and the Ceronda rivers, dominated by serpentinites and peridotites inherited from the Lanzo Ultramafic Complex, with smaller quantities of sialic components coming from the Stura di Lanzo alpine basin. A few loess layers lie on top of the glacio-fluvial and alluvial materials, deposited in different periods during the Pleistocene starting around 730 ka, although precise datings of the loess deposits is still missing.

This area is now mostly covered by crops. The native hardwood forests with predominance of oak (*Quercus robur* L.) and European hornbeam (*Carpinus betulus* L.) are preserved only in small and marginal portions of the area or in protected sites, such as La Mandria Regional Park.

The study area has a temperate climate, with a mean annual temperature (1971-2000) of 12°C and mean annual precipitation of 980 mm, with equinoctial distribution and winter minima. The oldest soils in the Lanzo terraced glacio-fluvial fan are strongly developed, characterized by the widespread presence of fragipan layers and Bt horizons, and by limited drainage. They are usually classified as Fragiudalf (from the 1:250.000 Regional Soil Map available on http://www.geoportale.piemonte.it/cms/, according to Soil Survey Staff, 2014). A typical soil of this area was selected in Fiano (Fig. 3.1, Table 3.1).

The observed soil profile (Table 3.2; Fig. 3.2) is a typical and complete profile developed on Pleistocene glaciofluvial terraces (Raimondo *et al*., 2019; Negri *et al*., 2021; Stanchi *et al*., 2021), characterized by a shallow surface layer (A and Bw

horizons) developed in recent loess, loose and friable and with a high biological activity in the organo-mineral horizon.

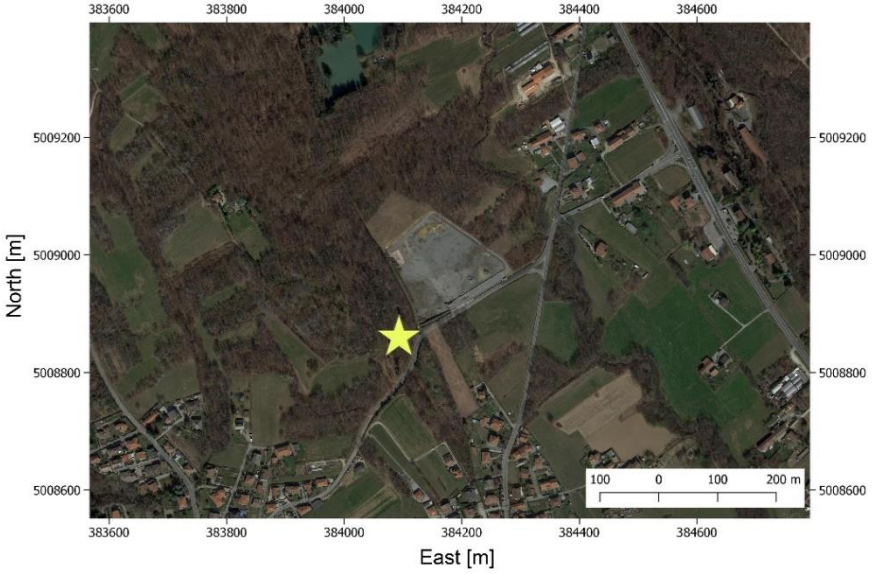

Figure 3.1. Aerial overview of the study area (Google Satellite image).

Table 3.1. Site characteristics of the Fiano profile.

Coordinates	45°12'53.38" N; 7°29'48.26" E
Elevation	430 m a.s.l.
Aspect	200
Slope	~ 1%
Climate	MAAT = 12°C; MAP: 980 mm
Vegetation	Hay meadows/oak-hornbeam forests
Geology	Alluvial deposits, mainly composed of ophiolitic rocks and minor sialic components
Morphology	Plateau, terraced alluvial fan
Landforms	Pleistocene terraced alluvial fan
Classification (WRB)	Fragic Luvisol (Siltic, Epidystric)

Table 3.2. Description of the representative soil profile on the Lanzo Pleistocene glaciofluvial terraces, located in Fiano (TO).

Profile description		
Horizon	**Boundaries (cm)**	**Description**
A	0-3	Moist colour dark yellowish brown (10YR 4/4); granular structure, with 2-7 mm aggregates (mostly by earthworms); no stone fragments; abundant fine to very coarse roots; clear wavy lower boundary.
Bw	3-50/65	Moist colour yellowish brown colour (10YR 5/8); friable, blocky subangular aggregates, weakly developed, and biogenic granular ones; no stone fragments; common fine to very coarse roots; abrupt wavy lower boundary.
2E/B(x)	50/65-90	Moist colour yellowish (10YR 6/3, 60%) and bright brown colour (7.5YR 4/6), with vertical streaks and glossae; friable when humid, quite hard when dry; moderately developed blocky subangular structure, secondarily medium, platy; scarce roots; nodular layer at the upper boundary; clear wavy lower boundary.
2Bcx	90-100	Moist colour bright brown (7.5YR 5/8), with light brown (7.5YR 6/3) and brown (10YR 4/3) mottles; no coarse fragments; subangular blocky structure; abundant Fe-Mn nodules; abrupt wavy lower boundary.
3Btx1	100-115/120	Moist colour yellowish brown (10YR 4/6), with grayish (10YR 6/2) and strong brown (7.5YR 4/6) mottles; no coarse fragments; moderately developed blocky subangular structure, secondarily fine platy, weakly developed; abundant streaks and nodules; scarce clay coatings in pores; clear wavy lower boundary.
3Btx2	115/120-165	Moist colour yellowish brown (10YR 4/6), with greyish (10YR 5/3), brown (7.5YR 4/4) mottles and black coatings (7.5Yr 2.5/2); no coarse fragments; moderately developed blocky subangular structure, secondarily fine platy, weakly developed; abundant streaks and scarce Fe-Mn nodules; common clay coatings in pores; abrupt wavy lower boundary.
4Btx3	165-215/225	Separated from 3Btx because of a much harder consistence and different spatial organization of streaks and mottles; much more abundant clay coatings; similar

		colours and structural aggregation. Abrupt wavy lower boundary.
5Btx4	215/225-255	Moist colour yellowish brown (10YR 5/8), with dark brownish (10YR 3/6) and reddish (5YR 4/6) and grey mottles (10YR 5/2); strong, coarse platy structural aggregation; common clay coatings; clear wavy lower boundary.
5Bvm1	255-265	Black (90%), with small bright yellowish-brown portions (10YR 6/8), grey (7.5YR 6/1) and a few red mottles (2.5YR 3/6); no coarse fragments; very strongly cemented; coarse platy structure; abrupt linear lower boundary.
6Bvm2	265-298	Black (60%), with small bright yellowish-brown portions (10YR 6/4), more abundant than above, and grey (7.5YR 6/1); no coarse fragments; moderately cemented; coarse platy structure; abrupt linear lower boundary.
7Bvm3	298-310	Black (80%), with small bright yellowish-brown portions (10YR 6/4), and grey (7.5YR 6/1); 10% highly weathered coarse fragments (mainly serpentinite); very strongly cemented; coarse platy structure; abrupt linear lower boundary.
7Bv	310-340	Black (50%), with bright yellowish-brown portions (10YR 6/4), and grey (7.5YR 6/1); 10% highly weathered coarse fragments (mainly serpentinite); weakly or not cemented; coarse platy structure; abrupt linear lower boundary.
8Btcg	340-350+	Moist colour bright brown (7.5YR 5/8), with reddish (5YR 4/6) and grey (10YR 5/2) portions; scarce (10%) coarse fragments, with different degrees of weathering; strong platy structure; abundant clay coatings and Fe-Mn nodules.

Below 50/65 cm, the consistence abruptly changes, and the first, weakly developed, fragipan horizon (2E/B(x)) limits water percolation and root development. The abrupt but wavy upper boundary of this horizon is marked by a thin sub-horizon enriched in Fe-Mn soft nodules and mottles. A strong reduction characterizes this horizon, with abundant grey glossae and mottles (2E), associated with smaller parts similar to the 2Bcx found immediately below (B(x)).

Another discontinuity is observed at ca. 100 cm, below which the consistence becomes harder, the structure (blocky subangular and platy) becomes stronger and the fragipan properties more expressed (3Btx).

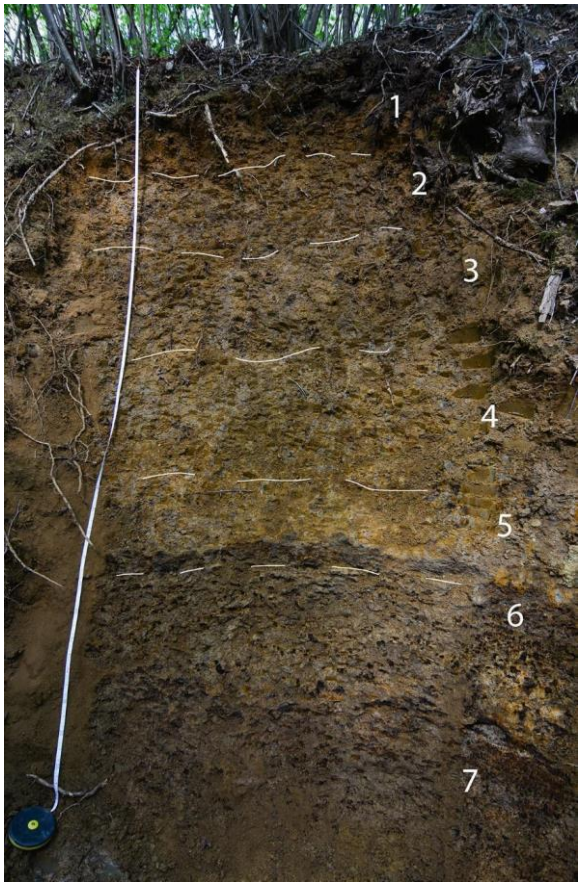

Figure 3.2. Representative soil profile on the Lanzo Pleistocene glaciofluvial terraces, located in Fiano (TO). Numbers indicate the various pedogenic cycles.

The first few clay coatings also appear in the pores and on a few aggregate faces. Other pedogenic discontinuities can be recognized below, each one characterized by a (non-linear) increasing development with depth. This occurs in the form of increasing redness of the soil matrix (rubification), increasing expression and definition of redoximorphic mottles (reddish, brown, grey or black), development of clay coatings in pore walls, expression of structural aggregation, particularly of the laminar component, and increasing fragic and plinthic properties (Fig. 3.3). All fragipan horizons had a firm to very firm consistence, increasing with depth. They

were hard when dry and brittle when moist, and underwent slaking upon water saturation.

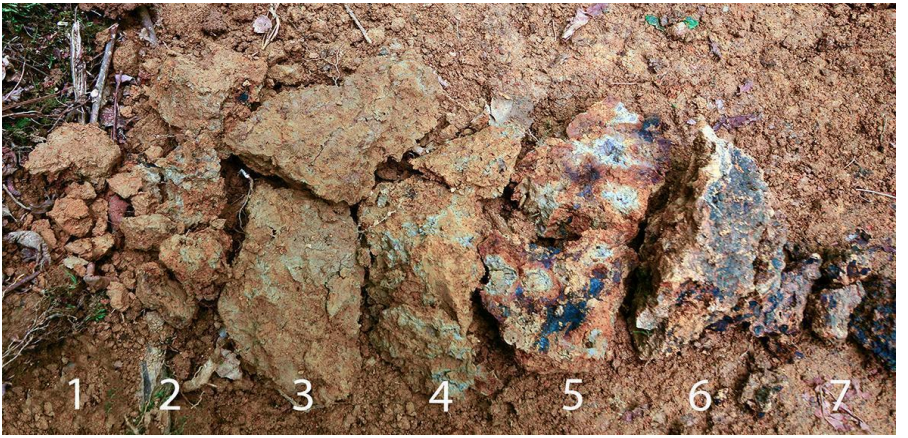

Figure 3.3. Structural aggregates from the different layers of the Fiano soil profile, showing the increasing degree of pedogenic development with depth. Numbers indicate the various pedogenic cycles.

Table 3.3. Main chemical data of the main horizons; strong cementation of Fe oxides might influence texture and FeD contents.

Horizon	Sand (g kg^{-1})	Silt (g kg^{-1})	Clay (g kg^{-1})	pH (H_2O)	OC (g kg^{-1})	CEC (cmol kg^{-1})	FeD (g kg^{-1})
Bw	28.1	47.8	24.1	5.2	6.8	10.7	44.7
2E/B(x)	27.0	39.5	33.5	5.8	2.5	15.6	42.8
3Btx1	18.4	48.8	32.8	5.8	1.8	14.0	40.4
4Btx3	24.4	42.6	33.0	6.2	1.5	14.2	20.0
5Btx4	31.6	42.2	26.6	6.2	1.3	23.1	35.6
6Bvm2				6.0	0.4	20.4	

From the chemical point of view (Table 3.3), we can observe that most of the soil horizons have little organic carbon contents, as it normally happens in fragipan (FAO, 2006). The pH values are quite low and increase with depth. Silt is the main fraction, as expected in loess-derived soils, but clay contents are particularly high, likely thanks to a high weathering degree. FeD is probably underestimated in deep horizons, as oxides are mostly concentrated in strongly cemented nodules. The CEC is low, as

expected in soil materials poor in organic C, when the clay fraction is rich in kaolinite (Raimondo *et al*., 2019).

To quantify variations in pedogenic development in the different layers recognized in the field, a modified version of the Profile Development Index (PDI), following the approach suggested by Harden (1982) and Harden and Taylor (1983), was applied to evaluate existing differences between horizons in a semi-quantitative way (Negri *et al*., 2021). In particular, 7 specific parameters obtained in the field were selected for the studied soil: rubification of the soil matrix, clay coatings development, structural aggregation shape and aggregate strength, mottles, nodules, expression of fragipan and presence and expression of plinthic/petroplinthic horizons.

The horizons were grouped according to the unit, or cycle, of belonging. The PDI values of horizons that belonged to the same cycle were summed, and the result was then normalized by the thickness of the layer, to take truncation into consideration. For those soil horizons that developed on loess, a poorly weathered loess layer nearby was considered as the starting point in the PDI determination. Its colour and structure were 10YR 5/4 and weakly developed, subangular blocky, respectively. For the deep horizons that formed from the alluvial sediments (6Bvm2), the fresh alluvium from nearby rivers was considered as a starting point; its colour was 5Y 5/4 and its structure was absent.

The results show that the pedogenic development degree increases with depth, according to an asymptotic trend (Fig. 3.4) that confirms the increasing age of the soil layers recognized in the field.

Each discontinuity separated layers with increasing fragic properties downward the profile, until the petroplinthic layers below 255 cm. Also, the development degree of platy structural aggregation increased with depth: both properties are associated to important reductions in permeability, which in turn are the main factor promoting the formation of Fe-Mn nodules just above the discontinuity. The development degree of these nodules also increases with depth (except for discontinuity 3-4). In other profiles in the area, these nodular layers become real plinthites, which however show an extremely large lateral variability within the same-age terraces.

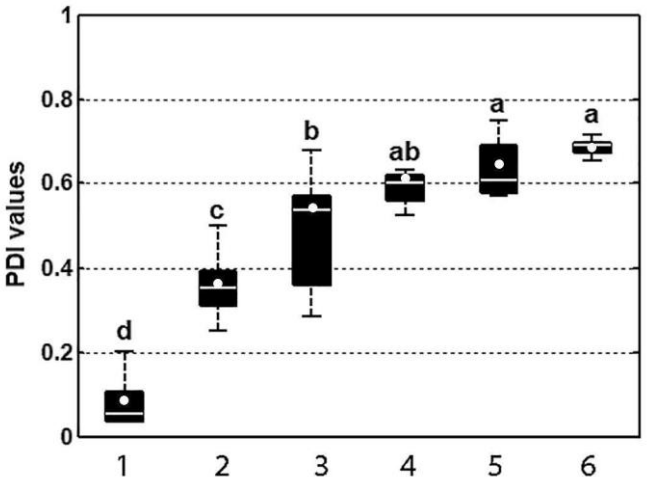

Figure 3.4. PDI index trend gradient with depth in the study area, in the different layers separated by pedogenic discontinuities; the values calculated in the observed profiles are shown as white points.

The increasing extent of pedogenic processes with depth were visible in the clay fraction as well. Chlorite was more abundant in the top horizons (Table 3.4), while it almost completely disappeared in layers 3-5 (Fig. 3.5). On the opposite, smectite increased from <5% in the surface Bw to 15-18% in layers 3-5. Vermiculite was most abundant in middle layers, while kaolinite had a similar trend as smectite, even if a rather high content was also observed in the top Bw horizon, likely evidencing the presence of already pedogenized materials in the weakly weathered youngest loess.

Table 3.4. Semiquantitative analysis of minerals in the clay fraction, derived from XRD diffraction patterns according to the method developed by Islam and Lotse (1986).

Horizon	Quartz	Illite	Chlorite	Vermiculite	10-14 and 14-14 interlayered	Smectite	Kaolinite
Bw	<5	<5	20	21	27	<5	21
2E/B(x)	<5	<5	7	23	18	8	36
3Btx1	<5	<5	<5	23	15	15	39
4Btx3	<5	<5	<5	30	12	13	38
5Btx4	<5	<5	<5	20	14	18	39

Thus, the main differences in clay mineralogy among the various aeolian depositions were related to the transformations of chlorite into smectite, partly vermiculite, which later partly transform into kaolinite.

The observed soil profile has hence the typical characteristics of the fragipan soils in the area. Its limitations are also typical: water infiltration is strongly slowed down, particularly at the Bw-2E/B(x) boundary, but also close to the other discontinuities, as shown by the nodular layers. Increasing fragic properties are associated with this reduced permeability. Increasing platy structural aggregation degree is another associated factor. This last property is likely caused by intense freezing conditions during glacial periods (Cremaschi and Van Vliet-Lanoë, 1990; Van Vliet-Lanoë, 1998).

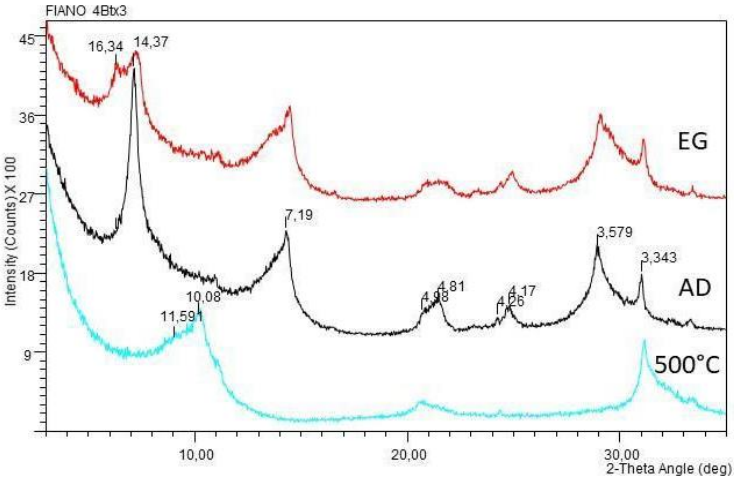

Figure 3.5. XRD patterns of the 4Btx3 soil horizon (d spaces in Ångstrom).

Intense polygenesis is thus one of the main characteristics of these soils on Pleistocene fluvio-glacial terraces: some properties are typically developed in humid and temperate climates characteristic of interglacial periods (i.e. clay illuviation and formation of clay coatings, redoximorphic features), others are related to cold, glacial phases and deep seasonal frost of permafrost (platy aggregation, sometimes brittleness and high bulk density), while petroplinthites usually require at least subtropical environments, also characteristic of certain interglacial periods. Each layer seems to have been subjected to an increasing number of glacial-interglacial variations with depth.

Chapter 3.2

Loess cycles in the Stura di Lanzo soils

Negri, S., Raimondo, E., D'Amico, M.E., Stanchi, S., Bonifacio, E.

Loess is a silty aeolian sediment whose formation is mainly due to the grinding action of glaciers on rocks. It can be produced also by frost shattering, aeolian abrasion and ballistic impact. The amounts of loess deriving by these residual processes, nevertheless, are negligible when compared to the huge yields generated by glacial abrasion. The resulting fine-grained material is then draped across the landscape by fluvial and aeolian action. Loess is first outwashed by proglacial flows, deposited in braided riverbeds in the fluvioglacial plain, exposed to freeze-thaw cycles and re-transported by wind. Loess has been associated with fragipan formation by many authors giving rise to the hydroconsolidation hypothesis (e.g., Barden *et al*., 1973; Assalay *et al*., 1998).

In the study area, the South-Western side of the Stura di Lanzo (SL) alluvial fan, river terraces are covered by a sheet of aeolian loess, up to 3 m thick at some sites. There is no agreement in the literature on the dating of this loess. Some authors stated that the deposition happened between 100 and 40 ka BP (Costantini *et al*., 2018), while other paleoclimatic investigations assess that at a nearby site the lowermost of four loess layers could be ascribed to Gl 5 (1.8–1.0 Ma, Billard and Orombelli, 1986). The whole area was not covered by glaciers during the Last Glacial Maximum (LGM), nor during more ancient glacial expansions, as the closest lobe of the ice stopped right behind the Lanzo Massif.

We recently applied several analytical techniques to confirm the discontinuities found in the field and to assess the origin of the loess beds in the Stura di Lanzo area (Negri *et al*., 2021). The abundance of coarse silt fraction suggested that most of the aeolic depositions originated from the Po plain, except for one cycle, with a probable origin from the Lanzo massif.

The different source of this cycle, represented in the Fiano soil profile by the horizons between 50/65 and 100 cm, is suggested also by image analysis (156 particles in the

10–200 µm range for each soil horizon). Mean gray value was lower for the particles belonging to this deposition ($P < 0.001$), pointing towards a darker colour, which is indeed typical of ultramafic materials. Differences were also visible in other image analysis-derived indexes: the particles of horizon 3Btx1 were, in Fiano, bigger than the others ($P < 0.001$), as visible in Fig. 3.6.

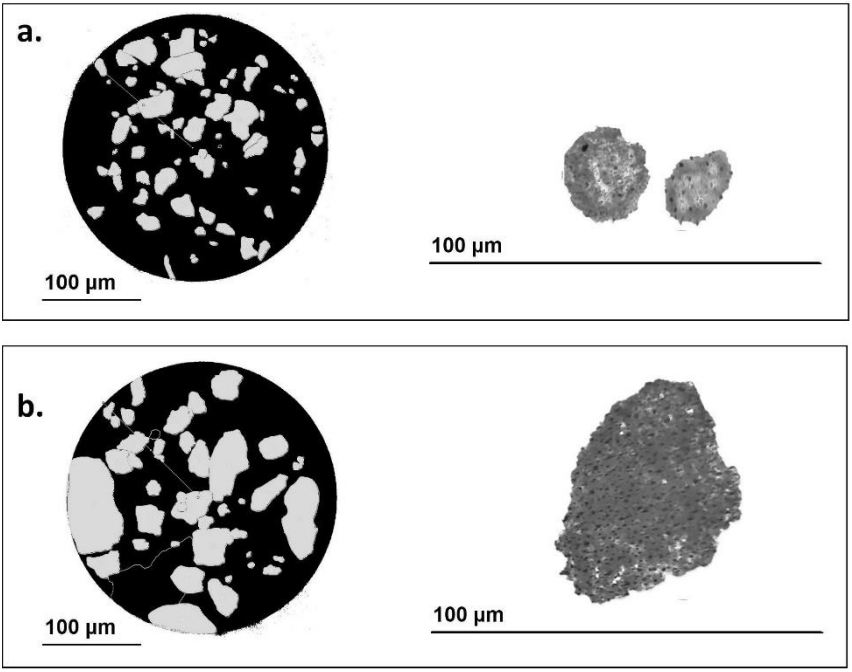

Figure 3.6. Examples of glass slides and single particles belonging to (a) 2E/B(x) and (b) 3Btx1. Samples belonging to the Fiano profile.

Roundness, which was significantly lower in the youngest cycle, according to our previous research, does not show any specific trend in the Fiano profile, while circularity increases with depth suggesting a greater smoothing degree in older depositions. This feature was not visible when the study area was considered as a whole, likely because the signs left by wind transport interfered with weathering in shaping the loess grains.

The particle size distribution indicated that the discontinuities found in the field corresponded to varying weathering level, although the classical S-shape of loess

deposits was present even in the oldest beds. The median size values in the loess beds of the Stura di Lanzo were of 6.5 ϕ (11.0 µm, Fig. 3.7a) in the youngest deposition and of 8 ϕ (3.9 µm) in the oldest one (Fig. 3.7b), with a bimodal or tri-modal distribution. The Fiano profile well reflected these trends.

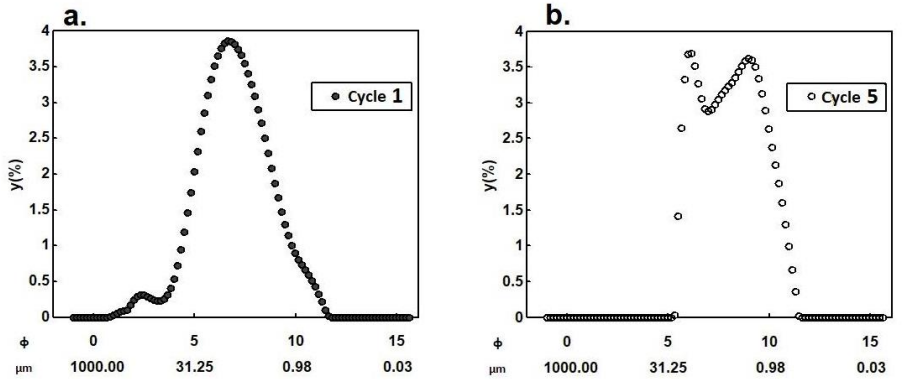

Figure 3.7. Laser PSD probability density curves of horizons belonging to (a) loess deposition 1; (b) loess deposition 5.

The dominant mode corresponded to the fine silt class, around 8–14 µm, also in the oldest depositions of the Fiano profile (here 12 µm), which in the 5Btx4 horizon corresponded however only to 56% of the total peak area (ca. 90% in the youngest depositions). Another important modal peak, always present, was visible in the clay class or slightly above its upper limit, from < 1 µm (in most cases) up to 4 µm. It is worthwhile to note that clay class diameter values were slightly higher in the horizons developed on the oldest loess deposition. The area of this finest modal class increased from young to old depositional cycles reaching 38% in the 5Btx4 of Fiano.

Chapter 3.3

Physical and geotechnical properties of fragipan-affected soils

Stanchi, S., Negri, S., D'Amico, M.E., Raimondo, E., Bonifacio, E.

Atterberg limits, in particular the plastic and liquid limit, represent threshold values for the gravimetric water content in remolded soil samples. They are commonly used in geotechnics and soil engineering (ASTM, 2010). At the plastic limit (PL), the soil sample shifts from semi-solid to plastic state, while at the liquid limit (LL) the transition from plastic to liquid state occurs. High liquid limits indicate high compressibility and swelling potential in soils.

The range of plastic behavior in soils is defined by the plastic index PI, computed as (LL-Pl). PI values >40% indicate very plastic behavior, i.e., a large interval of % water content where soil maintains its strength, while PI <7% is typical of non-plastic soils (Sovers, 1979). For low PI values, even a small change in soil moisture will result in significant changes in consistency, and scarce compressibility will be generally observed.

Poor plasticity is typical of sand and silt-rich soils, due to the physical and surface properties of the dominating size fractions. On the contrary, high plasticity is typically observed in clay-rich soils, such as the Fiano soil profile.

In a recent research (Stanchi *et al*., 2021) we checked the suitability of the standard method for LL and PL determination (ASTM, 2010), and of the pre-wetting duration, for fragipan-bearing soil samples. We demonstrated that, despite fragipan horizons display typical physical properties, widely described in the literature (e.g., Smalley *et al*., 2016; Bockheim and Hartemink, 2013), no adaptation of the method is needed. Therefore, a 3-hour pre-wetting was considered suitable for all soil samples, as no significant differences were observed in the Atterberg limits when different pre-wetting times were compared. This result was quite unexpected, considering the typical pore pattern and hydraulic properties of fragipan. It was therefore attributed to the size fraction used for LL and PL determination, and to the remoulding of

samples during the analysis, that makes them not directly comparable with undisturbed clods.

The liquid limit in the Fiano soil profile ranged from 39 to 43%, with the maximum value observed in the 2E/B(x) horizon (Table 3.5). No relevant variations were observed in LL in the fragipan-affected section of the profile. The plastic limit was in the range 30-38%, again with a maximum in the 2E/B(x) horizon. The resulting PI values ranged from 5 to 10. Thus, the samples were non-plastic or poorly plastic. PI was in general higher in the fragipan-affected samples. This trend was observed, with statistical significance, in the larger dataset analyzed by Stanchi *et al*. (2021).

Table 3.5. Atterberg limits and related properties for the soil profile located in Fiano (TO). Bv and Bc horizons were not analysed for Atterberg limits. LL: liquid limit; PL: plastic limit. PI: plastic index; SSA: specific surface area; A: activity index; Df: fragmentation fractal dimension.

Horizon	LL (%)	PL (%)	PI (%)	SSA ($m^2 g^{-1}$)	PI/LL	A	Df
Bw	39	30	9	17.50	0.229	0.37	2.794
2E/B(x)	43	38	5	35.00	0.115	0.15	2.869
3Btx1	42	35	7	34.30	0.166	0.21	2.834
3Btx2	41	31	10	37.80	0.241	0.30	2.838
4Btx3	41	33	8	37.10	0.186	0.23	2.835
5Btx4	40	33	7	36.40	0.182	0.28	2.803

As visible in Fig. 3.8, all samples fell in the section of the Casagrande chart (widely used in soil engineering) defined as “inorganic silts with medium compressibility and organic silts”.

A more recent version of the chart was however proposed by Moreno-Maroto and Alonzo-Azcarate (2018), where all soils with PI <LL/3 were defined as non-plastic, independent of their clay content, which is true for all our samples.

The activity index A, obtained as (PI/clay) (Table 1), despite a slight variability along the profile, was always <0.75, which indicates “inactive clays” such as kaolinite (Kaliakin, 2017), which was quite abundant in the study area as reported in Raimondo *et al.* (2019).

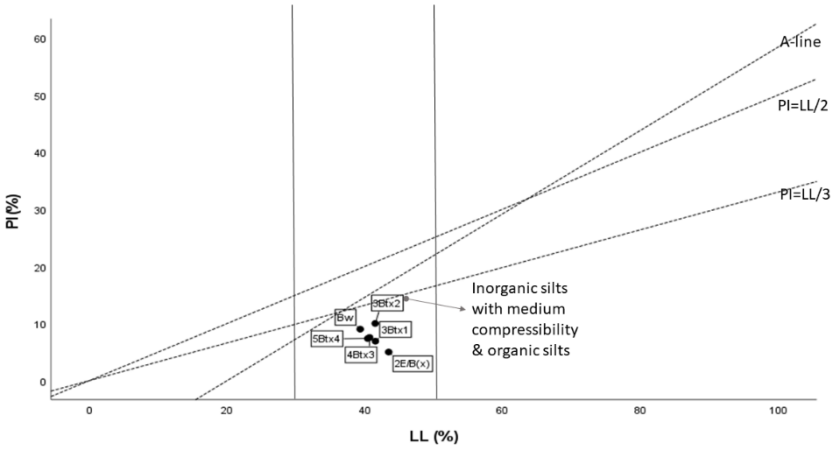

Figure 3.8. Casagrande chart as modified by Moreno-Maroto & Alonzo-Azcarate (2018).

The specific surface area (SSA) measured with the methylene blue spot test (ASTM, 1984) showed lower values in the Bw horizon (Table 3.5), while it was in the range 34-38 $m^2\ g^{-1}$ for deeper samples, with very slight variability among horizons. This is again in accordance with the high amounts of kaolinite, whose SSA varies from 30 to 55 $m^2\ g^{-1}$ (Khawmee *et al*., 2013).

The homogeneity in soil texture observed for the B-type soil horizons was reflected by the fragmentation fractal dimension Df, which is an indicator of the particle and aggregate-size distributions in soils (Stanchi *et al*., 2008). In general, Df values closer to 3 indicate a distribution dominated by finer classes, as it happens in clay-rich horizons, which is true for all the fragipan horizons in the soil profile.

The bulk density always exceeded 1.5 g cm^{-3} (data not shown) except for the top horizons, characterized by higher organic matter content. Such values could pose problems to root penetration and are therefore a severe limitation besides the mechanical properties of fragipan.

Chapter 3.4

Humus forms at La Mandria sites

Bonifacio, E., Samorè, A., D'Amico, M.E., Celi, L.

La Mandria Regional Park is one of the few remnants of forested areas close to Turin, being preserved as it has been used since the 16th century as a hunting reserve by the Savoia family, and later acquired by Regione Piemonte. It now comprises public and private areas, both suffering from the presence of red oak (*Q. rubra L.*). Because of its invasiveness, it has in several areas substituted the original *Quercus robur* L., *Q. petraea* (Matt.) Liebl. and *Carpinus sspp*. L. cover. The soils of the forested area are almost totally Typic Fragiudalfs, with the only exception of the slopes connecting the oldest and younger terraces. There, the long dating erosion has modified the profile and sometimes shifted the soils to Ruptic-Alfic Eutrudepts (IPLA, 2001).

The fast-growing red oak deeply impacts nutrient cycles. It is particularly important in an area where the soil is intrinsically at a low fertility because of its high degree of development. Red oak litter is indeed poorly decomposed, likely because of the presence of tannins that may inhibit microbial activity and organic matter turnover. Biocycling is, as a consequence, slowed down and nutrients are immobilized in the litter layers. This potentially contributes to the scarce success obtained in shifting back from the invasive species to the autochthonous vegetation (Bonifacio *et al*., 2015).

The fastest method to estimate litter turnover is to evaluate humus forms; the sequence of organic horizons, their thickness and continuity, and the structure of the top mineral horizon are the result of all factors interacting at the site and affecting biological activity. An updated taxonomy of humus forms has recently been developed (Zanella *et al*., 2018) and it was used to classify humus forms at two sites of La Mandria area (Fig. 3.9), one characterized by the presence of red oak (QR, *Quercus rubra*) and the other covered by autochthonous species (QC, i.e., *Querco-carpinetum*, mainly *Q. robur* i.e., English oak).

Figure 3.9. Study sites for humus forms and plant-soil relationships at La Mandria Regional Park.

The soils are Typic Fragiudalfs, but, as shown in Fig. 3.10, they sharply differ in the upper part of the profile. Further details about the relationships between plant and soils at these sites are given at Chapter 3.5. At each site, a soil profile and 4 additional pits within a radius of 12.5 m were opened to check for soil spatial variability, and humus forms were described according to Zanella *et al.* (2018).

QR sharply affected the upper part of the profile, with the presence of thick organic decomposed OH layers followed by a lower accumulation of organic matter in mineral horizons, that are lighter and more poorly structured than at the QC sampling points (Fig. 3.10). In most cases, below the A or the OH horizons at the QR sites an eluvial horizon was clearly visible, while at the QC sites the presence of the E horizon is more elusive, due to a better incorporation of organic matter.

The humus system at the QR site is a Mor (Table 3.6), as indicated by the presence of the OH horizon and the very low biotic activity in the top mineral layer; only fungal hyphae and small signs of arthropods activity were visible. The classification of humus forms is however more complicated: the presence of only a slightly zoogenic OH would point to Humimor, but this form lacks the zoogenic OF, which was instead always present. Hemimors are however characterized by a more evident biological activity in the OF horizon.

Figure 3.10. Soil profiles at the QR (left) and QC (right) sites.

The lack of the OH horizon clearly indicates a Mull humus system at the QC site and, because of the presence of several cm of OF, the assigned humus form was that of Dysmull. The coarse granular structure and the presence of earthworms also point to the Mull system, even if the pH of the horizons was however not in the typical range of the mull humus systems, being as low as 4.2.

Mor systems indicate a slow turnover of organic matter because of poor fertility conditions, harsh climate, or intrinsic recalcitrance to decomposition of plant residues. It is the typical humus form that is expected in high-elevation conifer stands, where earthworm and arthropod activity is impeded. On the other hand, Mulls are characterized by more favourable site conditions coupled with less recalcitrant organic matter.

Humus forms also reflect different C stocks. The storage of C and N in the litter layers is more than double under QR (3.5 Kg m^{-2} at the soil profile site) than at the QC profile (1.6 Kg m^{-2}) and this is only related to the different thickness of the horizons and to the presence of the OH. The OC concentration of OL and OF layers is indeed comparable (at QR: 45.6% OL, 43.6% OF; at QC: 46.8%, OL, 41.2% OF).

As the two sites are very close to each other (< 300 m distance), and the level of soil development (including leaching and clay translocation) has been shown to be the same, the striking differences that can be appreciated in the field are only caused by vegetation.

Table 3.6. Humus forms at the 5 observation points of the QR and QC sites, numbers in parentheses indicate the thickness of the horizons in cm.

Vegetation	Humipedon horizon sequence	Humus form
QR	OL (5) - OFzo (3)-OH (2) –A (3)	Humimor/Hemimor
	OL (2) – OFzo (2) – OH (1) –A (3)	Humimor/Hemimor
	OL (4) – OFzo (3) - OH/A (4)	Humimor/Hemimor
	OL (4) – OFzo (3) - OH/A (4)	Humimor/Hemimor
	OL (4) – OFzo (4) - OH/A (5)	Humimor/Hemimor
QC	OL (4) – OFzo (3) – A (4)	Dysmull
	OL (4) – OFzo (3) - A/AE (6)	Dysmull
	OL (3) – OFzo (3) – A (5)	Dysmull
	OL (4) – OFzo (4) – A (8)	Dysmull
	OL (3) – OFzo (3) – A (7)	Dysmull

Chapter 3.5

Nutrient biocycling at La Mandria sites

Seidel, F., Rolando, M., D'Amico, M.E., Celi, L., Bonifacio, E.

Invasive tree species often differ in plant internal nutrient cycling in comparison to native species prompting significant changes in soil properties by altering the biocycling of nutrients (Callaway and Aschehoug, 2000). This is possible due to a more efficient nutrient uptake, use, storage and/or higher nutrient reabsorption efficiency before leaf abscission resulting in a reduced litter quality and a reduced return of nutrients to the soil, depleting soil resources (Millard and Grelet, 2010). Thus, after the introduction of non-native species, non-resilient ecosystems may lose their ability to return to their original state and therefore, the restoration of natural native vegetation may become problematic (Bonifacio *et al*., 2015).

We selected two sites for this study at La Mandria Regional Park: one in the native English oak forest and one in an area that was once covered by English oak but is now a pure red oak stand (Fig. 3.11) to see the tree species effect on biocycling. Litter accumulation and the top part of the profiles differed, as shown in Chapter 3.4, suggesting that plant traits may play a role also in nutrient dynamics.

At each site 5 trees were selected, all comparable in age (ca. 60 years) and size (30-40 m height, 30-60 cm stem diameter at breast height). We sampled leaves and fine roots as the key contributors of organic matter to the soil, as well as the different organic horizons and the mineral soil (0-5 cm and 5-15 cm layers) during four phenological stages, namely the shoot growth, green leaf, pre- and post-abscission stage. Litter traps were installed to quantify leaf inputs (Fig. 3.12). The analysis is ongoing but preliminary data showed that red oak produced twice more litter than English oak. The nitrogen (N) to phosphorus (P) ratio of living leaves suggested that red oak was significantly more P limited throughout the year than English oak (Koerselman and Meuleman 1996).

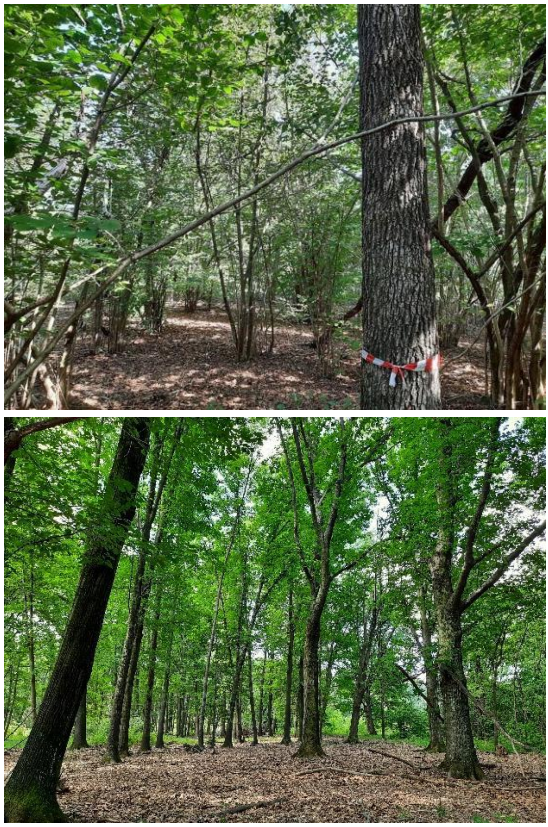

Figure 3.11. Quercus robur *and* Carpinus *forest (top) and* Quercus rubra *forest (bottom) at La Mandria Park.*

This was also reflected by the N reabsorption efficiency (NRE) that was higher in English oak while the P reabsorption efficiency (PRE) was higher in red oak. The produced litter (taken from litter traps) of both species did not differ in C or N content but P content was 4 times higher in English oak. Furthermore, fine root analysis showed that red oak soils have 18x more fine roots in the investigated layers which are mainly (95%) distributed in the OH horizon and are containing 30% less N and 50% less P with a higher C/N ratio than in the English oak plot.

Therefore, the relative input of C (g/kg plant tissue) into the soil via leaves and roots did not significantly differ between species, but the absolute amount did when taking the litter and root weight into account. The same was true for leaf and root N content

while leaf P input via litter was half and root P input was 9 times higher in red oak plots. Considering these observations on plant derived material, it becomes clear that we should expect an upwards shift of total C, N and P content in red oak soils in comparison to the English oak plots.

Figure 3.12. Litter traps installed for fresh litter collection at La Mandria Park.

The OL layer contained less N and P, with a wider C/N and N/P ratio under red oak compared with English oak. This was followed by an OF layer containing more C, N and available N under red oak which was similar in the OH layer where additionally P contents showed an increasing trend. Finally, the mineral soil layers (0-5 and 5-15 cm) showed that under English oak soil P and NO_3^- were higher while under red oak more NH_4^+ and organic C were present in addition to a wider C/N and N/P ratio.
Thus, we indeed found an upwards shift of total C, organic C as well as N, available N and total P content in red oak soils in comparison to the English oak plots away from the mineral soil and towards the organic layer (Fig. 3.13). Furthermore, as red oak was more efficient in P reabsorption from leaves and showed lower P in roots, it appears that the P balance of this ecosystem has been disturbed by the red oak invasion. P remained rather in tree tissues than being returned to the soil, as compared to English oak showing a higher P content in mineral soils. The biocycling of C, N and P was thus disrupted by the invasion of red oak due to the high P

resorption efficiency, the quality and quantity of litter and roots as a nutrient source for the soil.

In conclusion, soils under red oak in low fertility conditions are in fact degrading in quality with N and P accumulating in the organic layers reducing litter derived input to the mineral soil which could drive the ecosystem to a no-return threshold ultimately prohibiting successful restauration of these soils with native English oak forests without intensive management measures.

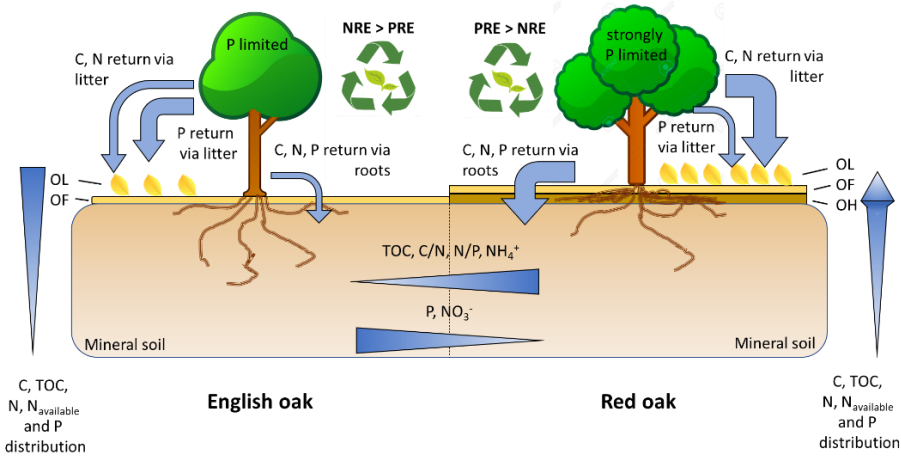

Figure 3.13. Graphical model showing the distribution of carbon (C), total organic carbon (TOC), nitrogen (N), available nitrogen ($N_{available}$), ammonium (NH_4^+), nitrate (NO_3^-), phosphorus (P), the C/N and C/P ratio as well as the N and P reabsorption efficiency (NRE and NRP respectively) between English oak and red oak plots in plant tissues (leaf, fine roots), organic layers (Litter (OL), fragmented (OF) and humified horizon (OH)) and mineral soil (0-5 cm and 5-15 cm).

Elementar, leader mondiale in analisi elementare di elementi quali carbonio, idrogeno, azoto, zolfo, ossigeno e cloro in matrici organiche e inorganiche, è in grado di offrirvi la più vasta gamma di analizzatori elementari disponibili sul mercato.

Analizzatori elementari CHNS
Strumenti per analisi di carbonio, idrogeno, azoto e zolfo, ossigeno e cloro in diverse matrici

Analizzatori TOC Liquidi e Solidi
Strumenti per analisi di carbonio organico totale in matrici ambientali quali ad esempio acque e rifiuti

Sistemi per analisi IRMS
Spettrometri di massa per analisi di isotopi stabili in solidi, liquidi e gas

Elementar Italia S.r.l.
Via Cavour n° 2
22074 Lomazzo (Co)
tel: +39 02.36714520
www.elementar.com
info-italia@elementar.com

elementar
EXCELLENCE IN ELEMENTS

Chapter 4

URBAN ENVIRONMENTS

Chapter 4.1

Historical tour of the urban sites recovered in the city of Torino and its surroundings

Ajmone Marsan, F.

The city of Torino (Fig. 4.1) has been, since the beginning of the industrial revolution in Italy (circa 1850), one of the most industrialized cities of the country focusing, in particular, on the metallurgical and related manufacturing.
The foundation of FIAT, which became a major car and other vehicles manufacturer, brought about the rise of complementary activities such as painting, plating, tires making. This area, together with the concentration of people, energy and materials, has accumulated a variety of soil pollutants owing to the historically permissive legislation on the matter (Ajmone Marsan and Zanini, 2013).

Figure 4.1. San Carlo square in the city of Torino.

In the late '80s, however, a process of de-industrialization began that saw the dismissal of a number of manufacturing plants (Gallino, 2003), leaving behind vast contaminated areas and large amounts of materials.

In Fig. 4.2, a survey of the derelict industrial sites in the city in 1989 is illustrated. The legend reports the area in m^2, the total area being 10.5 km^2. The largest sites are located to the north and the south of the city in what were the suburbs and are nowadays included in the urban area. Part of these areas were remediated and directed to new land uses while other severely contaminated sites are still waiting for a decisive intervention.

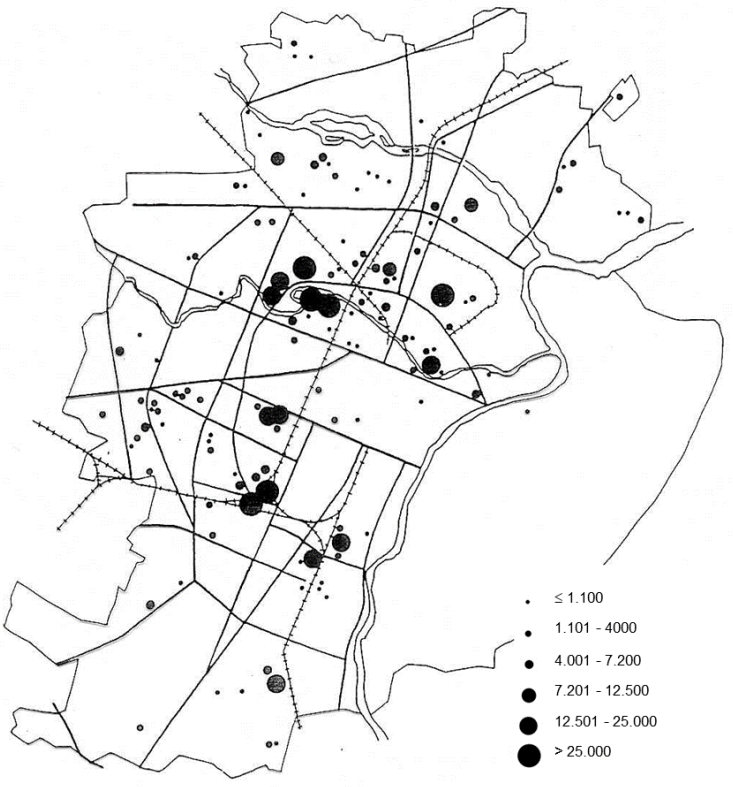

Figure 4.2. Derelict industrial sites in the city in 1989.

One of the most prominent transformations in the city has been what is now called Parco Dora, a former industrial site where FIAT metallurgical works and Michelin rubber plants were located. Fig. 4.3a illustrates the state of the site in 1950. The aerial photograph of Fig. 4.3b depicts the transformation of the Michelin plants into a park in 2015. Part of the area was used for residential purposes (see the building in the background).

Figure 4.3a. Parco Dora as it was in 1950. Source: Comune di Torino.

Figure 4.3b. Parco Dora as it appears currently.

Another important transformation that occurred in the city in the last 20 years and affected indirectly the soils of the urban area has been the construction of an underground line. This has produced – and still does – large amounts of excavated materials (Fig. 4.4) that could be used as “plant substrates”. The legislation on the matter has been very strict until 2017 so most of the material was just dumped. On the contrary, it is now possible, if the material is not contaminated, to use outside the site where it is produced.

Fig. 4.4. Excavated material waiting to be redistributed. Foto by Ajmone F.

Chapter 4.2

Main inorganic pollutants in Torino soils: case studies

Ajmone Marsan, F., Padoan, E.

The massive concentration of energy and matter - waste, in particular - in urban areas entails the dispersion of considerable amounts of contaminants in the environment. Metals, especially, have been released since the advent of industrialization and the soil appears to have been the ultimate sink (Ajmone Marsan and Biasioli, 2010; Ajmone Marsan and Zanini, 2013). Although in general point-source pollution rises immediate concern, the diffuse pollution is responsible for the major problems. This has been illustrated for the city of Torino, for which the contamination levels of the soils within the urban area were compared with those of the surrounding soils (Biasioli *et al.*, 2006) (Fig. 4.5).

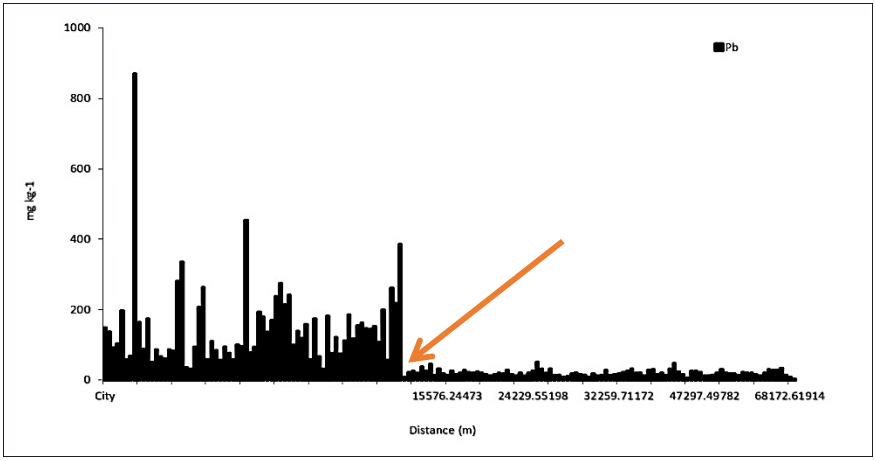

Figure 4.5. The distribution of lead (Pb) in the soils of Torino and surroundings. The arrow points to the city limit. Source: Biasioli et al., 2006.

Subsequent studies confirmed that the main metal contaminants in the Torino urban area are lead, copper, zinc, chromium and nickel, of traffic and industrial origin (Biasioli and Ajmone Marsan, 2007; Biasioli *et al*., 2012). As an example, the distribution of lead in the city of Torino is depicted in Fig. 4.6. A specific investigation revealed that also mercury is widespread in urban soils (Rodrigues *et al*., 2006).

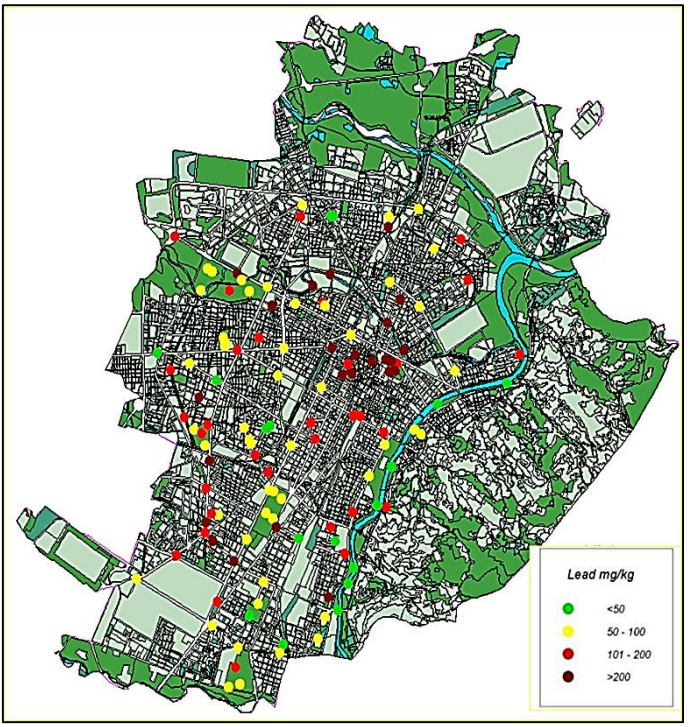

Figure 4.6. Distribution and concentration of Pb in specific areas of Torino.

However, a number of problems emerged that hamper the study of urban soils and those of Torino in particular. The first is the extreme variability – horizontal and vertical – of the soil properties, including the pollutant concentration, in view of the interferences, mixing and removing, that usually affect the soils of a city (Madrid *et al*., 2006). Secondly, due to the very nature of soil distribution in a city, it is not

possible to adopt a random sampling so the illustration of the contamination can only be by points.

In addition, for the soils of Torino, the geological substrate is characterized by high concentration of Cr, Ni, and Co due to the presence of serpentinic minerals and this interferes with a consistent determination of the level of soil contamination in the city (Fig. 4.7 A,B)

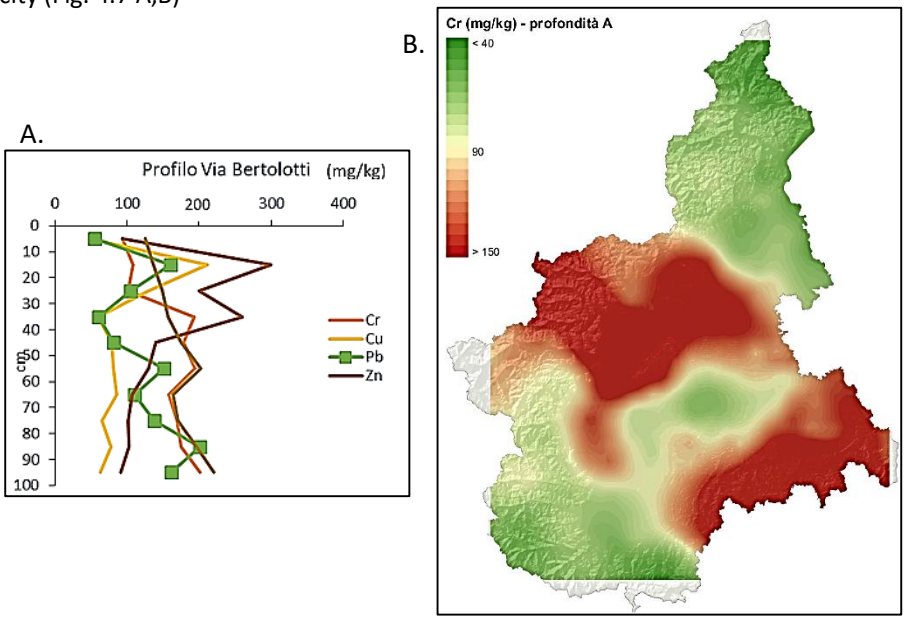

Figure 4.7. A. Concentration of principal metals in the profile of via Bertolotti. B. Spatial distribution of Cr in the soils of the Piemonte region (depth 0-10 cm). Torino lies in the middle of the red patch in the middle of the map. From Arpa Piemonte (2020)

More than the presence of the metals per se, the major cause of concern is their transfer, or potential transfer, to other environmental compartments such as water, air and ultimately to living organisms.

The release of the contaminant from urban soils was studied under anaerobic conditions (Ajmone Marsan *et al.*, 2019) (Fig. 4.8).

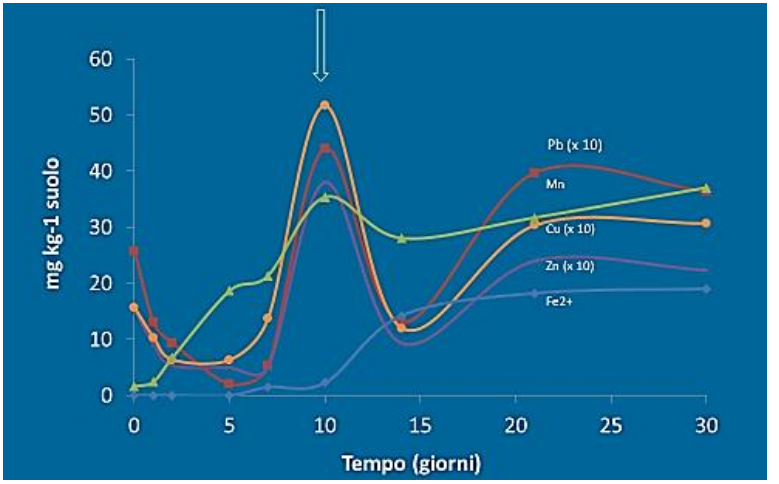

Figure 4.8. Metal release in anaerobiosis.

The metal bioaccessibility of metals was investigated in the soils of a peri-urban area (Poggio *et al*., 2009), and was followed by a study of the bioaccessibility of metals in soils and road dust along an urban-periurban transect (Padoan *et al*., 2017) (Fig. 4.9).

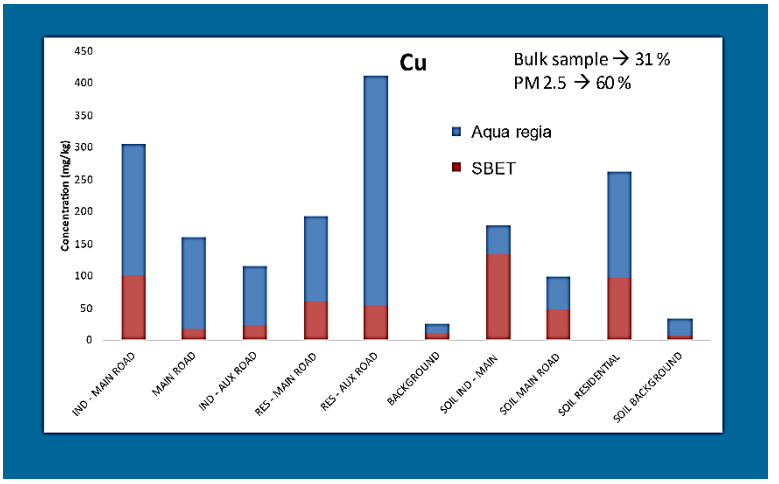

Figure 4.9. Copper (Cu) in road dust and soil (simple bioaccessibility extraction test, SBET).

More recently, the study was extended to the health risk assessment of potentially toxic elements in the soils of Torino (Li *et al*., 2021) (Fig. 4.10).

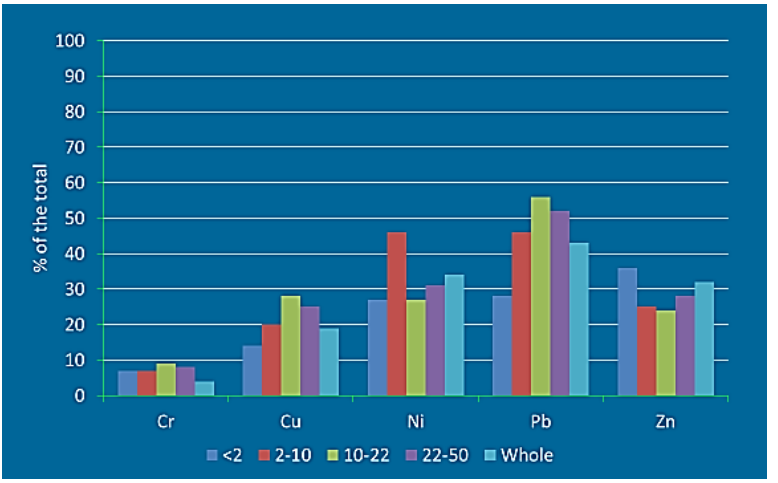

Figure 4.10.Metal bioaccessibility in soil particles (simple bioaccessibility extraction test, SBET).

Chapter 4.3

Phytotechnologies for soil remediation

Padoan, E., Schiavon, M.

General overview

A variety of conventional physical and chemical technologies can be exploited for the reclamation of contaminated lands, but they are generally very expensive and poorly sustainable. In addition, they may greatly affect soil fertility, up to disturbing the whole ecosystem. Alternatively, cost effective, environment-friendly and aesthetically pleasing technologies can be employed that make use of plants and associated microorganisms to remove pollutants from the contaminated soils (Pilon-Smits, 2005; Ashraf et al., 2019). These green technologies are globally termed "*phytoremediation*", but differ from each other depending on the contaminant, the type of substrate to remediate, and the intended use of the land (Pilon-Smits, 2005; Ashraf et al., 2019). Thus, phytoextraction is the approach that foresees the use of plants with elevated capacity to take up and translocate metals/loids to the above ground tissues. Plants should be appreciably tolerant to the contaminant and produce great biomass. Depending on whether the species is herbaceous or arboreal, the aerial part of plants is completely or partially removed. Post-harvest disposal of the contaminated plant material must be then managed through advanced techniques like composting and compaction, combustion and gasification, phytomining and pyrolysis. Phytostabilization is applied in areas where the concentration of inorganic contaminants is not very high. Plants in this case are not required to accumulate high concentrations of metals/loids. Rather, the interaction between their roots, soil and root-associated microorganisms creates a steady environment that prevents contaminants from being lost in the surrounding areas. Such an approach could be supported by the addition of chelating agents to the soil that promote the immobilization of inorganic contaminants. Phytovolatilization, instead, may be applied when soils are rich in contaminants that plants take up and further convert

into volatile, less toxic species. As an example, this approach might be valuable for the remediation of soils contaminated with mercury and selenium.

The effectiveness of phytoremediation technologies depends on several factors, such as the characteristics of the substrate to be cleaned up, the intensity of contamination and the plant species employed. Indeed, plants differ in their capacity to accumulate, resist or tolerate metals and metalloids. Based on this, they are classified as (i) indicators, if metal/loid uptake and root-to-shoot translocation are regulated so that leaf concentration is related to the metal/loid concentration in soil; (ii) excluders, if they own mechanisms that prevent or limit the entry of metal/loids in their roots and their further translocation to the aerial parts; (iii) accumulators, when metal/loids are actively concentrated inside their tissues, irrespective of the metal/loid concentration in soil. In the last case, plants must possess efficient enzymatic and non-enzymatic defensive mechanisms that avoid generation of oxidative stress in cells or scavenge reactive oxygen species (ROS). In addition, there are plants that are termed hyperaccumulators because they exhibit extraordinary capacity to accumulate certain metals or metalloids in their leaves without showing any visible symptom of toxicity. However, the limited biomass produced by these plants represents a constraint for their use in soil reclamation in most cases.

In phytoextraction and phytovolatilization technologies, metal accumulators are generally preferred. It must be noted, however, that the acquisition of metals/loids by plants can be hampered by the presence of competing elements that are essential for the plant metabolism and physiological functions. These nutrients occur in forms that are chemically similar to those of the contaminant species. For instance, chromium in the form of chromate or bichromate makes use of sulfate transporters to enter the root cells, therefore competing with sulfate ions for the uptake (Schiavon *et al*., 2007, 2008, 2012). On the other hand, arsenate is chemically more similar to phosphate, with which it may enter in competition during plant absorption processes (Zhao *et al*., 2009).

Thus, having a broad knowledge of all chemical, physical and biological factors that control the speciation of contaminants in soil and taking into account possible uptake competition events between elements are essential to achieve effective soil reclamation. In the further sections, we report an example of a study evaluating the competition between chromium and sulfur for the uptake by plants and a phytoremediation study conducted in Torino.

Metal interactions with nutrients: the case of Cr(VI) and its analog sulfur

Brassica juncea is among the most suitable plant species to be used for phytoremediation purposes. This species produces a large biomass and exhibits great capacity to accumulate metal/loids and translocate them to the shoot. Therefore, it is very efficient in the remediation of soils containing high levels of inorganic pollutants, including chromium (Cr),

Chromium, as reported above, is one of the main contaminants occurring in certain areas of Torino affected by metal contamination. The main species of this element are the trivalent (Cr(III)) and hexavalent (Cr(VI)), which can interconvert depending on several soil factors. The trivalent form is the most stable in the environment and primarily occurs as iron chromite ($FeOCr_2O_3$). Cr(VI), instead, generates compounds that are listed as highly toxic to living organisms and carcinogenic to humans and most animals. In particular, Cr(VI) mainly occurs as oxyanion chromate (CrO_4^{2-}) or dichromate ($Cr_2O_7^{2-}$), and in these forms is taken up by plants through sulfate transporters. This is because of two main reasons. First, plants do not possess any specific mechanism for the uptake of Cr, as this element is not required for their vital metabolism. Second, Cr in the form of chromate or dichromate is chemically similar to sulfate, therefore it can bind to sulfate transporters and be accumulated in plants. The assumption that Cr(VI) compounds use the sulfate transport system to enter the plant roots is old, but stronger evidence was achieved in the last two decades. Two studies conducted using *B. juncea* and *Zea mays* unequivocally proved that Cr(VI) and sulfate compete for the uptake (Schiavon *et al*., 2007, 2008, 2012) (Fig. 4.11 A-D).

Because of Cr(VI) – sulfate competition, S uptake rates are reduced and Cr accumulation increases. Therefore, S concentration in plants is expected to decrease. This effect should hypothetically increase the expression of sulfate transporters, generally up-regulated by low S availability or decreased S concentration in tissues. However, chromate was shown to act as a repressor of high and low affinity sulfate transporters, either under low or high S supply. It is likely that plants reduce the expression of sulfate transporters after Cr enters the root cells as a resistance mechanism to prevent further, excessive, accumulation of this toxic element.

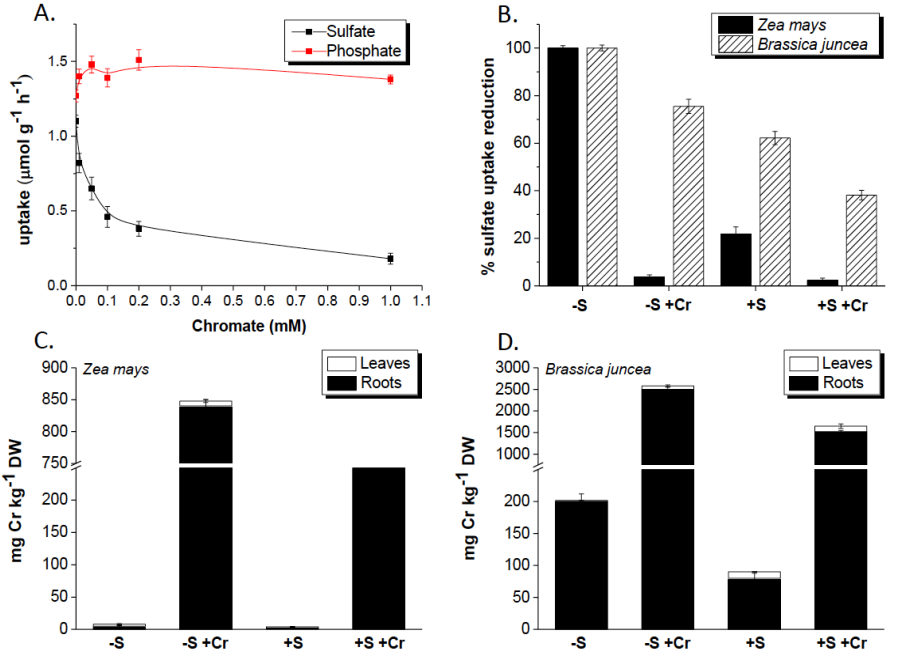

Figure 4 11. A. Variation of sulfate and phosphate uptake rates in maize plants in relation to increasing chromate concentration in the external medium. Uptake was measured within a 10 min pulse. B. Effects of sulfate and chromate combinations on sulfate uptake after 2 days of Cr application in maize and B. juncea plants (when present, Cr and S were equimolar, i.e. 0.2 mM). C.-D. Accumulation of total Cr in leaves and roots of maize and B. juncea plants subjected to different sulfate and chromate combinations. (From Schiavon et al., 2007, 2008).

The significance of Cr(VI) - sulfate competition is hence noteworthy as S, beyond being an essential macronutrient for plants, is involved in many detoxification processes by forming compounds like thiols (e.g., cysteine and glutathione) that reduce oxidative stress (Hasanuzzaman *et a*l., 2017), or phytochelatins and metallothioneins, which bind a number of metals and metalloids and deliver them to the vacuoles (Cobbett and Goldsbrough, 2002). To compensate for the reduced entry of S into the roots because of competition with Cr(VI), maize and *B. juncea* plants tend to retain ROS detoxifying S compounds in their below-ground apparatus, where Cr

accumulated the most. Conceivably, part of these compounds can also be transferred from the shoot to the root via phloem.
The possibility that transport systems for other macronutrient might be involved in Cr(VI) uptake cannot be ruled out, but phosphate transporters, for instance, do not mediate chromate transport, or are negligibly involved (Fig. 4.11 A), Schiavon *et al.*, 2007).
The Cr(VI) - S competition for the uptake is only one example of heavy metal-nutrient interactions, but other types of interactions exist, for instance between arsenate and phosphate (Zhao *et al.*, 2009). In *B. juncea*, phosphate application attenuates As accumulation (Grifoni *et al.*, 2015). Such interaction can be affected by additional elements, like S in the form of thiosulphate, which can determine the concurrent decrease of P and increase of As in *B. juncea* tissues.

Phytoremediation with short rotation forestry: case study (C.so Mortara)

A phytoextraction trial was performed during the renovation of a former industrial area in the northern part of Torino. It is noteworthy that in a former industrial area, currently embedded into a residential neighborhood, the aesthetic appeal is pivotal for the remediation approach to gain acceptance. In addition, the area should return to public utility (i.e., as an urban park) when restoration and decreased PTE concentration are achieved.
Hyperaccumulator plants have a low economic value, thus the use of short rotation coppice crops (SRC) has been promoted in recent years, combining phytoremediation needs with the production of valuable biomass on the contaminated land (Desjardins et al., 2018).
Plants used for SRC often have an additional value as ornamental, thus this remediation type shows the additional benefits of a green infrastructure. In Table 1, the plant species and genotypes used in the study presently described are reported.

Table 4.1. Species and genotypes used in the experiments.

Code	Genotype	Species
P1	ORION	*Populus ×canadensis Mönch*
P2	BALDO	*P. deltoides Marsh.*
P3	VILLAFRANCA	*P. alba* L.
S1	SI64-017	*Salix alba* L.
S2	MOS310	*S. viminalis* L.
S3	DRAGO	*S. babylonica* L.
R1	NORD	*Robinia pseudoacacia* L.
R2	SUD	*R. pseudoacacia* L.
R3	ENERGY	*R. pseudoacacia* L.

The selected area (Fig. 4.12) contained soil heavy metal concentrations (Co, Cr, Cu, Ni, Pb, Zn) above the legislative limits defined for green and residential areas (values of soil characterization and elemental composition are reported in tables 2 and 3). High values in the groundwater were determined for Ni, due to the soil parent material, and for Cr(VI), due to the previous industrial activities.

Figure 4.12. Experimental plot in C.so Mortara (Torino) before planting and during the second year. The surface of the experimental plot was about 0.1 ha.

Table 4.2. Chemico-physical characterization of the soil (n=32). Average values. TN: Total Nitrogen; TC: Total Carbon; Org.C: Organic Carbon; Olsen P: bioavailable Phosphorus; CEC: Cation Exchange Capacity.

	pH	**TN**	**Org. C**	**$CaCO_3$**	**Sand**	**Silt**	**Clay**	**Skeleton**	**Olsen P**
			mg/kg		%	%	%	%	mg/kg
Mean	8.4	1.1	19.3	124	65.3	29.1	5.6	38.2	13.1
S.D.	0.1	0.01	0.14	0.4	3	2.9	1	4.4	1.8

Table 4.3. Concentration of selected heavy metals in soil (n=32). Average values.

	Cr		**Cu**		**Ni**		**Pb**		**Zn**	
mg/kg	Total	DTPA	Total	DTPA	Total	DTPA	Total	DTPA	Total	DTPA
Mean	191	<0.5	97	8.3	185	1.3	215	27.7	447	12.6
S.D.	14		35	1.5	4	0.2	34	2.5	82	12.2

To identify the best cost-effective agronomic management of the parcels for the cost reduction, annual or biennial coppicing turnovers were studied. As an example, Zn and Cu results are reported. With a biennial management, the most productive clone for Cu phytoextraction was R1, while P1 yielded more using annual coppicing (Fig. 4.13).

Zinc phytoextraction was more efficient, bearing results in line with literature studies during field trials (Guidi Nissim et al., 2018). Accumulation yields were higher with annual coppicing for poplar clones. Salix and Robinia clones performed better on biennial management.

The root system contained between 9 and 11% of total Zn, which was thus the fraction of Zn not removed in the trial. However, the translocation of PTEs to above-ground tissues of plants is of primary importance in the management of a phytoremediation trial. From Fig. 4.13 it is evident that leaves carried an important share of the PTE uptake. Although the total uptake was not very high, the transfer of metals to the leaves accounted for 39% of total Zn accumulation in clone P1, and for 8-13% in willow clones (S1 and S3).

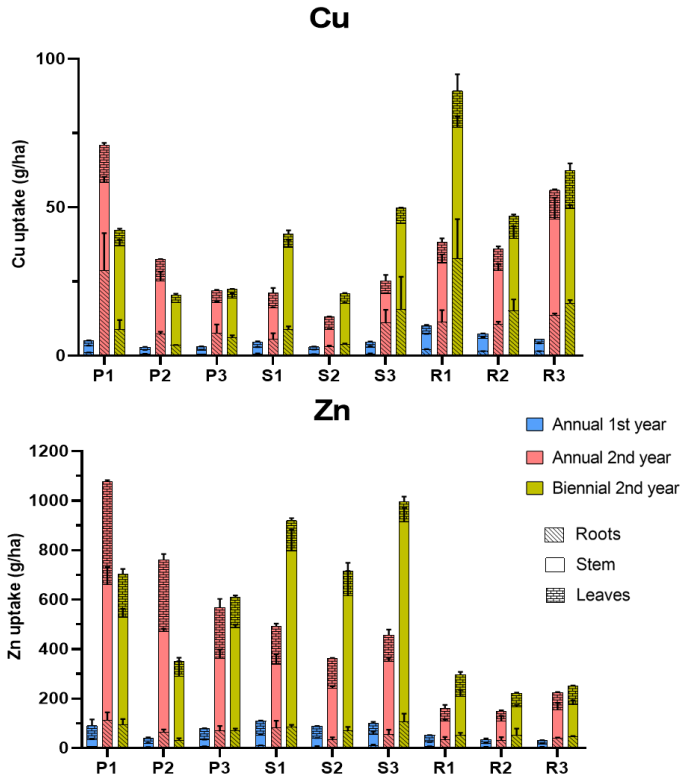

Figure 4.13. Estimated phytoextraction rates for the studied clones in the plant tissues. For each clone, tissue uptakes are stacked (from Padoan et al., 2020).

A successful phytoextraction should include the collection of leaves, a practice hardly used in field trials, as it will increase costs. In an urban context, the leaf harvest will be easier, as the city is already acquainted with the collection of leaves on the streets, and thus has suitable equipment.

Chapter 4.4

The contribution of soils to urban air quality

Padoan, E, Ajmone Marsan, F.

Particulate matter (PM) is recognized as one of the major risk factors to health worldwide. Over the last decades, broad attention has been addressed on effective remediation and regulation of vehicle exhaust emissions. As a result, about half of the current traffic emissions derive from non-exhaust processes, such as the suspension of soil and particles previously deposited on road surfaces (road dust, RD) due to vehicle-induced turbulence and wind, and direct emissions from the wear of brakes, tires, and road surfaces (Amato, 2018). Unfortunately, this share is predicted to grow in the future.

The study of road and soil dust is fairly challenging because RD particles are a complex mixture of solid and liquid particles originating from multiple sources.

In studies aimed to identify RD sources, mineral sources were always detected in very small size particles (<10 μm), generally of highly variable chemical composition. This was because they can derive from road wear, deposition of urban background mineral dust, soil from urban works or resuspended by wind, desert dust in Mediterranean areas and others.

Overall, soil dust has been poorly characterized in the RD composition of European cities. Therefore, we performed a study intended to evaluate RD pollution in urban and periurban areas of Torino and present methods to identify the soil contribution to urban air quality.

The average concentration values of most of the metals identified and quantified in roadside soils and in bulk (<2 mm) RD samples (Table 4.3) were similar. Only lead (Pb) concentration was significantly lower in RD compared to bulk soil. Lead, having a widespread distribution in urban soils due to an almost unique anthropic source (leaded gasoline), represents a perfect example for the use of a metal as a soil tracer contributing to urban pollution, both to RD and PM.

Table 4.4. Mean, minimum and maximum elemental pseudo-total contents in bulk soils and road dust in Torino. Values are expressed in mg/kg. (From Padoan et al., 2017).

	Cd	Cu	Cr	Ni	Sb	Pb	Zn
				Soils			
Mean	0.6	128	405	254	5.4	319	286
Min	0.2	26	147	145	1.5	38	96
Max	1.9	433	1048	465	13	1213	618
				Road dust			
Mean	0.8	181	519	294	7.7	74	200
Min	0.2	17	299	161	0.4	16	51
Max	1.7	717	1248	678	33	189	827

During a second sampling campaign (2016-2017), the inhalable (<10 µm) fraction of RD was investigated. The effect of soil on RD buildup was evident based on elemental concentrations determined at the different sampling sites. Typical traffic pollutants, such as Cu, were more abundant in residential sites, followed by suburban and industrial areas (Fig. 4.14).

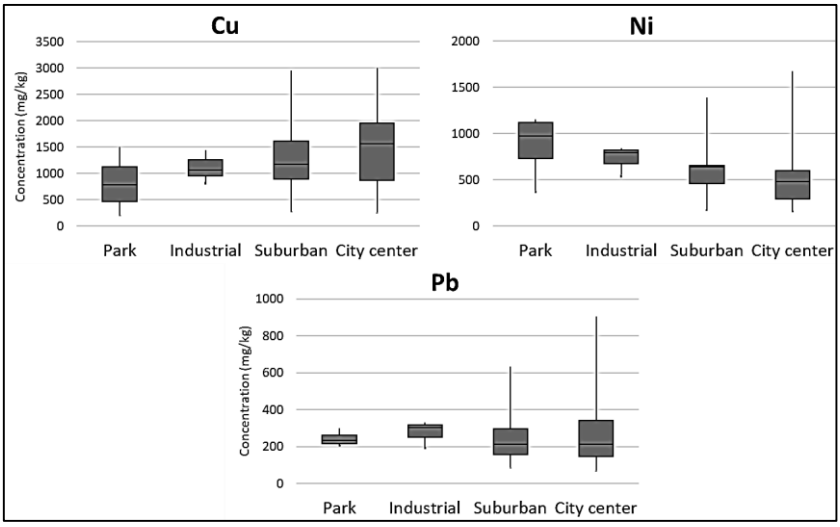

Figure 4.14. Elemental concentration ranges of selected species in suspendable RD (<10 µm) in 2018 according to sampling areas..

Conversely, mineral and lithological elements like Ni, were more occurring in parks and industrial areas. In the latter case, streets where the sampling was performed were mostly surrounded by arable fields, but had a very high share of heavy-duty vehicles (HDV). Lastly, the concentration of some elements (e.g., Pb) was irrespective of the land use. Such a behavior could be partly explained by assuming a prevalent source existing in all sampled sites, as for instance the soil, although some studies found brake wear and wheel clips as major sources of Pb in roads.
Statistical and chemometric methods could also be applied to a larger set of samples to identify the main sources of RD and estimate their contributions to the individual samples. In Torino, a source apportionment analysis using a Positive Matrix Factorization (PMF) model was performed on the dataset. The model identified the soil contribution as a constant source during both winter and summer seasons, accounting on average to 25% of the total dust mass in Torino (Fig. 4.15).

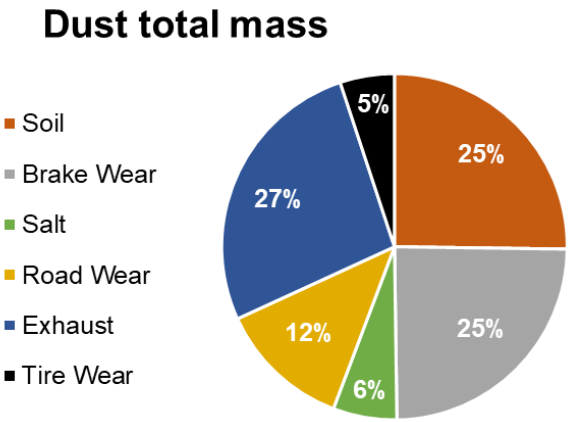

Figure 4.15. Dust contribution from sources calculated using the PMF model for Torino in 2018.

acea PINEROLESE

L'INNOVAZIONE È IL NOSTRO TERRITORIO

Chapter 5

RICE AGROECOSYSTEMS

Chapter 5.1

Rice paddy soils: Formation of hydromorphic soils

D'Amico, M.E., Said-Pullicino, D.

The study site is located in Zeme (Province of Pavia, NW Italy), situated in the low section of the Po plain between the Sesia and Agogna rivers, which includes the distal part of the glaciofluvial Würmian flat and is characterized by the presence of bumps of Holocene fluvial dynamics and levelling due to the more recent agricultural processes (Fig. 5.1). The study area has a temperate climate, with a mean annual temperature of 12.5 °C and mean annual precipitation of 830 mm.

Figure 5.1. Aerial overview of the study area (Google Satellite image; coordinate system WGS84/UTM 32 N).

Soils develop on alluvial sediment with a maximum elevation of 105 m a.s.l., characterized by a high groundwater level during spring, up to 30–50 cm below surface (Table 5.1).
Two adjacent plots were identified for this excursion, one under maize (*Zea mays*) monocropping and another under paddy rice (*Oryza sativa*) monocropping established about 30 years ago. Comparison between these two cropping systems allowed for the evaluation of agricultural management-induced effects on soil formation and functioning. Whereas maize is an upland crop, rice is cultivated in flooded paddies with water management involving continuous flooding for most of the growing season from seeding till ripening stages, except for one or two short mid-season drainage periods.

Table 5.1. Site characteristics of the Zeme profile.

Coordinates	45°11′ 31.8″ N, 8°40′ 3.7″ E
Elevation	105 m a.s.l.
Slope	~ 0%
Climate	MAAT = 12.5°C; MAP = 830 mm
Vegetation	Maize / paddy rice
Geology	Mixed, sandy to sandy loamy glaciofluvial deposits
Morphology	Basal level of the Po Plain
Landforms	LGM terraced glaciofluvial plain
Classification (WRB)	Anthraquic Luvisol (Epidystric) - Lamellic Endogleyic Luvisol

The comparison of two soil profiles without (Profile 1) and with (Profile 2) paddy management evidences extremely strong and fast processes, which are initiated by paddy rice cultivations (Fig. 5.2; Table 5.2). Non-paddy soils have few mottles, which increase with depth thanks to high seasonal water table; mottles become common only below 70 cm, in the Bgw horizon (Fig. 5.3). The Bt horizon has very well-developed clay lamellae, which evidence clay illuviation in a rather coarse soil matrix dominated by sand (Fig. 5.3). This demonstrates a rather long-lasting pedogenesis in an undisturbed pedo-environment. Pedogenic Fe oxyhydroxides showed a maximum in the Bt horizon (noticeable from dithionite-extractable Fe), but the difference with the overlying horizons was not particularly evident, evidencing weak reduction in surface horizons (Table 5.3).

Profile 1
Lamellic Endogleyic Luvisol
(maize monocropping; non-paddy management)

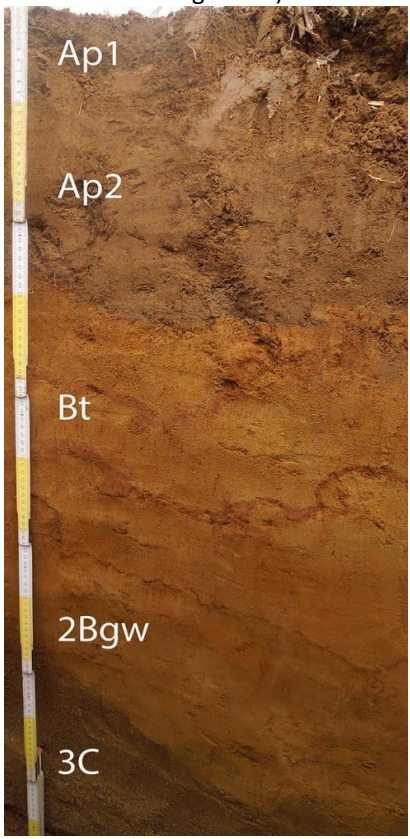

Profile 2
Anthraquic Luvisol (Epidystric)
(rice monocropping; paddy management)

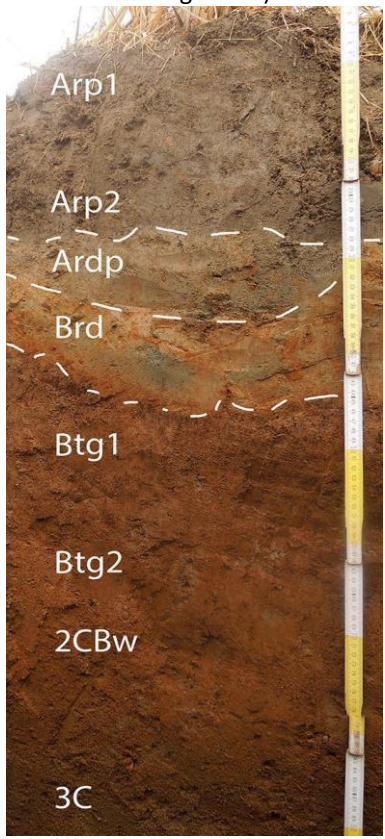

Figure 5.2. Soil profiles under non-paddy and paddy management.

Table 5.2. Detailed description of the soil profiles.

Profile 1 description – Non-paddy management		
Horizon	**Boundaries (cm)**	**Description**
Ap1	0-15 cm	Brown colour (10YR 4/3); massive, a few weakly developed granular aggregates; very scarce stone fragments, including pieces of glass, bricks etc.; common fine and very fine roots; clear wavy lower boundary
Ap2	15-30 cm	Brown colour (10YR 4/3); massive, a few weakly developed angular blocky aggregates; very scarce stone fragments, including pieces of glass, bricks etc.; abrupt wavy lower boundary
Bt	30-70 cm	Brown colour (7.5YR 4/4); massive, extremely weak angular blocky aggregates; wavy, prominent clayey lamellae crossing the whole horizon, with dark reddish colour (5YR 3/4), stone fragments absent; scarce roots; clear wavy lower boundary
2Bgw	70-85 cm	Yellowish brown (10YR 5/6); few weakly visible strong brown mottles (5%, 7.5YR 4/6); not structured (single grain), soft consistence; abrupt wavy lower boundary.
3C	85-110+ cm	Loose sand; yellowish brown (10YR 5/4); few weakly visible mottles

Profile 2 description – Paddy management		
Horizon	**Boundaries**	**Description**
Arp1	0-13 cm	Dark greyish brown colour (2.5Y 4/2); very few dark brown mottles (7.5YR 3/4); weakly developed granular structure; very scarce stone fragments, including pieces of glass, bricks etc.; abundant fine and very fine roots; clear wavy lower boundary
Arp2	13-25 cm	Dark greyish brown colour (2.5Y 4/2); very few dark brown mottles (7.5YR 3/3); very few Fe-Mn concretions; moderately developed subangular blocky structure; very scarce stone fragments; common fine and very fine roots; clear wavy lower boundary
Ardp	25-34 cm	Dark greyish brown colour (10YR 4/2); common dark brown mottles (7.5YR 3/4); oxidized root channels, with dark red covers (2.5YR 3/6); very few Fe-Mn concretions; massive, lumpy-crumbly, strongly compacted; absent stone fragments;

		very scarce fine and very fine roots; abrupt wavy lower boundary
Brd	34-43 cm	Brown colour (10YR 5/3); abundant strong brown mottles (7.5YR 4/6) and olive grey reduced zones (5Y 5/2) and dark greenish grey (gley1 4/10Y); massive, lumpy-crumbly, strongly compacted; absent stone fragments; very scarce fine and very fine roots; abrupt wavy lower boundary
Btg1	43-53 cm	Brown colour (10YR 3/4); few mottles; common (5-15%) black Fe-Mn concretions, particularly close to the upper boundary; massive, extremely weak angular blocky aggregates; more clay than above and below; stone fragments absent; scarce roots; clear wavy lower boundary
Btg2	53-80 cm	Brown colour (10YR 3/4); abundant dark brown mottles (>50%, 7.5YR 3/4), scarce olive grey reduced zones (2.5Y 5/2); common Fe-Mn concretions; massive, with few blocky angular aggregates and single grains; clear wavy lower boundary.
2CBw	80-90 cm	Dark yellowish brown (10YR 4/4); few weakly visible mottles
3C	90-110+ cm	Loose sand; dark yellowish brown (10YR 3/4); very few Fe-Mn concretions (<1%).

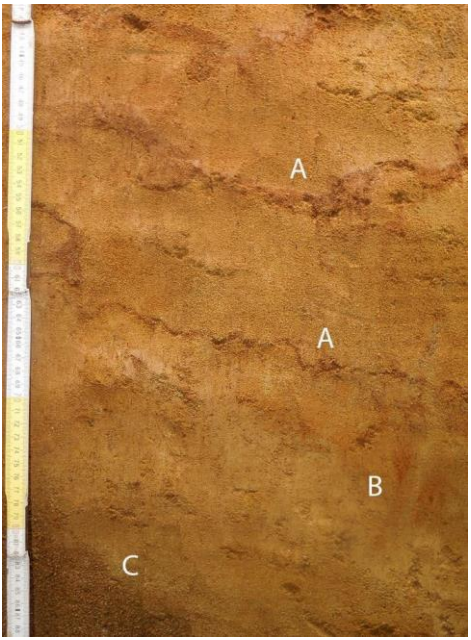

Figure 5.3. Clay lamellae in the non-paddy soil Bt horizon (A), mottles in the 2Bgw horizon (B) and the abrupt wavy boundary with the sandy alluvial substrate (C).

Table 5.3. Chemical and physicochemical analysis of the soil samples.

Profile 1 – Non-paddy management											
Horizon	BD ($g\ cm^{-3}$)	Sand ($g\ kg^{-1}$)	Silt ($g\ kg^{-1}$)	Clay ($g\ kg^{-1}$)	pH_{H2O}	pH_{CaCl2}	OC ($g\ kg^{-1}$)	N ($g\ kg^{-1}$)	Fe_o ($g\ kg^{-1}$)	Fe_d ($g\ kg^{-1}$)	Fe_o/Fe_d
Ap1	1.48	586	288	127	4.9	4.1	6.94	0.78	3.57	7.41	0.48
Ap2	1.66	605	274	121	4.7	4.0	7.61	0.82	3.57	7.20	0.50
Bt	1.55	664	204	131	5.4	4.8	2.26	0.23	3.45	11.7	0.29
2Bgw	1.51	547	347	106	6.6	5.9	1.51	0.14	1.65	9.48	0.17
3C	1.49	951	17	32	6.6	5.8	0.46	0.03	0.63	3.70	0.17

Profile 2 – Paddy management											
Horizon	BD ($g\ cm^{-3}$)	Sand ($g\ kg^{-1}$)	Silt ($g\ kg^{-1}$)	Clay ($g\ kg^{-1}$)	pH_{H2O}	pH_{CaCl2}	OC ($g\ kg^{-1}$)	N ($g\ kg^{-1}$)	Fe_o ($g\ kg^{-1}$)	Fe_d ($g\ kg^{-1}$)	Fe_o/Fe_d
Arp1	1.42	561	311	128	5.7	4.9	11.7	1.09	1.44	2.67	0.54
Arp2	1.49	565	308	127	5.4	4.8	11.4	1.10	1.51	2.72	0.55
Arpd	1.82	591	296	114	5.9	5.1	6.20	0.68	2.48	4.02	0.62
Brd	1.93	531	289	180	6.5	5.7	3.23	0.37	5.06	10.1	0.50
Btg1	1.74	520	280	199	6.7	5.9	2.39	0.29	4.67	12.1	0.39
Btg2	1.64	610	166	224	6.6	5.9	2.44	0.33	5.15	14.4	0.36
2CBw	1.61	704	105	190	6.6	5.9	2.16	0.41	4.21	12.0	0.35
3C	1.46	880	27	93	6.6	5.8	1.82	0.21	1.58	4.85	0.33

The paddy soil has extremely different morphological characteristics, caused by the artificial creation of a hard impermeable layer (plough pan) and the resulting intense seasonal waterlogging, particularly in the surface horizons (Anthraquic conditions; Fig. 5.2; Table 5.2). The tillage layer (Arp horizons) is thus characterized by intense waterlogging and reduction, which causes substantial Fe and an almost complete Mn loss. In particular, oxalate-extractable Fe is reduced by ca. 70%, while dithionite extractable Fe by 75-80% (Table 5.3). Strong reduction also characterizes the plough pan (Aprd and Bgrd horizons). As a result of this Fe loss in the topsoil, Fe is more concentrated in the subsoil horizons of the paddy soil. A nodular layer is thus formed at the upper limit of the B horizon below the plough pan. Short-range-ordered (SRO) metal oxides are also concentrated in the Btg1 horizon, evidenced by the large value of the ratio between oxalate and dithionite-extractable Fe (Table 5.3). Rice, like most wetland plants, transports oxygen via aerenchyma from the atmosphere to the roots and O_2 release into the rhizosphere results in the presence of roots channels covered by oxidized Fe coatings. This is particularly visible in the Aprd horizon, where distinct zones can be distinguished around root channels as shown by the different colours (Fig. 5.4).

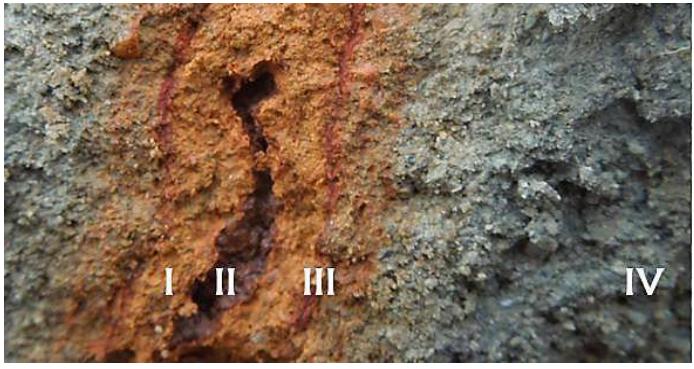

Figure 5.4. Oxidized mottles and Fe plaque in a rice root channel in the Arpd horizon. (Details: I, 5YR 5/8; II, 2.5YR 3/6; III, 2.5YR 4/8; IV, 1 gley).

Micro-scale spatial element distribution along transects from the root channels into the rhizospheric soil matrix evaluated by nano-scale secondary ion mass spectrometry (NanoSIMS) and image analysis have allowed to distinguish three distinctive zones extending from single rice roots: (i) an inner zone composed of

oxide-encrusted residues of root cells and their fragments; (ii) a thin intermediate zone comprising precipitated Fe (hydr)oxides and organic matter, but also rhizodeposits with Al compounds retained therein; and (iii) a silicate-dominated outer zone, which reflects the transition from the rhizosphere to the bulk soil (Fig. 5.5; Kölbl *et al*., 2017).

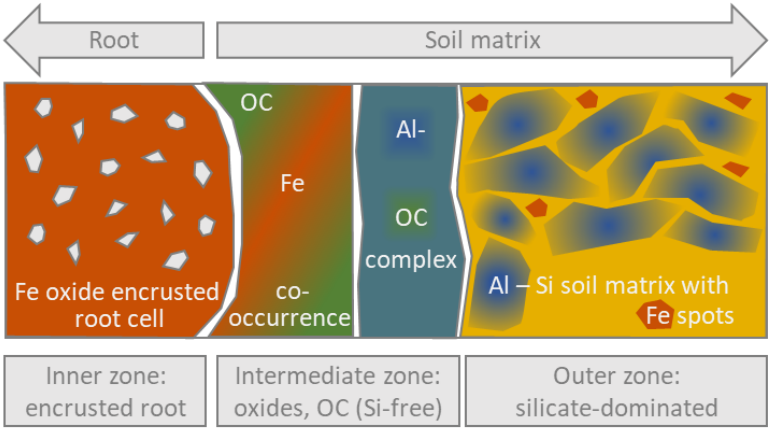

Figure 5.5. Schematic representation of element distributions in different distinctive zones extending from rice root channels to soil matrix as evaluated by NanoSIMS and image analysis (Source: Kölbl et al., 2017).

Chapter 5.2

Rice agroecosystems and climate change

Said-Pullicino, D., Bertora, C., Giannetta, B., Romani, M., Celi, L.

Rice is the most important staple food crop of the world's population feeding about 3.23 billion people, with 159 Mha under cultivation globally (FAO, 2017). Paddy soils are not only important soil resources for sustaining global food security through rice production, but also constitute the largest anthropogenic wetland with key ecosystem functions. In around 75% of this land, rice is grown in flooded paddies that result in anoxic soil conditions throughout a major part of the cropping period. Redox processes in these agro-ecosystems govern the biogeochemical cycling of carbon (C), and related ecological functions. In fact, paddy soils may serve as both a source and sink of atmospheric C and thus play an important role in global C cycling, and consequently on climate change.

Wetland rice soils conserve a large proportion of the global terrestrial C stocks (ca. 10 Pg; Kirk, 2004). The larger accumulation of organic matter (OM) in soils under paddy management with respect to other arable ecosystems has been widely recognized to contribute to the C sink functions of rice agro-ecosystems. This has often been assumed to be due to the post-harvest incorporation of large amounts of crop residues together with the retarded decomposition of OM under waterlogged conditions during several months of paddy field flooding every year. However, there is growing evidence questioning this assumption. All soil organic C accumulation mechanisms, driven by retarded decomposition, chemical recalcitrance and specific organo-mineral associations and inclusions are not yet well understood, and their role in driving C accrual in these redox-active soils remains to be investigated in detail. The interaction of OC with soil minerals and its subsequent stabilization against microbial mineralization largely depend on soil redox conditions. In the study site object of this excursion, topsoil OC stocks in the soil under paddy management (Profile 2) were 55% larger than those found in the adjacent non-paddy soil (Profile 1; Fig. 5.6a). Moreover, the paddy soil also showed subsoil OC stocks (30–100 cm)

that were 2.6-fold greater with respect to the non-paddy soil. Apart from affecting OC stocks, paddy management caused notable differences in the amounts, depth distribution and crystallinity of Fe oxides along the soil profile with respect to the non-paddy soil (Table 5.3). Topsoil horizons in Profile 2 were depleted in both short-range ordered (SRO) and crystalline Fe oxides and consequently pedogenetic Fe oxide stocks were 33 % lower with respect to the non-paddy soil Profile 1 (Fig. 5.6b), even though paddy topsoils still showed a greater proportion of Fe_o.

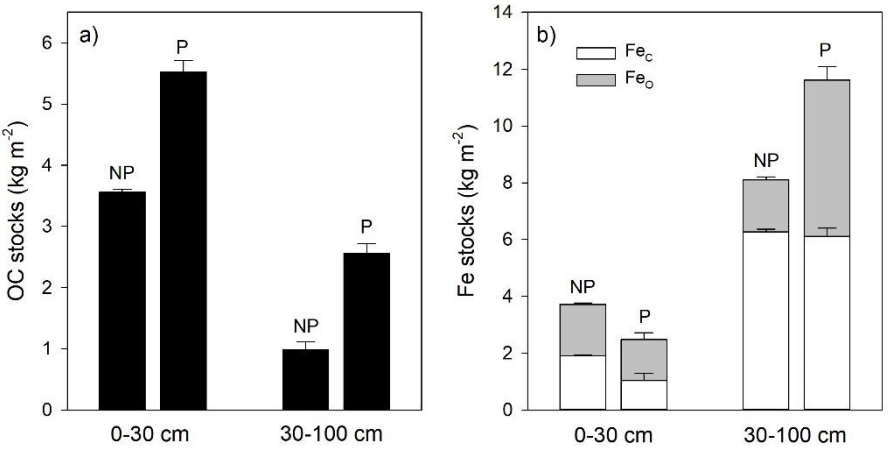

Figure 5.6. Organic C (a), and short-range ordered (Fe_o) and crystalline (Fe_c) Fe oxide (b) stocks in topsoil (0–30 cm) and subsoil (30–100 cm) horizons under non-paddy (NP; Soil profile 1) and paddy (P; Soil profile 2) management. Error bars represent standard error. (Source: Said-Pullicino et al., 2021).

On the other hand, Btg1 horizons just beneath the plough pan in soil Profile 2 were enriched in Fe oxides, particularly SRO oxides. This accounted for a 43% increase in subsoil Fe oxide stocks with respect to the adjacent non-paddy soil.

Anoxic conditions in the plough layer of paddy soils during the cropping season causes the reductive dissolution of Fe oxides leading to an increase in porewater Fe(II) concentrations and release of associated dissolved organic C (DOC) into solution. Subsequent oxidative precipitation of dissolved Fe(II) can occur either in the topsoil with the re-establishment of oxic conditions or in the O_2-rich rice rhizosphere, or in the more oxic subsoil following transport into deeper mineral horizons through percolation. This leads to the observed redistribution of pedogenetic Fe along the soil

profile and the formation of new mineral phases, mainly SRO oxides more or less associated with phyllosilicate particles (Sodano *et al.*, 2016) or Fe-OC coprecipitates (Sodano *et al*., 2017), which can contribute to the retention of OC both in the topsoil and subsoil.

Water management practices in rice paddies strongly affect the temporal trends in porewater DOC and Fe^{2+} concentrations over the cropping season, with important implications on dissolved/colloidal C and Fe mobilization from the topsoil into the subsoil. Figure 5.7 shows the trends in porewater DOC and Fe^{2+} concentrations at different depths as a function of the duration of field flooding during the cropping season, by comparing three water management systems involving water seeding with continuous flooding (WFL), dry seeding with flooding at tillering stage (DFL), and dry seeding with intermittent irrigation (DIR). Cropping systems managed under continuous flooding led to the accumulation of important amounts of DOC together with the important release of Fe^{2+} due to the reductive dissolution of Fe (hydr)oxides. Adoption of dry seeding and delayed flooding resulted in much lower DOC and Fe^{2+} concentrations in the first part of the cropping season with respect to water seeding and continuous flooding, while maintaining rice cropping under aerobic conditions by intermittent irrigation resulted in lowest DOC and Fe^{2+} contents throughout the soil profile. Together with the effects of different water management on the hydrology of these soils, the transport of DOC and Fe^{2+} from the topsoil to the subsoil was dependent on the combination of hydrological flow regime and the resulting soil moisture conditions. Over a cropping season, as much as 33–51 g C m^{-2} and 25–42 g Fe m^{-2} were lost by percolation from the silty-loam textured topsoil under continuous flooding, representing an important input of organic C and transfer of pedogenic Fe into the subsoil, possibly contributing to the formation of stable SOC in the deeper mineral horizons with important implications on C accumulation. In contrast, total DOC percolation was reduced by about 25% with the adoption of dry seeding (18–46 g C m^{-2}), and by 90% with intermittent irrigation (3.7–4.2 g C m^{-2}). Although substantial DOC and Fe fluxes reported for these poorly-developed, coarse-textured paddy soils under continuous flooding could contribute to increasing deep-soil C stocks, the contribution of these aforementioned processes to the C sink functions of rice paddies across different soil types remains an open question.

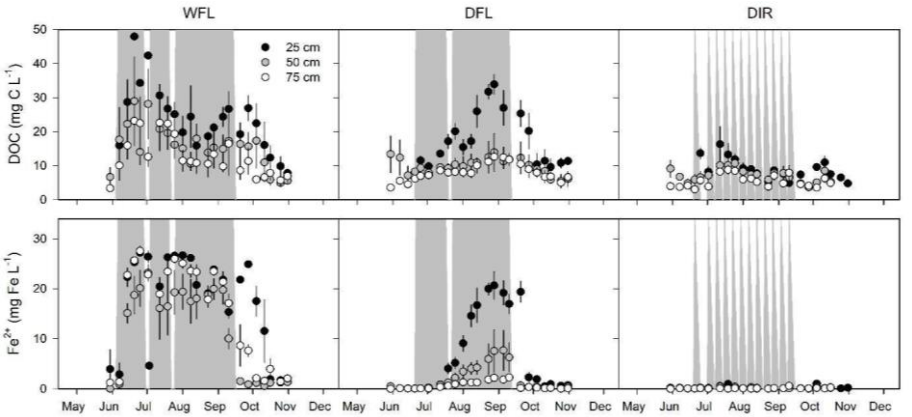

Figure 5.7. Variations in DOC and Fe^{2+} concentrations at different soil depths over a rice cropping season as a function of water management practices involving water seeding and continuous flooding (WFL), dry seeding and flooding at tillering stage (DFL), and dry seeding and intermittent irrigation (DIR). Shaded areas represent the presence of floodwater. (Source: Said-Pullicino et al. 2016).

Rice fields also represent an important global source of atmospheric methane (CH_4), one of the major greenhouse gases (GHG) responsible for global warming. Annual release rates of CH_4 from rice paddies are estimated to range between 31 and 112 Tg y^{-1}, about 5-19% of the global CH_4 emissions (Forster *et al.*, 2007). Considering that CH_4 has a global warming potential that is about 25 times that of CO_2, these emissions can partially or totally offset the C sequestration potential of these soils. Various agricultural management practices involving alternative crop residue and water management strategies have been shown to be effective in mitigating CH_4 emissions from rice paddies (Peyron *et al.*, 2016; Bertora *et al*., 2018). Figure 5.8 reports the effectiveness of different water and crop residue management practices in mitigating cumulative methane emissions over a rice cropping season from temperate rice paddies. Since the establishment of strictly anaerobic soil conditions (< –200 mV) is a prerequisite for methanogenic activity, a strong positive correlation between cumulative CH_4 emissions and soil flooding days suggests that the permanence of ponding water in the fields may control CH_4 production.

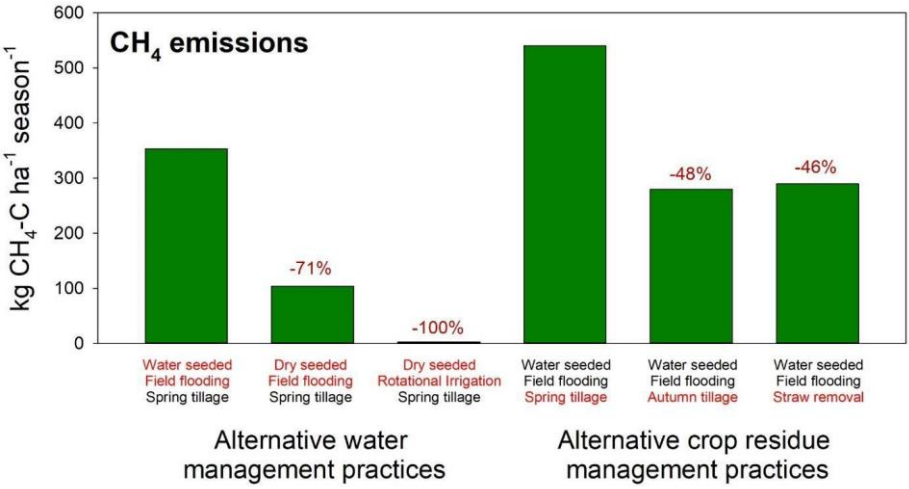

Figure 5.8. Cumulative methane emissions over a cropping season from temperate rice paddies as a function of different water and crop residue management practices. (Sources: Peyron et al., 2016; Bertora et al., 2018).

In fact, results suggest that whereas the conventional system based on water seed and continuous flooding resulted in highest total annual fluxes, any reduction in the permanence of ponding water in the field proved to be effective in mitigating CH_4 emissions by 70% in the case of dry seeding and delayed flooding, and up to 100% in the case of intermittent irrigation.

Since substrate availability for methanogens is another driver of CH_4 production, crop residue management practices can also influence cumulative CH_4 emissions. Early crop residue incorporation in autumn or straw removal were both effective in mitigating overall CH_4 fluxes with respect to the conventional practice that involves spring tillage, water seeding and continuous flooding (Fig. 5.8). Whereas methanogenic pathways occurring during the anaerobic degradation of organic matter are well characterized, the understanding of abiotic and biotic factors that control the contribution of different C sources to CH_4 production (e.g., crop residues, root exudates, organic amendments, soil organic matter), as well as the temporal and spatial dynamics of methanogenic and methanotrophic microbial communities under alternating redox conditions is far from complete.

In conclusion, rice paddies are major contributors to global GHG emissions but at the same time hold an important potential to sequester C. The balance between C source and sink functions of these agro-ecosystems is not always clear due to the high variability induced by different management practices and soil types. Moreover, soil processes driving the trade-off between CH_4 emissions and C sequestration are still not fully understood, especially due to the complex interactions between plants, soils and microorganisms. Future research initiatives should aim to further unravel the contribution of different processes to the C source/sink function of rice paddies across different soil types, as these outcomes will have important implications on the adoption of future paddy field management strategies concerning the management of belowground C pools and fluxes, and the mitigation of GHG emissions in a wider vision of improving the sustainability of modern rice cropping systems, while maintaining the physiological requirements of rice plants and grain yields that lie at the basis of the farmers' livelihoods.

Chapter 5.3

Adaptation of the rice plant to water management and grain nutritional quality

Sacchi, G.A.

Global warming and competition between lowland rice and other seasonal crops, along with industrial and civic requirements for water, may cause physical and/or economic water shortages for rice cultivation. It is expected that several million hectares of currently lowland irrigated rice systems will experience water scarcity by 2050. Development of water-saving techniques is thus essential to improve the sustainability of irrigated rice systems. In this regard, alternate wetting and drying (AWD), which involves intermittent field irrigation without maintaining standing water, has been shown to be effective in increasing rice water use efficiency (WUE) compared to continuous flooding (PF). Several studies ascertained that AWD could markedly improve WUE up to more than 60%. Nevertheless, its effects on rice yield are variable and not completely understood due to the action of multiple factors, such as the severity and duration of the dry periods, the number of dry-wetting cycles during the season, and the local microclimatic conditions. Furthermore, limited information about the adaptability of rice cultivars to AWD is available.

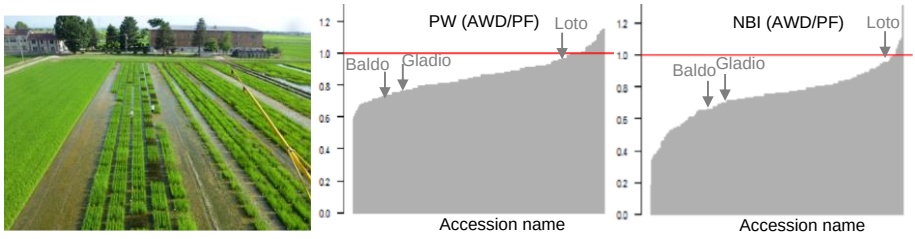

Figure 5.9. Experimental field at CREA – Vercelli (left); distribution of phenotypic value ratio (AWD/PF) for yield/panicle (PW) (center); Nitrogen Balance Index (NBI) (right). (Source: Volante et al., 2017).

For this reason, about 300 japonica rice accessions belonging to the rice germplasm collection hold at the Research Centre for Cereal and Industrial Crops (CREA, Vercelli), including most of the Italian varieties usually grown under PF, were phenotypically characterized for traits related to phenology, physiology and yield within a two year-period in field conditions under PF and AWD (Fig. 5.9). The yield performance, as assessed by grain yield/panicle (PW), was in general reduced by AWD (Fig. 5.9). As suggested by the values of Nitrogen Balance Index (NBI) retrieved in the flag leaves at flowering (Fig. 5.9), the accessions showing the best yield under AWD were able to better use the added N-fertilizer.

The possibility that yield losses due to AWD could be balanced by better grain quality and nutritional value was tested in three accessions showing different sensitivity to AWD (Baldo, Gladio and Loto, Fig. 5.10). In both seasons, the water-saving management reduced yields of Baldo and Gladio but not of Loto. AWD did not affect apparent amylose content and N-protein concentration (indicators of rice grain quality) in Loto's brown grains, but increased their content in total tocols, γ-oryzanol, and flavonoids, as well as their antioxidant activity. These findings suggest that the adoption of varieties tolerant to AWD-related stresses, such as Loto, could combine yield and nutritional benefits to improve the product quality.

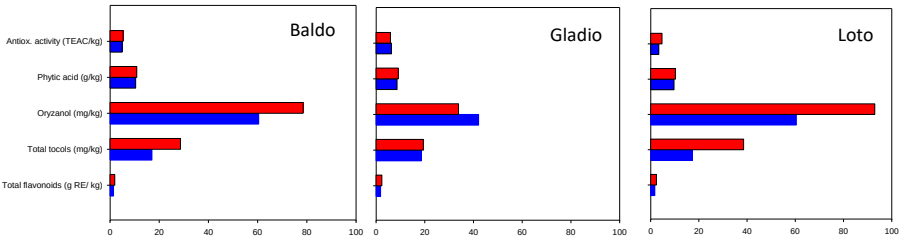

Figure 5.10. Total concentration of health-promoting compounds and antioxidant activity in the brown grain of three varieties under permanent flooding (blue bars) or alternate wetting and dry (red bars). (source: Orasen et al. 2019).

Water management strongly controls soil redox-driven reactions and microbial activity, with consequent effects on macro- and micro-nutrient plant availability and uptake. Several studies indicate that AWD promotes crop N- and P-use efficiency while determining a different effect on plant availability and uptake of essential microelements (mainly Fe and Zn). A ionomic approach using the same japonica rice panel grown under PF and AWD showed that Fe, Zn, and Cu grain density increased

with AWD on average 1.3-, 1.6- and 2.0-times, respectively, compared to PF. Such an effect was genetic-dependent. Thus, AWD management could improve N- and P-use efficiency and microelement nutritional values of rice grains; however, possible negative consequences on grain safety cannot be ruled out, because toxic elements can additionally accumulate (see Chapter 5.5).

Genotypes can show different yield stability and grain quality under AWD conditions. Identifying the genomic basis of this variability could be helpful in developing new rice genotypes more adapted to water-saving technologies. Valuable information was obtained by genotype-phenotype association studies (GWAS) after identifying 30,000 single nucleotide polymorphism (SNPs) in the CREA' s rice panel by genotype-by-sequence. Several markers associated traits (MTAs) were identified, corresponding to physiological and agronomic responses to AWD. More of them are apparently linked to plant responses to drought stress imposed by AWD. With respect to the ionomic approach, an interesting MTA (MTA_8_Zn), localized into chromosome 8 (Fig. 5.11) and related to Zn accumulation in grain was identified in both water management techniques.

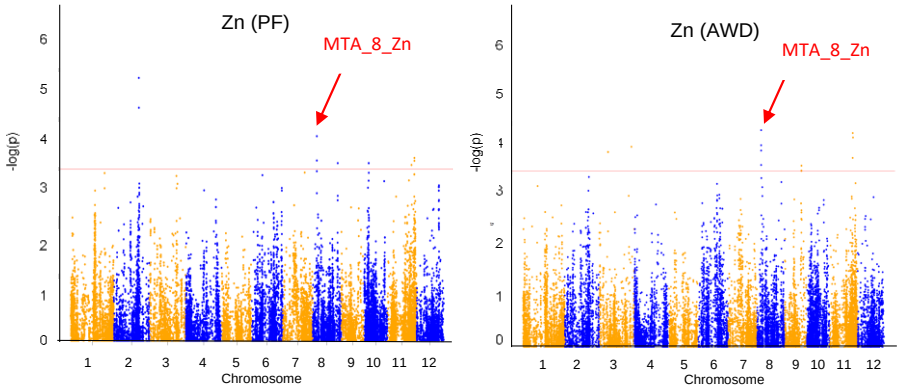

Figure 5.11. Manhattan plots of the significant associations detected for the concentration of Zn in the brown grain of the rice panel grown under PF or AWD conditions.

Within MTA_8, the gene OsABCG18 coding for a cytokinin transporter is included, whose activity is related to grain yield, root system architecture, and Zn nutrition in rice. This result in particular highlights how the plasticity of root system architecture can play a role in plant adaptive responses to environmental conditions with interesting effects on quantitative and qualitative traits of rice yield.

Chapter 5.3

Food safety: managing inorganic contaminants in rice paddies

Martin, M., Romani, M., Tenni, D., Beone, G.M., Fontanella, M.C.

Rice accumulates larger concentrations of arsenic (As) compared to other cereal crops, even when cultivated in uncontaminated soils, as a consequence of growing under flooded conditions. The spatial distribution of As along the soil profile and its temporal release into the soil solution generally follow Fe and Mn reduction pathways that are also affected by organic matter quantity and quality. The complexity of As chemistry in soil is increased by microbially-mediated reactions that are not only able to reduce arsenate to the more soluble and toxic arsenite, but are also responsible for the formation of a number of organic As compounds, mostly represented by methylated forms, such as dimethylarsinic acid (DMA) or monomethylarsinic acid (MMA). When rice soils become strictly anaerobic, As can also react with sulfur, forming thiolated As compounds that can also include one or more methyl groups (Wang *et al*., 2020a and b). Most As in rice grain is in the form of inorganic arsenite with small amounts of arsenate. Organic As detected in rice tissues and grain is mostly DMA with traces of MMA, although recently thio- and methylthioarsenates have been detected in rice. In particular, dimethylmonothioarsenate can be found in rice grain at concentrations comparable to DMA (Planer-Friedrich *et al*., 2021).

While the threshold set for the commercialization of husked (0.25 mg inorganic As kg^{-1}) and white rice (0.20 mg inorganic As kg^{-1}) in the EU is seldom exceeded, in Italian rice, almost half of the rice produced in our territories does not meet the stricter requirements for the preparation of rice-based baby foods (0.10 mg inorganic As kg^{-1}) (Tenni *et al*. 2017).

Besides As, cadmium (Cd) is another inorganic contaminant in rice, particularly because several strategies aimed at counteracting As uptake by the rice plant may

result in an increase in Cd uptake. The limit for Cd in rice for adult consumption has just been changed from previous 0.20 mg kg^{-1} to 0.15 mg kg^{-1}, while the maximum Cd content in rice for baby food is 0.04 mg kg^{-1}.

*Table 5.4. Total As and Cd in Lomellina paddy rice topsoils (*n *= 170) and in samples of white rice (*n *= 82).*

	Soil (mg kg^{-1})		White rice (µg kg^{-1})	
	As	**Cd**	**As_{TOT}**	**Cd**
Mean	9.81	0.20	152.6	56.3
Median	6.50	0.18	142.4	27.6
S.D.	10.80	0.12	59.5	72.0
Max	89.62	0.82	315.0	386.0
Min	1.92	*b.d.l.*	47.0	*b.d.l.*

Besides a few outliers, soil As concentrations in the soils of Lomellina (Table 5.4) are in line with the European mean (9 mg kg^{-1}), as well as Cd (0.20 mg kg^{-1}). All rice grain samples analyzed are generally below the threshold for inorganic As (mean, 126 µg kg^{-1} As_i, representing over 80% of the total) and for total Cd, with very few exceptions. The relationship between the concentration of As in soil and in the rice grain is weak, often masked by soil heterogeneity even in the relatively small area examined between Garlasco, SE, to Robbio, NW. However, stronger correlations appear when soils are grouped for physicochemical similarity and similar agronomic management (Figure 5.12). The soil characteristics most commonly related to rice As uptake were soil texture and organic C content. Conversely, Cd content in rice did not show any relationship with soil Cd contents, probably due to the very low concentrations and the predominant effect of water management.

Several strategies have been adopted to limit As concentration in rice by primarily acting on water management. It has been proven that growing rice aerobically greatly decreases its As content. However, more oxidizing soil conditions are associated with lower pH and sulfide oxidation, diminishing the stability of Cd-bearing minerals. Thus, increased Cd concentrations often accompany the decrease of As content in aerobic rice. A fine tuning of water management is thus required to decrease As uptake while avoiding an increase in Cd.

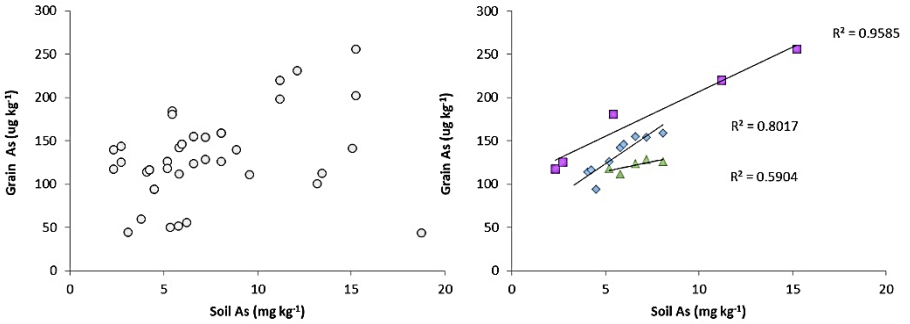

Figure 5.12. Relationship between As concentrations in (a) the rice grain and soil sampled from some paddy fields in Lomellina, and (b) grouped on the basis of homogeneous soil properties and agronomic practices.

The occurrence of a short drying at the stage of stem elongation can be exploited to lower As concentration in soil solution when rice plants are particularly sensitive to As uptake (Fig. 5.13). The effect is clearly reflected by plant uptake and storage in the rice grain in semi-controlled environments (Zecchin *et al.*, 2017), but the results are encouraging even when applied at farm level (Fig. 5.14). The effectiveness, however, improves in soils with rapid drainage. Conversely, drying the soil later in the cropping season, after rice flowering, would not decrease As, while it would largely increase Cd concentration in grain.

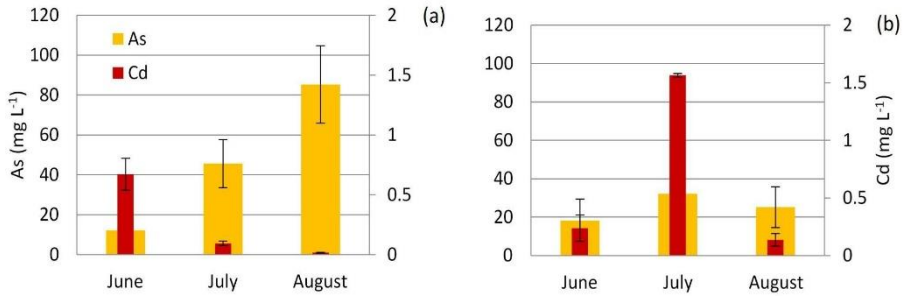

Figure 5.13. As and Cd in soil solution during the cropping season in two adjacent paddy fields in Mortara (PV): (a) water sowing and continuative submersion; (b) dry sowing with 10 days drying at stem elongation.

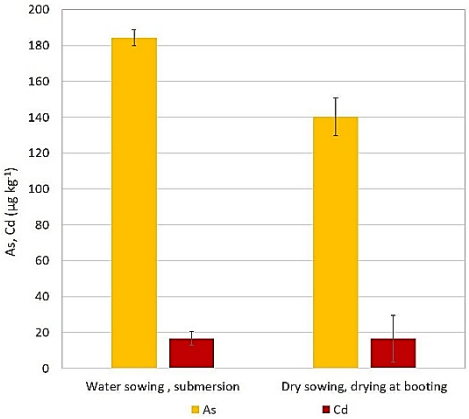

Figure 5.14. As and Cd in rice grain grown in two adjacent paddy fields in Mortara (PV): water sowing and continuative submersion, and dry sowing with 10 days drying at stem elongation.

The effect of crop residues, organic amendment, and green manure is still debated. While the effect of organic inputs is normally beneficial for Cd immobilization, easily degradable organic materials can fuel microbially induced reductive reactions and As dissolution. The use of silicon and sulfur fertilization, although largely treated in literature, does not seem to improve the quality of rice grain at field level, while liming has proven to be effective in limiting Cd uptake (Figure 5.15).

Figure 5.15. Total As and Cd contents in rice grain of plants grown with different amendments in a paddy field in Castello d'Agogna (PV). Rice was dry sown and continuously submerged.

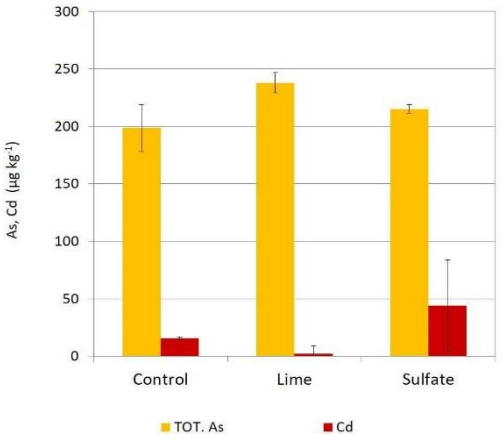

Even in a relatively homogeneous environment, such as the paddy rice fields of the western Po plain, presently there is not a single solution suitable for all rice farms;

however, good results can be achieved by combining different strategies tailored on soil physicochemical characteristics, agronomic practices and climatic trends. Rice samples high in Cd are normally low or even very low in As the reason mostly depending on water management, but also related to varietal characteristics. While in the recent past rice was typically sowed in water and the crop was kept under submersion for the whole growing season, presently dry sowing with retarded submersion is becoming the prevalent technique; moreover, water scarcity is becoming increasingly common in spring and summer, so that alternating wetting and drying may be a forced practice in driest seasons. A trend with decreasing As, while increasing Cd in rice grain may thus become increasingly common in future years, requiring progressive adjustments of the combined techniques.

AZIENDA AGRICOLA

MARTINENGO LUIGI

VIA STRADA PER ROSASCO, 2
LANGOSCO (PV)
luigimartinengo@tiscali.it


CAFFÈ VERGNANO 1882
CAFFÈ VERGNANO 1882

BIBLIOGRAPHY

Aeschimann, D., Lauber, K., Moser, D.M., Theurillat, J.p., Michel, A. Flora alpina: atlante delle 4500 piante vascolari delle Alpi. Zanichelli, 2004.

Ajmone Marsan, F., Biasioli, M., 2010. Trace elements in soils of urban areas. Water Air Soil Pollut., 213, 121–143.

Ajmone Marsan, F., Zanini, E. Soils in urban areas. In: The soils of Italy, World soils Book Series. Costantini, E.A.C., Dazzi, D., (Eds), Springer Science+Business media, 2013.

Ajmone-Marsan, F., Padoan, E., Madrid, F., Vrščaj, B., Biasioli, M., Davidson, C.M., 2019. Metal release under anaerobic conditions of urban soils of four European cities. Water, Water Air Soil Pollut., 230, 53.

Amato, F. Non-Exhaust Emissions, An Urban Air Quality Problem for Public Health; Impact and Mitigation Measures. Accademic Press, 2018.

ARPA Piemonte, 2020. Dipartimento Valutazioni Ambientali - Sviluppo dello studio sulla contaminazione diffusa del suolo, per la definizione di valori di fondo naturale ed ai fini della valutazione di situazioni di inquinamento diffuso ai sensi del D.Lgs. 152/2006. Relazione tecnica di Fabietti G.

Ashraf, S., Ali, Q., Zahir, Z.A., Ashraf, S., Asghar, H.N., 2019. Phytoremediation: Environmentally sustainable way for reclamation of heavy metal polluted soils. Ecotoxicol. Environ. Saf. 174, 714-727.

Assalay, A.M., Jefferson, I., Rogers, C.D.F. Smalley, I.J., 1998. Fragipan formation in loess soils: development of the Bryant hydroconsolidation hypothesis. Geoderma 83, 1-16.

ASTM, 1984. Standard Test Method for Methylene Blue Index of Clay. C 837-81 Section XV, vol. 15.02.

ASTMD 4318-10e1, 2010. Standard Test Methods for Liquid Limit, Plastic Limit, and Plasticity Index of Soils. ASTM International, West Conshohocken, PA.

Barden, L., Mcgown, A., Collins, K., 1973. The collapse mechanism in partly saturated soil. Eng. Geol. 7(1), 49-60.

Balestrini, R., Arese, C., Freppaz, M.,Buffagni, A., 2013. Catchment features controlling nitrogen dynamics in running waters above the tree line (central Italian Alps), Hydrol. Earth Syst. Sci. 17, 989-1001.

Bertora, C., Cucu, M.A., Lerda, C., Peyron, M.,..., Said-Pullicino, D., 2018. Dissolved organic carbon cycling, methane emissions and related microbial populations in temperate rice paddies with contrasting straw and water management. Agric. Ecosyst. Environ. 265, 292-306.

Bhatia, M.P., Das, S. B., Xu, L., Charette, M.A., Wadham, J.L., Kujawinski, E.B., 2013. Organic carbon export from the Greenland ice sheet. Geochim. Cosmochim. Acta 109, 329-344.

Biasioli, M., Barberis, R., Ajmone Marsan, F., 2006. The influence of a large city on some soil properties and metals content. Sci. Total Environ., 356, 154-164.

Biasioli, M., Ajmone-Marsan, F., 2007. Organic and inorganic diffuse contamination in urban soils: the case of Torino (Italy). J. Environ. Moni., 9, 862-868.

Biasioli, M., Fabietti, G., Barberis, R., Ajmone-Marsan, F., 2012. An appraisal of soil diffuse contamination in an industrial district in northern Italy. Chemosphere 88, 1241-1249.

Billard, A., Orombelli, G., 1986. Quaternary glaciations in the French and Italian piedmonts of the Alps. Quat. Sci. Rev. 5, 407-411.

Bockheim, J.G., Hartemink, A.E., 2013. Soils with fragipan in the USA. Catena 104, 232-242.

Bonifacio E., Petrillo M., Petrella F., Tambone F., Celi L., 2015. Alien red oak affects soil organic matter cycling and nutrient availability in low fertility well-developed soils. Plant Soil 395, 215-229.

Callaway, R.M., Aschehoug, E.T., 2000. Invasive plants versus their new and old neighbors: a mechanism for exotic invasion. Science 290, 521-523.

Cobbett, C., Goldsbrough, P., 2002. Phytochelatins and metallothioneins: roles in heavy metal detoxification and homeostasis. Annu. Rev. Plant Biol. 53, 159-182.

Colombo, N., Bocchiola, D., Martin, M., Confortola, G.,..., Freppaz, M., 2019. High export of nitrogen and dissolved organic carbon from an Alpine glacier (Indren Glacier, NW Italian Alps). Aquat Sci. 81(4), 1-13.

Costantini, E.A.C., Carnicelli, S., Sauer, D., Priori, S.,...., Lorenzetti, R., 2018. Loess in Italy: genesis, characteristics and occurrence. Catena 168, 14-33.

Cremaschi, M., Van Vliet-Lanoë, B., 1990. Traces of frost activity and ice segregation in Pleistocene loess deposits and till of northern Italy: Deep seasonal freezing or permafrost? Quat. Int. 5, 39-48.

Delgado-Baquerizo, M., Eldridge, D.J., Maestre, F.T.,..., Singh, B.K., 2017. Climate legacies drive global soil carbon stocks in terrestrial ecosystems. Sci. Adv. 3(4).

Desjardins, D., Brereton, N.J.B., Marchand, L., Brisson, J., Pitre, F.E., Labrecque, M., 2018. Complementarity of three distinctive phytoremediation crops for multiple-trace element contaminated soil. Sci. Total Environ. 610, 1428-1438.

Ding, J., Wang, T., Piao, S., Smith, P.,..., Zhao, L., 2019. The paleoclimatic footprint in the soil carbon stock of the Tibetan permafrost region. Nat. Commun. 10(1), 4109.

Ernakovich, J.G., Hopping, K.A., Berdanier, A.B., Simpson, R.T.,..., Wallenstein, M.D., 2014. Predicted responses of arctic and alpine ecosystems to altered seasonality under climate change. Glob Chang Biol. 20(10), 3256-3269.

FAO, 2006. Guidelines for Soil Description. FAO, Rome.

FAO, 2017. FAOSTAT: FAO Statistical Databases.

Forno, M.G., De Luca, D.A., Bonasera, M., Bucci, A.,..., Taddla, G., 2018. Synthesis on the Turin subsoil stratigraphy and hydrogeology (NW Italy). Alp. Mediterr. Quat. 31(2), 147-170.

Forster, P., Ramaswamy,V., Artaxo, P., Berntsen, T.,..., Van Dorland, R. Changes in Atmospheric Constituents and in Radiative Forcing. In: Climate Change 2007: The Physical Science Basis. Contribution of Working Group I to the Fourth Assessment Report of the Intergovernmental Panel on Climate Change. (eds Solomon, S., Qin, D., Manning, M., Chen, Z., *et al.*) Cambridge University Press, 2007.

Gallino L. La scomparsa dell'Italia industriale. Einaudi, 2003.

Gordon, J.E., Barron, H.F., 2013. The role of geodiversity in delivering ecosystem services and benefits. Scott. J. Geol. 49(1), 41-58.

Gray, J.M. Geodiversity: Valuing and Conserving Abiotic Nature. Wiley Blackwell: Chichester, II, 2013.

Grifoni, M., Schiavon, M., Pezzarossa, B., Petruzzelli, G., Malagoli, M., 2015. Effects of phosphate and thiosulphate on arsenic accumulation in the species Brassica juncea. Environ. Sci. Pollut. Res. 22(4), 2423-2433.

Guidi Nissim, W.; Palm, E.; Mancuso, S.; Azzarello E., 2018. Trace element phytoextraction from contaminated soil: a case study under Mediterranean climate. Environ. Sci. Poll. Res. 25, 9114-9131.

Hack, H., Bleiholder, H., Buhr, L., Meier, U.,..., Witzenberger, A., 1992. Einheitliche Codierung der phänologischen Entwicklungsstadien mono- und dikotyler Pflanzen – Erweiterte BBCH-Skala, Allgemein Nachrichtenbl. Deut. Pflanzenschutzd., 44, 265-270.

Harden, J.W., 1982. A quantitative index of soil development from field descriptions: examples from a chronosequence in Central California. Geoderma 28, 1-28.

Harden, J.W., Taylor, E.M., 1983. A quantitative comparison of soil development in four climatic regimes. Quat. Res. 20, 342-359.

Hasanuzzaman, M., Nahar, K., Anee, T.I., Fujita, M., 2017. Glutathione in plants: biosynthesis and physiological role in environmental stress tolerance. Physiol. Mol. Biol. Plants 23(2), 249-268.

Hood, E., Scott, D., 2008. Riverine organic matter and nutrients in southeast Alaska affected by glacial coverage. Nat. Geosci. 1(9), 583-587.

Hood, E., Battin, T.J., Fellman, J., O'neel, S., Spencer, R.G., 2015. Storage and release of organic carbon from glaciers and ice sheets. Nat. Geosci. 8(2), 91-96.

Hütsch, B.W., Augustin, J., Merbach., W., 2002. Plant rhizodeposition-an important source for carbon turnover in soils. J. Plant. Nutr. Soil 165, 397-407.

IPLA - Regione Piemonte 2001. Carta dei suoli 1:50.000. Rev. 2020. http://www.geoportale.piemonte.it/

Islam, A.K.M.E., Lotse, E.G., 1986.Quantitative mineralogical analysis of some Bangladesh soils with X-ray, ion exchange and selective dissolution techniques. Clay Miner., 21, 31-42.

Kaliakin V.N. (Ed.). Soil Mechanics: calculations, principles, and methods. Elsevier, 2017.

Khawmee, K., Suddhiprakarn, A., Kheoruenromne, I., Singh, B., 2013. Surface charge properties of kaolinite from Thai soils. Geoderma 192, 120-131.

Kirk, G. The Biogeochemistry of Submerged Soils. John Wiley & Sons, 2004.

Koerselman, W., Meuleman, A.F.M., 1996. The vegetation N:P ratio: a new tool to detect the nature of nutrient limitation. J. Appl. Ecol. 33, 1441-1450.

Kölbl, A., Schweizer, S.A., Mueller, C., Höschen, C.,…, Kögel-Knabner, I., 2017. Legacy of rice roots as encoded in distinctive microsites of oxides, silicates, and organic matter. Soils 1, 2.

Li, X., Ding, Y., Xu, J., He, X., Han, T.,…, Li, Q., 2018. Importance of mountain glaciers as a source of dissolved organic carbon. J. Geophys. Res. Earth Surf. 123(9), 2123-2134.

Li, Y., Ajmone-Marsan, F., Padoan, E., 2021. Health risk assessment via ingestion and inhalation of soil PTE of an urban area. Chemosphere (in press).

Madrid, L., Diaz-Barrientos, E., Ruiz-Cortés, E., Reinoso R.,…, Ajmone-Marsan, F., 2006. Variability in concentrations of potentially toxic elements in urban parks from six European cities. J. Environ. Monit., 8, 1158-1165.

Magnani, A., Viglietti, D., Godone, D., Williams, M.W., Balestrini, R., Freppaz. M., 2017. Interannual Variability of Soil N and C Forms in Response to Snow—Cover duration and Pedoclimatic Conditions in Alpine Tundra, Northwest Italy. Arct. Antarct. Alp. Res. 49, 227-242.

Millard, P., Grelet, G.A., 2010. Nitrogen storage and remobilization by trees: Ecophysiological relevance in a changing world. Tree Physiol. 30, 1083-1095.

Moreno-Maroto, J.M., Alonzo-Azcarate, J., 2018. What is clay? A new definition of “clay” based on plasticity and its impact on the most widespread soil classification systems. Appl. Clay Sci. 161, 57-63.

Negri, S., Raimondo, E., D’Amico, M.E., Stanchi, S., Basile, A., Bonifacio, E., 2021. Loess-derived polygenetic soils of North-Western Italy: a deep characterization of particle size, shape and color to draw insights about the pas. Catena 196, 104892.

Nord, E.A., Lynch, J.P., 2009. Plant phenology: A critical controller of soil resource acquisition. J. Exp. Bot. 60(7), 1927-1937.

Orasen, G., De Nisa, P., Lucchini, G., Abruzzese, A.,…, Sacchi, G.A., 2019. Continuous flooding or alternate wetting and drying differently affect the accumulation of health-promoting phytochemicals and minerals in rice brown grain. Agronomy 9, 628.

Padoan, E., Rome, C., Ajmone Marsan, F., 2017. Bioaccessibility and size distribution of metals in road dust and roadside soils along a peri-urban transect. Sci. Total Environ. 601-602, 89-98.

Padoan E., Passarella I., Prati M., Bergante S., Facciotto G., Ajmone-Marsan F., 2020. The Suitability of Short Rotation Coppice Crops for Phytoremediation of Urban Soils. Appl. Sci. 10, 307.

Peyron, M., Bertora, C., Pelissetti, S., Said-Pullicino, D.,..., Sacco, D., 2016. Greenhouse gas emissions as affected by different water management practices in temperate rice paddies. Agric. Ecosyst. Environ. 232, 17-28.

Perotti, L., Carraro, G., Giardino, M., De Luca, D.A., Lasagna, M., 2019. Geodiversity evaluation and water resources in the Sesia Val Grande UNESCO Geopark (Italy). Water 11 (10), 2102.

Perrone, G., Morelli, M., Piana, F., Fioraso, G.,..., Tallone, S., 2013. Current tectonic activity and differential uplift along the Cottian Alps/Po Plain boundary (NW Italy) as derived by PS-InSAR data. J. Geodyn., 66, 65-78.

Piana, F., Fioraso, G., Irace, A., Mosca, P.,…, Vigna, G.B., 2017. Geology of Piemonte Region (NW Italy, Alps-Apennines interference zone). J. Maps 13, 395-405.

Pilon-Smits, E., 2005.Phytoremediation. Annu. Rev. Plant. Biol., 5, 15-39.

Pintaldi E, D'Amico M. E., Colombo N., Martinetto E.,..., Freppaz, M. Hidden paleosols on a high-elevation Alpine plateau (NW Italy): evidence for Lateglacial Nunatak? Submitted to Glob. Planet. Change.

Pintaldi E., Quaglia, E., Viglietti, D., Pittarello, M.,..., Freppaz, M. Snowbed communities and soil C and N dynamics during a four-year investigation in the NW-Italian Alps. Submitted to Arct. Antarct. Alp. Res.

Pintaldi, E., D'Amico, M.E., Colombo, N., Colombero, C.,..., Freppaz, M., 2021. Hidden soils and their carbon stocks at high-elevation in the European Alps (North-West Italy). Catena 198, 105044.

Planer-Friedrich, B., Blanco, A.E.C., Kerl, C.F.J. 2021. Detection of thioarsenates in rice grains and rice products. Agric. Food Chem. 69, 2287-2294.

Poggio, L., Vrščaj, B., Schulin, R., Hepperle, E., Ajmone Marsan, F., 2009. Metals pollution and human bioaccessibility of topsoils in Grugliasco (Italy). Environ. Pollut. 157, 680-689.

Raimondo, E., Falsone, G., D'Amico, M.E., Stanchi, S., Celi, L., Bonifacio, E., 2019. Characteristics of fragipan B horizons developed on different parent material in North-Western Italy. Arch. Agron. Soil. Sci. 65, 308-321.

Rodrigues, S., Pereira, M.E., Duarte, A.C., Ajmone-Marsan, F.,…, Vrščaj, B., 2006. Mercury in urban soils: a comparison of local spatial variability in six European cities. Sci. Total Environ., 368, 926-936.

Said-Pullicino, D., Miniotti, E.F., Sodano, M., Bertora, C.,..., Celi, L., 2016. Linking dissolved organic carbon cycling to organic carbon fluxes in rice paddies under different water management practices. Plant Soil 401, 273-290.

Said Pullicino, D., Giannetta, B., Demeglio, B., Missong, A.,..., Celi, L., 2021. Redox-driven changes in water-dispersible colloids and their role in carbon cycling in hydromorphic soils. Geoderma 385, 114894.

Sakai, A., Ohsawa, M., 1993. Vegetation pattern and microtopography on a landslide scar of Mt Kiyosumi, central Japan. Ecol. Res. 8, 47-56.

Schiavon, M., Wirtz, M., Borsa, P., Quaggiotti, S., Hell, R., Malagoli, M., 2007. Chromate differentially affects the expression of a high-affinity sulfate transporter and isoforms of components of the sulfate assimilatory pathway in Zea mays (L.). Plant biology (Stuttgart, Germany) 9(5), 662-671.

Schiavon, M., Pilon-Smits, E.A., Wirtz, M., Hell, R., Malagoli, M., 2008. Interactions between chromium and sulfur metabolism in Brassica juncea. J. Environ. Qual. 37(4), 1536-1545.

Schiavon, M., Galla, G., Wirtz, M., Pilon-Smits, E.A.,..., Malagoli, M., 2012. Transcriptome profiling of genes differentially modulated by sulfur and chromium identifies potential targets for phytoremediation and reveals a complex S-Cr interplay on sulfate transport regulation in B. juncea. J. Hazard. Mater. 239-240, 192-205.

Singer, G.A., Fasching, C., Wilhelm, L., Niggemann, J.,..., Battin, T.J., 2012. Biogeochemically diverse organic matter in Alpine glaciers and its downstream fate. Nat. Geosci. 5(10), 710-714.

Slemmons, K.E., Rodgers, M.L., Stone, J.R., Saros, J.E., 2017. Nitrogen subsidies in glacial meltwaters have altered planktonic diatom communities in lakes of the US Rocky Mountains for at least a century. Hydrobiologia 800(1), 129-144.

Smalley, I.J., Bentley, S.P., Markovic, S.B., 2016. Loess and fragipans: Development of polygonal-crack-network structures in fragipan horizons in loess ground. Quat. Int. 399, 288-1233.

Sodano, M., Said-Pullicino, D., Fiori, A.F., Catoni, M., Martin, M., Celi, L., 2016. Sorption of paddy soil-derived dissolved organic matter on hydrous iron oxide-vermiculite mineral phases. Geoderma 261, 169-177.

Sodano, M., Lerda, C., Nisticò, R., Martin, M.,..., Said-Pullicino, D., 2017. Dissolved organic carbon retention by coprecipitation during the oxidation of ferrous iron. Geoderma 307, 19-29.

Soil Survey Staff. Keys to Soil Taxonomy. Soil Survey Staff, USDA-SCS Natural Soil Survey Center, XII, 2014.

Sovers, G. Introductory Soil Mechanics and Foundations: Geotechnical Engineering. Macmillan, IV, 1979.

Stanchi, S., Bonifacio, E., Zanini, E., 2008. Mass-Size Fractal Dimension of Primary and Aggregated Particles and Soil Profile Development. Soil Science 173, 87-95.

Stanchi, S., Negri, S., D'Amico, M.E., Raimondo, E., Bonifacio, E., 2021. Atterberg limits fail in recognizing fragipan horizons. Catena 202, 105282.

Sterling, A.A., Peco, B., Casado, M.A., Galiano, E.F., Pineda, F.D., 1984. Influence of Microtopography on Floristic Variation in the Ecological Succession in Grassland. Wiley on behalf of Nordic Society Oikos Stable 42(3), 334-342.

Stibal, M., Šabacká, M., Žárský, J., 2012. Biological processes on glacier and ice sheet surfaces. Nat. Geosci. 5(11), 771-774.

Tenni, D., Martin, M., Barberis, E., Beone, G.M.,..., Romani M., 2017. Total As and As speciation in Italian rice as related to producing areas and paddy soils properties. J. Agric. Food Chem. 65, 3443-3452.

Tian, L., Zhao, L., Wu, X., Fang, H.,..., Chen, H., 2017 Vertical patterns and controls of soil nutrients in alpine grassland: Implications for nutrient uptake. Sci. Total Environ. 607-608, 855-864.

Van Vliet-Lanoë, B., 1998. Frost and soils: implications for paleosols, paleoclimate and stratigraphy. Catena 34 (1-2), 157-183.

Vione, D., Colombo, N., Said-Pullicino, D., Bocchiola, D.,..., Freppaz, M., 2021. Seasonal variations in the optical characteristics of dissolved organic matter in glacial pond water. Sci. Total Environ.759, 143464.

Volante, A., Desiderio, F., Tondelli, A., Perrin, R.,..., Valè, G., 2017. Genome-Wide Analysis of japonica Rice Performance under Limited Water and Permanent Flooding Conditions. Front. Plant Sci. 8, 1862.

Wadham, J.L., Hawkings, J., Telling, J., Chandler, D.,..., Nienow, P., 2016. Sources, cycling and export of nitrogen on the Greenland Ice Sheet. Biogeosciences 13(22), 6339-6352.

Wang, J., Kerl, C.F., Hu, P., Martin, M.,..., Planer-Friedrich, B., 2020a. Thiolated arsenic species observed in rice paddy pore waters. Nat. Geosci. 13 (4), 282-287.

Wang, J., Halder, D., Wegner, L., Brüggenwirth, L.,,..., Planer-Friedrich, B., 2020b. Redox Dependence of Thioarsenate Occurrence in Paddy Soils and the Rice Rhizosphere. Environ. Sci. Technol. 54 (7), 3940-3950.

Wilson, P. Block/Rock Streams. In: The Encyclopedia of Quaternary Science. Elias, S.A. (Ed), Elsevier, 2013.

Zanella, A., Ponge, J.F., Jabiol, B., Sartori, G.,...,Viola, F., 2018. Humusica 1, article 5: terrestrial humus systems and forms-keys of classification of humus systems and forms. Appl. Soil. Ecol. 122, 75-86.

Zecchin, S., Corsini, A., Martin, M., Romani, M.,..., Cavalca, L., 2017. Rhizospheric iron and arsenic bacteria affected by water regime: Implications for metalloid uptake by rice. Soil Biol. Biochem. 106, 129.

Zhao, F.J., Ma, J.F., Meharg, A.A., McGrath, S.P., 2009. Arsenic uptake and metabolism in plants. New Phytol. 181(4), 777-794.

AUTHORS LIST

Ajmone Marsan Franco, Università di Torino, DISAFA. franco.ajmonemarsan@unito.it
Beone Gian Maria, Università Cattolica del Sacro Cuore, DiSTAS. gian.beone@unicatt.it
Bertora Chiara, Università di Torino, DISAFA. chiara.bertora@unito.it
Bocchiola Daniele, Politecnico di Milano, DIIAR-CIMI. daniele.bocchiola@polimi.it
Bona Francesca, Università di Torino, DBIOS; ALPSTREAM. francesca.bona@unito.it
Bonifacio Eleonora, Università di Torino, DISAFA. eleonora.bonifacio@unito.it
Cat Berro Daniele, SMI. d.catberro@nimbus.it
Celi Luisella, Università di Torino, DISAFA. luisella.celi@unito.it
Colombo Nicola, Università di Torino, DISAFA; NATRISK. nicola.colombo@unito.it
Confortola Gabriele, Politecnico di Milano, DIIAR-CIMI. gabriele.confortola@gmail.com
D'Amico Michele Eugenio, Università di Torino, DISAFA, present address: Università di Milano, DiSAA. michele.damico@unimi.it
Fenoglio Stefano, Università di Torino, DBIOS;. stefano.fenoglio@unito.it
Fontanella Maria Chiara, Università Cattolica del Sacro Cuore, DiSTAS. mariachiara.fontanella@unicatt.it
Freppaz Michele, Università di Torino, DISAFA; NATRISK. michele.freppaz@unito.it
Giannetta Beatrice, Università di Torino, DISAFA, present address: Università di Verona, Dipartimento di Biotecnologie. beatrice.giannetta@univr.it.
Giardino Marco, Università di Torino, DST; NATRISK. marco.giardino@unito.it
Godone Danilo, CNR-IRPI. danilo.godone@irpi.cnr.it
Lombardi Giampiero, Università di Torino, DISAFA. giampiero.lombardi@unito.it
Lonati Michele, Università di Torino, DISAFA. michele.lonati@unito.it
Martin Maria, Università di Torino, DISAFA. maria.martin@unito.it
Mercalli Luca, SMI. l.mercalli@nimbus.it
Negri Sara, Università di Torino, DISAFA. sara.negri@unito.it

Padoan Elio, Università di Torino, DISAFA. elio.padoan@unito.it
Pintaldi Emanuele, Università di Torino, DISAFA. emanuele.pintaldi@unito.it
Pittarello Marco, Università di Torino, DISAFA. marco.pittarello@unito.it
Raimondo Elisa, Università di Torino, DISAFA. elisa.raimondo@unito.it
Ravetto Enri Simone, Università di Torino, DISAFA. simone.ravettoenri@unito.it
Rolando Morena, Università di Torino, DISAFA. morena.rolando@unito.it
Romani Marco, Centro Ricerche sul Riso, ENR. m.romani@enterisi.it
Sacchi Gian Attilio, Università di Milano, DiSAA. gianattilio.sacchi@unimi.it
Said-Pullicino Daniel, Università di Torino, DISAFA. daniel.saidpullicino@unito.it
Salerno Franco, CNR-IRSA. salerno@irsa.cnr.it
Samoré Andrea, EGAP Parchi Reali. andrea.samore@parchireali.to.it
Schiavon Michela, Università di Torino, DISAFA. michela.schiavon@unito.it
Seidel Felix, Università di Torino, DISAFA, present address: Thünen Institute - AK. felix.seidel@thuenen.de
Stanchi Silvia, Università di Torino, DISAFA. silvia.stanchi@unito.it
Tenni Daniele, Centro Ricerche sul Riso, ENR. d.tenni@enterisi.it

We would like to acknowledge **Elementar**, **ACEA Pinerolese Industriale**, **Forte di Bard**, **Caffé Vergnano** and **Azienda Agricola Martinengo** for the support they gave to the organization of this 2nd joint meeting on Soil and Plant System Sciences 2021.

We also thank the municipalities of **Gressoney La Trinite'** and **Alagna Valsesia** which host our field investigations, as well as **Monterosaski** for the logistic support.

We thank the **La Mandria** Park for allowing us to use their sites for our research and for the help its staff has given us on many occasions for many years.

We thank the municipality of **Turin** for hosting investigation on urban environments.

We would also like to thank **Ente Nazionale Risi** and its staff, often active partners in our projects, for their contribution in managing most field trials within their rice experimental platform in Castello d'Agogna, and for their continuous support in transferring research outcomes to rice farmers.